DIGITAL CAMERA IDENTIFICATION USING SENSOR PATTERN NOISE FOR FORENSICS APPLICATIONS

Ashref Lawgaly

A thesis submitted in partial fulfilment of the requirements of the University of Northumbria at Newcastle for the degree of Doctor of Philosophy

Research undertaken in the
Faculty of Engineering and Environment

January 2017

DECLARATION

I declare that no outputs submitted for this degree have been submitted for a research degree of any other institution. I also confirm that this work fully acknowledges opinions, ideas and contributions from the work of others. Any ethical clearance for the research presented in this commentary has been approved. Approval has been sought and granted by the Faculty Ethics Committee.

I declare that the Word Count of this Commentary is *34,483* words

Name: Ashref Lawgaly

Signature: Lawgaly

Date: 28/04/2016.

Acknowledgements

First, I would like to express my deep gratitude to my lord, Almighty ALLAH, for generously giving me endless precious bounties. Without His guidance and mercy, this work would have never reached this stage. I would like to state genuine gratitude to Dr. Fouad Khelifi for his generous provision of his time and advice. Personality, my special thanks goes to my wife Sumeia Elkazza for her constant encouragement and support. Also, many thanks for my mother and my mother in low for their support during the study period and their wishes. Finally, I would like to thank all my colleagues for their essential help and encouragement.

Publications

The following papers have been published.

- A. Lawgaly, F. Khelifi, and A. Bouridane, “Image sharpening for efficient source camera identification based on sensor pattern noise estimation,” in Proc. International Conference on Emerging Security Technologies, Cambridge, UK, Sep. 2013.
- A. Lawgaly, F. Khelifi, and A. Bouridane, “Weighted averaging based sensor pattern noise estimation for source camera identification,” in Proc. International Conference on Image Processing (ICIP), Paris, France, Oct. 2014.
- M.Al-Ani, F.Khelifi, A. Lawgaly, and A. Bouridane, “A novel image filtering approach for sensor fingerprint estimation in source camera identification”, Advanced Video and Signal Based Surveillance (AVSS), 12th IEEE International Conference. Karlsruhe, 25-28 Aug. 2015.
- Shaikh, M.K., Lawgaly, A., Tahir, M.A. and Bouridane, A. (2016) 'Modality identification for heterogeneous face recognition', Multimedia Tools and Applications, pp. 1-16.
- A. Lawgaly, and F. Khelifi, “Sensor Pattern Noise Estimation Based on Improved Locally Adaptive DCT Filtering and Weighted Averaging for Source Camera Identification and Verification,” IEEE Transactions on Information Forensics and Security.

ABSTRACT

Nowadays, millions of pictures are shared through the internet without applying any authentication system. This may cause serious problems, particularly in situations where the digital image is an important component of the decision making process for example, child pornography and movie piracy. Motivated by this, the present research investigates the performance of estimating Photo Response Non-Uniformity (PRNU) and developing new estimation approaches to improve the performance of digital source camera identification. The PRNU noise is a sensor pattern noise characterizing the imaging device. Nonetheless, the PRNU estimation procedure is faced with the presence of image-dependent information as well as other non-unique noise components. This thesis primarily focuses on efficiently estimating the physical PRNU components during different stages. First, an image sharpening technique is proposed as a pre-processing approach for source camera identification. The sharpening method aims to amplify the PRNU components for better estimation. In the estimation stage, a new weighted averaging (WA) technique is presented. Most existing PRNU techniques estimate PRNU using the constant averaging of residue signals extracted from a set of images. However, treating all residue signals equally through constant averaging is optimal only if they carry undesirable noise of the same variance. Moreover, an improved version of the locally adaptive discrete cosine transform (LADCT) filter is proposed in the filtering stage to reduce the effect of scene details on noise residues. Finally, the post-estimation stage consists of combining the PRNU estimated from each colour plane aims to reduce the effect of colour interpolation and increasing the amount of physical PRNU components. The aforementioned techniques have been assessed on two image datasets acquired by several camera devices. Experimental results have shown a significant improvement obtained with the proposed enhancements over related state-of-the-art systems. Nevertheless, in this thesis the experiments are not including images taken with various acquisition different resolutions to evaluate the effect of these settings on PRNU performance. Moreover, images captured by scanners, cell phones can be included for a more comprehensive work. Another limitation is that investigating how the improvement may change with JPEG compression or gamma correction. Additionally, the proposed methods have not been considered in cases of geometrical processing, for instance cropping or resizing.

Table of Contents

List of Abbreviations

PRNU:	Photo Response Non-Uniformity.
CCD:	Charged Coupled Device.
CMOS:	Complementary Metal Oxide Semiconductor.
ICs:	Integrated Circuits.
CFA:	Colour Filter Array.
DIP:	Digital Image Processor.
RGB:	Red-Green-Blue.
YMCG:	Yellow-Magenta-Cyan-Green.
SPN:	Sensor Pattern Noise.
DFT:	Discrete Fourier Transform.
DWT:	Discrete Wavelet Transform.
DCT:	Discrete Cosine Transform.
SCI:	Source Camera Identification.
WA:	Weighted Averaging.
LADCT:	Locally Adaptive Discrete Cosine Transform.
FT:	Fourier Transform.
MRA:	Multiresolution Analysis.
JPEG:	Joint Photographic Experts Group.
GIF:	Graphics Interchange Format.
PNG:	Portable Network Graphics.
TIFF:	Tag Image File Format.
EXIF:	Exchangeable Image File.
SVM:	Support Vector Machine.
EM:	Expectation Maximization.
FPN:	Fixed Pattern Noise.

PNU: Pixel Non-Uniformity.

DSLR: Digital Single Lens Reflex.

MLE: Maximum Likelihood Estimator.

DNA: Deoxyribonucleic acid.

RSC: Removing Shared Components.

PCA: Principal Component Analysis.

MAP: Maximum A posteriori Probability.

PCE: Peak Correlation Energy.

CCN: Circular Cross-Correlation Norm.

FIR: Finite Impulse Response.

CRF: Camera Response Function.

SNR: Signal to Noise Ratio.

UM: Unsharp Masking.

FPR: False Positive Rate.

FNR: False Negative Rate.

TPR True positive Rate.

TP: True Positive.

FN: False Negative.

TN: True Negative.

FN: False Negative.

ECG: Electrocardiography.

EER: Equal Error Rate

List of Tables

List of Figures

CHAPTER 1 **INTRODUCTION**

1.1 Motivation

Many businesses, organisations and individuals currently use digital image devices in everyday life due to their undeniable advantages. Digital image devices have been used in many applications, for example consumer photography, medical diagnosis and in the military sector. Prime examples of digital devices are smart phones and digital cameras, which provide simple and effective ways of capturing and saving digital images of daily activities. However, these digital images can easily be changed based on low-cost image editing software, which requires little work or knowledge. The accessibility of such tools and their simplicity of use increase the risk of images being used in our daily lives and they may also be inadmissible as evidence in a court of law. This may cause serious issues, particularly in situations where the photo is an important part of the decision-making process in crimes, involving child pornography and movie piracy situations. Consequently, in order to increase the trustworthiness of digital images, copyright protection and image authentication should be identified. Motivated by this, the present research will investigate the performance of existing techniques which are based on estimating photo response non-uniformity (PRNU), in order to contribute to the development of new estimation approaches to improve the performance of digital camera identification.

1.2 Background

1.2.1 Digital imaging applications

Any operation that tries to enhance or analyse a visual image is known as image processing. Currently, several common areas are included in the field of digital image processing. For example, bioresearch and biomedical laboratories utilize digital applications to visualize systems in biological samples, digital image systems such as the matching of DNA material and Classification. Moreover, the digital image can be operated on-board exploratory spacecraft and in earthbound telescopes. These instruments can use digital image processing methods in order to enhance, restore and analyse extra-terrestrial imagery. Also, for resource management purposes, satellite images from every square mile of the Earth's surface can be examined. Data from these images can be used to analyse crop yields and damage owing to frost, disease, and other factors (Baxes, 1994). Moreover, digital imaging is used for medical diagnostic purposes, for instance in physiology, ophthalmology, anatomy, and dentistry. Finally, digital imaging systems can be used for military purposes. For instance, automated interpretations of earth satellite imagery can be used in order to identify military threats or sensitive targets and to track targets in real time for smart-bomb and missile-guidance systems (Gonzalez and Woods, 2008).

1.2.2 Digital image authentication

Image authentication plays an important role in security and communication to make digital images a reliable means for testifying to incident and providing legally acceptable evidence in the courtroom. However, pictures can be edited, transmitted

and distributed easily with recent technologies such as Bluetooth and Internet without applying an authentication system. Also when editing software is used it is often effectively impossible to differentiate between an original image and one that has been modified. Consequently, to improve the trustworthiness of digital images, image authentication techniques must be applied. Digital image authentication involves methodologies utilized to analyse and determine whether an image has been amended after it was taken. Rey and Dugelay (2002) pointed out that certain criteria should be considered in obtaining a powerful image authentication system. These criteria could be summarized as follows

1. Localisation of modified regions: the system must have the ability to identify any malicious modification of a part of a digital image and confirm other regions as authentic.
2. Restoration of altered regions: the system must have the capability to reconstruct, partially destroyed or changed regions to allow the user to realise what the original content of the modified regions was.
3. Sensitivity: the authentication system has to be sensitive to different types of manipulation such as changing or cropping the digital picture in specific regions.
4. Tolerance: the system should tolerate a loss of information which can be due to applying compression algorithms and other non-malicious manipulations.

Digital image authentication techniques can be divided into two groups based on either data-hiding techniques or non-data-hiding techniques. The former, include hashing and watermarking schemes based on adding an element of authentication data into an image in order to guarantee its authenticity (Li, 2009) .Nonetheless, it has been reported that one of the drawbacks of hashing and watermarking techniques is that it

has to be operated inside the digital image device, and as a consequence this may cause a reduction in the use of this technique within the image authentication field. In non-data-hiding-based digital image authentication, some unique patterns which could exist due to the image acquisition process and any post-processing procedure are applied. One of the major techniques in this technique is PRNU. This approach was created to serve as a camera fingerprint either to identify the source of an image, or for detecting image forgeries (Farid, 2009). Additionally, camera fingerprinting could be used for forensic tasks in a number of ways. Firstly, it could be used to verify the presence of a specific PRNU fingerprint in the image and it also has the ability to identify forged areas by determining the non-appearance of the PRNU fingerprint in specific regions of the image. Additionally, in order to identify the PRNU fingerprint, it may be likely to reconstruct some aspects of the processing history; for instance, the PRNU can be applied as a template in order to estimate some geometrical processing, such as rotation or scaling. As a final point, the PRNU is beneficial for determining the individual brand of digital camera or distinguishing among a scan image and a digital camera (Fridrich, 2009a). Numerous methodologies can be used in image authentication, as indicated above however; the principal focus of this research is the links between digital image content and the original source based on the PRNU.

1.2.3 Image acquisition sensors

Currently, the most popular type of imaging sensors utilized in scanners, digital cameras, and camcorders are the charged coupled device (CCD) and complementary metal oxide semiconductor (CMOS). Each contains a large number of photo detectors, named pixels, which are generated from silicon and are responsible for converting

photons into electrons using the photoelectric effect (Fridrich, 2009a). Li and Nathan (2005) reported that the CCD image sensor is a silicon based on integrated circuit (IC), containing a dense matrix of photogates or photodiodes that could be operated by translating light energy in the form of photons into electronic charges. The key function of the CCD is collecting the photogenerated electrons in its potential wells through the CCD's exposure to energy; and the hole is then forced away from the potential well. After that, it will eventually move into the silicon substrate. Therefore, the higher the amount of electrons which collect on that pixel, the lighter that is incident on a particular pixel will be. When the CCD gate voltages are changed, the depth of the potential wells is also altered. This action can allow the transfer of the photogenerated electrons among the registers to the "read-out" circuit. The output signal could be at that time moved to the computer for image processing. Meanwhile the use of CMOS has the benefit compared to the CCD in that it is produced in the same manner as memory chips, which can make a possible decrease in cost and power. Also, it may be possible to add other circuitry in order to combine voltage measurement, and amplifiers on the same chip resulting in even more cost savings. Nevertheless, currently, the CMOS sensors cannot be utilized in high-level specification cameras since they generate more additional noise than the CCD (Li and Nathan, 2005).

1.2.4 Digital image acquisition model

The majority of information about the camera pipeline may remain copyrighted information belonging to the manufacturer; nevertheless, the universal sequence of image acquisition and the structure of the digital camera can be similar among common types of digital cameras.

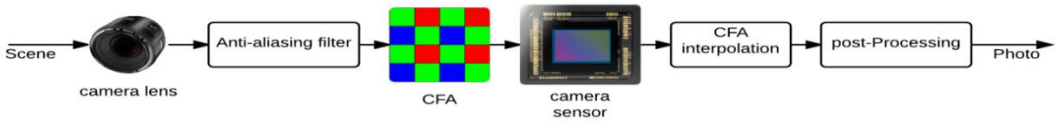

Figure 1-1 Digital image acquisition procedure for digital camera (Source: Li, 2009)

Figure 1-1 illustrates the basic components of a digital camera which are the lens, filters, image sensor, colour filter array (CFA) and digital image processor (DIP). Tran Van *et al.* (2007) pointed out that; every component adjusts the input by using a particular technique with a particular set of parameters. When an image is captured, the light is passed across the lens and this may cause certain distortion, for instance, chromatic aberration and spherical aberration. Consequently various filters, for example an anti-aliasing filter is exploited. Such a filter is applied in order to decrease aliasing, which may occur due to the spacing among pixels. Subsequently, with the aim of generating a colour image, the light goes through an additional filter named a colour filter array (CFA). Every pixel on the lens sensor could be allocated one of three or four colours. A demosaicing process is then utilized in order to assign every pixel the intensities of the other two colours by interpolating the colour information within a neighbourhood. As demonstrated in figure 1-2, the colour filter array patterns can be RGB (red-green-blue) or YMCG (yellow-magenta-cyan-green) colour spaces, for a 4 × 4 block of pixels (Li, 2009).

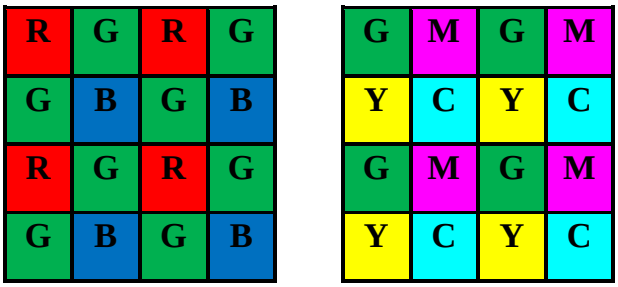

Figure 1-2 CFA patterns: (a) RGB, (b) YMCG (Source: Mikkilineni et al., 2006).

The light next passed on to the imaging sensor which is the key part of every digital camera. Such sensor contains a vector of photo detectors each cell is matched to one pixel of the final image and each pixel becomes an equivalent signal linked to the light's intensity, which is converted into a digital signal. These imaging sensors do not respond to colour, they merely capture the brightness of light; thus, the sensor is used after the colour filter array. Lastly, several image processing operations such as gamma correction, enhancing, colour correction, white balancing, and image formatting may be applied before the image is saved, and the nature of these operations could differ from one manufacture to another (Khanna *et al.*, 2006). Based on a simplified description of an imaging pipeline for each colour band, let **I**[i] be the digital signal representation before applying the demosaicing and the light intensity at pixel i is denoted as $\mathbf{Y}[i]$, where $i = 1,2, \dots n$. In this thesis, all matrices shown in boldface font are in vector form and all the processes could be element-wise. A basic model of the sensor output could be expressed as:

$$\mathbf{I} = g^{\gamma}.[(\mathbf{1} + \mathbf{K})\mathbf{Y} + \mathbf{\Lambda}]^{\gamma} + \mathbf{\Theta}_q \qquad 1.1$$

where g represents the colour channel gain, γ is the gamma correction factor which is approximately equal to 0.45, **K** denotes the zero-mean multiplicative factor responsible for the unique component of the sensor.

Also, in some research papers this component is known as the sensor camera fingerprint. Furthermore, the combination of all extra additive noise sources such as shot noise; read-out noise and dark current noise are denoted as $\boldsymbol{\Lambda}$. The gain factor g modifies the pixel intensity level based on the sensitivity of the pixel in each colour band in order to achieve the correct white balance. Finally, $\boldsymbol{\Theta}$ represents quantization noise. In order to factor out the most dominant component $\mathbf{Y}$ from equation 1.1, the Taylor expansion $(1+x)^{\gamma} = 1 + \gamma x + O(x^2)$ is applied, which gives:

$$\mathbf{I} = (g\mathbf{Y})^{\gamma}.[\mathbf{1} + \mathbf{K} + \Lambda/\mathbf{Y}]^{\gamma} + \boldsymbol{\Theta}_q = (g\mathbf{Y})^{\gamma}.[\mathbf{1} + \gamma\mathbf{K} + \gamma\,\Lambda/\mathbf{Y}]^{\gamma} + \boldsymbol{\Theta}_q \qquad 1.2$$

In order to avoid introducing several different notations, the symbols can be absorbed as follows: $\mathbf{I}^{(0)} = (gY)^{\gamma}, = \gamma\mathrm{K}$. This could leads to a sensor output model which could be written as:

$$\mathbf{I} = \mathbf{I}^{(0)} + \mathbf{I}^{(0)}\mathbf{K} + \boldsymbol{\Theta} \qquad 1.3$$

where $\mathbf{I}^{(0)}$ is the sensor output in the absence of noise, $\mathrm{I}^{(0)}\mathrm{K}$ is the sensor camera fingerprint (PRNU), and $\Theta = \gamma^{(0)}\,\Lambda/\mathbf{Y} + \boldsymbol{\Theta}_q$ is the compound independent random noise component. This research mainly focuses on the efficient extraction of PRNU in order to improve the performance of identification in terms of small images.

1.3 Scope of research

Multimedia data including text, image, video and audio can be obtained from a variety of devices for instance cameras, computers, mobile phones, printers, and scanners. These devices may produce data with different patterns as a result of different physical device with diverse parameters being used inside such digital devices; this may therefore lead to diverse patterns in output. The present research concerns the

identification of the source of digital images which have been taken by specific digital cameras. Although several techniques can be used to identify the source of images, such as analogous to bullet scratches and some statistical features, this research is based on the analysis of digital camera components such as imaging sensors in order to identify the original source. Moreover, the research compares the performance and efficiency of the proposed techniques with existing state-of-the-art algorithms.

1.4 Objectives

Several objectives are considered in order to achieve the aim of this PhD research. These objectives can be summarized as follows

- To explore how a digital image is obtained from digital camera.

  This objective is covered in Chapter 1.

- To explore some types of image representation in the transform domain, such as DFT, DWT and DCT.

  This objective is covered in Chapter 2

- To explore and evaluate the performance of existing state-of-the-art image authentication techniques, especially, photo response non-uniformity techniques.

  This objective is covered in Chapter 3.

- To design and develop a new pre-processing algorithm to improve PRNU estimation.

  This objective is covered in Chapter 4

- To design and develop a new approach for efficient PRNU estimation.

  This objective is covered in Chapter 5.

- To design and develop a new filtering schema based on PRNU estimation.

  This objective is covered in Chapter 6.

- To evaluate the effect of colour PRNU.

  This objective is covered in Chapter 7.

1.5 Thesis contributions

In this dissertation, several techniques have been proposed for efficient PRNU estimation in order to improve image source identification. The main contributions of this dissertation can be summarized as follows.

- Image sharpening as a pre-processing technique for a source camera identification system

As a first stage towards the development of a new system for source camera identification (SCI), image sharpening is performed for efficient PRNU estimation. Such estimation depends on the difference among a set of digital images and their smoothed versions in order to capture the characteristics of the sensor. Hence, this procedure can use a part of the sensor noise content which is concentrated in the high frequency range and present in edges, textured and contours regions of the digital images. The proposed image sharpening technique aims to amplify these PRNU components for better estimation, therefore improving the performance of source camera identification. Considerable improvements are gained by the proposed technique, as validated in comparison with two recent source camera identification techniques.

- In the estimation stage, a new weighted averaging (WA) technique is presented.

Most existing techniques estimate the PRNU through the constant averaging of residue signals extracted from a specific number of digital images. This is based on the hypothesis that every residue signal is a noisy observation of the sensor pattern noise. This theory is well justified in practice since the digital images are taken under diverse conditions, making the corresponding residue signals different from each other. For example saturated pixels can produce more undesirable noise in residue signals. Also, bright digital images deliver better PRNU estimation than darker ones. Motivated by this observation, a weighted averaging technique is presented for effective PRNU estimation. The presented technique is validated by comparison with two PRNU estimation techniques from the literature and experimental results show considerable improvements.

- An improved version of the locally adaptive discrete cosine transform (LADCT) filter is proposed in the filtering stage.

A new source camera identification system relying on an improved version of the locally adaptive discrete cosine transform (LADCT) filter is proposed for accurate PRNU estimation. This proposed filter aims to reduce the effect of scene details on noise residues. The LADCT can exceed other filters that operate on full images and it performs well on images affected by image-dependent noise including the multiplicative noise. This provides a logical reason for adopting this filter because the PRNU is also multiplicative.To the best of the present author’s knowledge, this filter has not been used before in the field of digital image forensics.

- In the post-estimation stage, a new PRNU estimation technique based on colour combination is presented.

The camera sensors can exhibit a physical noise pattern in one colour component only at every pixel position, while the other components can be estimated through interpolation involving the neighbouring pixels. Some PRNU estimation techniques depend on the green or gray scale version of images in order to extract the PRNU, while other researchers estimated the PRNU from each channel individually and then combined them linearly to derive a colour-to-luminance PRNU. However, a linear combination with fixed weights may include some interpolation noise if a particular color location does not correspond to the physical light information. Also, if only the green channel is used, the physical PRNU information which could exist in other colour components (red and blue) is not taken into account. The post-estimation stage consists of concatenating the PRNU estimated from each colour plane in order to exploit the presence of physical PRNU components in different channels. Experimental results have shown a significant gain obtained with the proposed colour combination technique and the superiority of the overall system when compared with state of the art source camera identification systems.

1.6 Thesis outline

The thesis is organized as follows. A mathematical description of the DWT, DCT and DFT is presented in chapter 2. Chapter 3 is devoted to surveys of the latest state-of-the-art image authentication techniques. With the aim to amplify the PRNU components for better estimation, an efficient pre-processing approach is examined with some existing methodologies in chapter 4. Chapter 5 focuses on a weighted averaging (WA) technique for superior PRNU estimation. This is followed by a presentation of experimental results for WA and various source camera identification techniques. Chapter 6 describes a new filtering scheme based on an improved version of the locally adaptive discrete cosine transform (LADCT) filter. The experimental results on images of different sizes are also provided in this chapter. Chapter 7 introduces a digital camera identification using colour PRNU combination. Chapter 8 provides the conclusion of the thesis and recommendations for future work.

CHAPTER 2 IMAGE REPRESENTATION IN THE TRANSFORM DOMAIN

2.1 Motivations

The conventional approach for estimating the PRNU is based on image filtering and the most powerful filters operate in the transform domain. Motivated by this, this chapter investigates the most widely used decorrelating transforms. An image transform provides a meaningful and practical method to change the statistical properties of the original image. The transform domain offers a number of attractive features such as energy compaction and decorrelation. Regarding the former, most of the signal data may be concentrated in a small number of low-frequency components of the transform. Decorrelating transforms can eliminate linear dependencies from the data, consequently making a set of components such that, when individually quantized and entropy coded, the resulting symbol stream can be considerably reduced when compared with utilizing quantization directly on the image data (Bracewell, 1999).

2.2 Spatial domain representation

A radiograph could be seen as a spatial representation of an object in a two-dimensional area of varying exposure intensity. A neutral radiographic image is a 2-D light intensity function, $f(x, y)$, where x and y are spatial coordinates, and the value of f at (x, y) is commensurate with the illumination or intensity of the picture at that location.

A digital image could be defined as a two-dimensional matrix or a sequence of two-dimensional matrices (one for each colour band). A digital image can consist of a determinate number of components, each of which needs a particular value and position, and these components are named pixels (Graham, 1998). Digitised illumination values are named the grey level, and a digital image is represented as follows:

$$f(x,y) = \begin{bmatrix} f(1,1) & f(1,2) & \cdots & f(1,N) \\ f(2,1) & f(2,2) & \cdots & f(2,N) \\ \vdots & \vdots & & \vdots \\ f(N,1) & f(N,2) & & f(N,N) \end{bmatrix} \quad 2.1$$

The quality of a digital image could rely on the total number of lines and pixels, together with the range of brightness values in the image. These characteristic are named as image resolutions (Petrou and Petrou, 2010). Figure 2-1 illustrates the effect of digitization, where the 2-D continuous image has been divided into 16 rows and 16 columns.

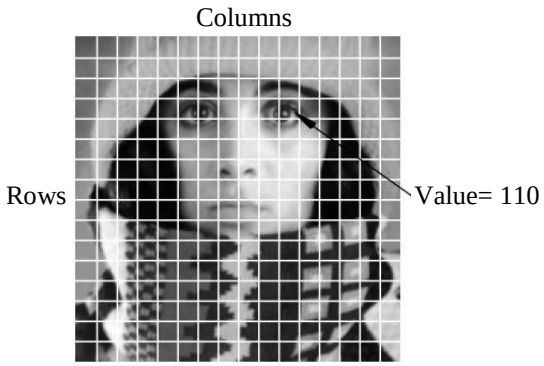

Figure 2-1 Digitization of a continuous image. (Source: Ravirajaet al., 2015)

2.3 Discrete Fourier transform

The Fourier transform (FT) is well known for providing an approach to solving problems in linear systems. In image processing, the FT has been an essential tool which can be applied to decompose a signal into its cosine and sine components (Bracewell, 1999). In a one-dimensional signal, the FT of a complex valued function $X(f)$ could be defined as:

$$X(f) = \int_{-\infty}^{+\infty} x(t)e^{-i2\pi ft}\,dt\,, f\ \in \Re. \qquad 2.2$$

where the independent variable t represents time, while f represents the ordinary frequency. The signal in Fourier domain can be reconstructed to the signal $x(t)$ by applying the inverse transform as:

$$x(t) = \int_{-\infty}^{+\infty} X(f)e^{i2\pi ft}\,df\,, t\ \in \Re. \qquad 2.3$$

The interpretation of the Fourier signal is aided by expressing it in a polar coordinate formula as

$$X(f) = |X(f)|e^{i\phi(f)} \qquad 2.4$$

where |X(f)| refers to the amplitude and Φ(f) refers to the phase of X(f).

If X(f) ⇔ x(t) this indicates that $X(f)$ and $x(t)$ are a Fourier transform pair. Jain (1989) reported that the FT offers a number of properties as follows:

- Linearity

$$ax_1(t) + bx_2(t) \iff aX_1(f) + bX_2(f) \qquad 2.5$$

- Convolution

$$x_1(t) * x_2(t) \iff X_1(f)X_2(f) \qquad 2.6$$

- Scaling

$$x(at) \Leftrightarrow \frac{1}{|a|} X\left(\frac{f}{a}\right) \quad 2.7$$

- Time shift

$$x(t - t_0) \Leftrightarrow e^{-i2\pi f t_0} X(f) \quad 2.8$$

- Modulation

$$x(t)e^{-i2\pi f_0 t} \Leftrightarrow X(f - f_0) \quad 2.9$$

- Parseval's theorem

$$\int_{\Re} |x(t)|^2 = \int_{\Re} |X(f)|^2 \quad 2.10$$

Sonka *et al.* (1999) mentioned that the two-dimensional Fourier transform and its inverse could be defined as

$$F(u,v) = \int_{-\infty}^{+\infty} \int_{-\infty}^{+\infty} f(x,y) e^{-2\pi i(xu+yv)} \, dx \, dy \quad 2.11$$

$$f(x,y) = \int_{-\infty}^{+\infty} \int_{-\infty}^{+\infty} F(u,v) \, e^{2\pi i(xu+yv)} \, du \, dv \quad 2.12$$

The discrete Fourier transform (DFT) has been widely applied in image filtering, image description and image data compression. The DFT is the sampled FT and consequently does not include all frequencies forming an image, but just a collection of samples which is sufficient to perfectly describe the spatial domain image. The number of frequencies corresponds to the total of pixels in the spatial domain image. The two dimensional DFT of a square image N × N is defined by:

$$F(k,l) = \sum_{i=0}^{N-1} \sum_{j=0}^{N-1} f(i,j) e^{-i2\pi(\frac{ki+lj}{N})} \quad 2.13$$

where $f(i,j)$ represent an image in the pixel domain and the exponential part is the base function, which corresponds to every point $f(k,l)$ in the Fourier domain. As shown in equation 2.13, the $f(k,l)$ can be gained by multiplying the pixel image by the corresponding base function and then summing the results. It is worth noting that the base functions are cosine and sine waves with increasing frequencies, $f(0,0)$ denotes the DC-component of the image that matches the average brightness, while $f(N-1,N-1)$ denotes the maximum frequency. The DFT could be re-converted to the pixel domain by applying the inverse Fourier transform, which could be defined as:

$$f(i,j) = \frac{1}{N^2} \sum_{k=0}^{N-1} \sum_{l=0}^{N-1} F(k,l)\, e^{i2\pi(\frac{ki+lj}{N})} \qquad 2.14$$

2.4 Discrete cosine transform

The discrete cosine transform (DCT) is an additional sinusoidal transform which could be linked to the DFT. The DCT has been generally applied in applications for image feature extraction, filtering, and compression (Sonka *et al.*, 1999). There are four definitions of the DCT and often denoted as DCT-I, DCT-II, DCT-III and DCT_IV, and the most commonly used DCT, in image processing and compression is DCT-II. This could be defined for a square (N × N) image as:

$$C(k,l) = \alpha(k,l) \sum_{i=0}^{N-1} \sum_{j=0}^{N-1} f(i,j) \cos\left(\frac{(2i+1)k\pi}{2N}\right) \cos\left(\frac{(2j+1)l\pi}{2N}\right) \qquad 2.15$$

Where

$$\alpha(k,l) = \begin{cases} \frac{1}{N} & for\ k,l = 0 \\ \frac{2}{N^2} & for\ k,l = 1,2,\dots,N-1 \end{cases}$$

One of the key advantages of the DCT is that it produces a real valued output image, and this could make the DCT faster than the DFT transform. The cosine transform computation could be based on the Fourier transform, and all *N* coefficients of the DCT can be calculated using a 2N-point fast Fourier transform. Moreover, the DCT has outstanding energy compression for highly correlated data. Indeed, the DCT has the ability to discard coefficients representing high frequency components without seriously changing the way an image looks to the human eye. Lukin *et al.* (2010) claimed that DCT-based filters have demonstrated good efficiency for eliminating different types of noise such as Poisson and film-grain noise that contaminate which signal through an additive or a multiplicative rule.

2.5 Discrete Wavelet Transform

Wavelets represent another method for decomposing a complex signal into sums of basis functions. Such a mathematical tool allows the analysis of signals and signal-generating procedures characterized by non-stationary behaviour (Abry, 1997). The wavelet is basically a function that, unlike the Fourier transform, has not only a frequency linked to it, but also a scale (Parker, 1997). Moreover, Burrus *et al.* (1998) pointed out that the signal $x(t)$ could often be described, analysed or processed better if expressed as a linear decomposition by:

$$x(t) = \sum_{j,k} a_{j,k}\, 2^{j/2}\, \psi(2^j t - k) \qquad 2.16$$

where $a_{j,k}$ represents a set of two-dimensional coefficients which are normally named the discrete wavelet transform (DWT) of $x(t)$, while the $\psi_{j,k} = 2^{j/2}\, \psi(2^j t - k)$ is basis functions. This function is created from a single function (named the mother

wavelet or generating wavelet) by changing the two parameters j and k, when the index k changes, the location of the wavelet can be moved in time or space. This can allow the expansion to clearly represent the location of events in space or time. Meanwhile when the parameter j is changed, the shape of the wavelet can change in scale. This permits a representation of detail or resolution.

2.5.1 Multiresolution analysis

Multiresolution analysis (MRA) integrates and unifies methods from a range of disciplines, including quadrature mirror filtering from digital speech recognition, pyramidal representation from image processing and sub-band coding from signal processing. As its suggests name, the multiresolution principle is concerned with the representation and analysis of digital images or signals at more than one resolution where features that might be undetected at one resolution may be more easier to detect at another. In MRA, a scaling function is used to build a sequence of approximations of an image or function where each differs by a factor of 2 in resolution from its nearest neighbouring approximations. After that, wavelets functions are used to encode the difference in information between adjacent approximations (Gonzalez and Woods, 2008). The scaling functions could be expressed in terms of integer translations of the basic scaling function by:

$$\varphi_k(t) = \varphi(t-k) \qquad k \in Z \ , \qquad \varphi \in L^2 \tag{2.17}$$

where the subspace of $L^2(\Re)$ spanned by these functions can be expressed as:

$$V_0 = \overline{Span(\varphi_k(t))}_k \tag{2.18}$$

A two-dimensional family of functions can be produced from the basic scaling function by scaling and translation by:

$$\varphi_{j,k}(t) = 2^{j/2}\varphi(2^j t - k) \quad 2.19$$

The subspace spanned over k for any j, is defined as:

$$V_j = \overline{Span(\varphi_{i,j}(t))}_k \quad 2.20$$

This means that if $x(t) \in V_j$, and then it can be expressed as

$$x(t) = \sum_k a_k \, \varphi(2^i t - k) \quad 2.21$$

The basic requirement of multiresolution analysis is:

$$V_0 \subset V_1 \subset V_2 \subset \ldots \subset L^2 \quad 2.22$$

Therefore, the spaces V_j satisfy an intuitive scaling condition.

$$x(i) \in V_j \Leftrightarrow x(2t) \in V_{j+1} \quad 2.23$$

The important features of a signal could better be described by also utilizing a number of wavelet functions $\psi_{j,k}(t)$ that span the differences between any two neighbouring scaling subspaces, V_j and V_{j+1} (Burrus *et al.*, 1998). The orthogonal complement of V_j in V_{j+1} is W_j. This can be expressed as:

$$V_1 = V_0 + W_0 \quad 2.24$$

which can be extended to:

$$V_n = V_0 + W_0 + W_1 + \cdots + W_{n-1} \quad 2.25$$

Hence, a signal $x(t) \in V_n$ could be defined as:

$$x(t) = \sum_k a_k \, \varphi(t - k) + \sum_{j=0}^{n-1} \sum_k d(j,k)\psi_{j,k}(t) \quad 2.26$$

The decomposition of $x(t)$ with n resolutions (or scales) could be represented as:

$$x(t) = \sum_k a_{j-1,k} \, 2^{(j-1)/2}\varphi(2^{j-1}t - k) + \sum_k d_{j-1,k} \, 2^{(j-1)/2}\psi(2^{j-1}t - k) \quad 2.27$$

where

$$a_{j-1,k} = \sum_{m} h(m-2k)a_{j,k} \qquad 2.28$$

and

$$d_{j-1,k} = \sum_{m} g(m-2k)a_{j,k} \qquad 2.29$$

The first summation in equation 2.27 can give a function that is a low resolution or coarse approximation of $x(t)$. In the second summation, when the index *j* is increased, a finer resolution function can be added, which adds increasing detail. Equations 2.28 and 2.29 denote a digital filtering procedure which could be followed by a down-sampling (sometimes named a sampler or a decimator) by a factor of 2. The down-sampler can take a signal $x(n)$ as an input and generates an output of $y(n) = x(2n)$. These equations illustrate that the wavelet and scaling coefficients at several ranks of scale could be achieved by convolving the expansion coefficients at scale j by the time-reversed recursion coefficients $\mathrm{h}(-\mathrm{n})$ and $\mathrm{g}(-\mathrm{n})$ and then down-sampling to give the extension coefficients at the next level of j-1. In other words, the scale *j* coefficients can be filtered by two finite impulse response (FIR) digital filters with coefficients $\mathrm{h}(-\mathrm{n})$ and $\mathrm{g}(-\mathrm{n})$, after which the down-sampler gives the next coarser scaling and wavelet coefficients. The implementation of equations 2.28 and 2.29 with two stages of wavelet decomposition is shown in figure 2-2. Similarly, a reconstruction of the original fine-scale coefficients would be created from a combination of the scaling function and wavelet coefficients at a coarse resolution.

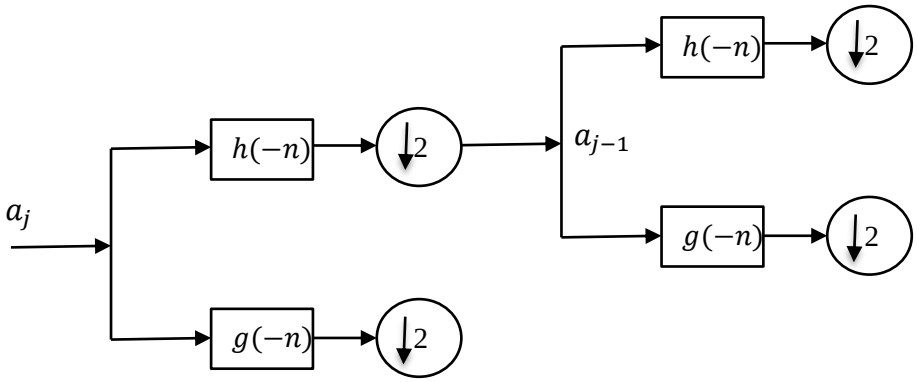

Figure 2-2 Two-stage wavelet decomposition

2.5.2 Two-dimensional wavelet transform

For two-dimensional data for example images, the most generally utilized procedure for wavelet decomposition uses separable one-dimensional wavelets and scaling functions. Such a type of two-dimensional DWT can produce a decomposition of approximation coefficients at level *j* in four components: the approximation at level *j* - *1* ($a_j - 1$), and other details in three locations, which are diagonal $d_{j-1}^{(d)}$, horizontal $d_{j-1}^{(h)}$, and vertical $d_{j-1}^{(v)}$ (Mallat, 1999). Figure 2-3 shows a sample of a one-stage decomposing image 'Lena'. In a similar manner, the reverse procedure could be applied in order get the original two-dimensional signal.

(a) (b)

Figure 2-3 One-step 2-D wavelet decomposition: (a) original image, (b) Decomposed image.

2.6 Spatial and Transform Domain Filtering Methods

Filters play a significant role in the image de-noising process. It is a technique for modifying or enhancing an image. There are two basic approaches to image de-noising, spatial filtering methods and transform domain-filtering methods. A conventional technique to remove noise from image data is to employ spatial filters, which could be further considered into linear and non-linear filters. Spatial filters can employ a low pass filtering on sets of pixels with the hypothesis that the noise occupies the higher region of frequency spectrum. Generally, spatial filters remove noise to a reasonable extent however may lead to blurring images, which in turn makes the edges in images invisible. The transform domain filtering approaches could be sub-divided according to the choice of the basis functions. Figure 2-4 illustrate the basic for filtering in the frequency domain. Spatial-frequency filtering denotes usage of low pass filters based on Fast Fourier Transform (FFT). In frequency smoothing methods, the removal of the noise can be achieved by designing a frequency domain filter and adapting a cut-off frequency when the noise is decorrelated from the useful signal in the frequency domain. However, such methods may be seen as time consuming and rely on the cut-off frequency and the filter function behaviour. Additionally, they could create artificial frequencies in the processed image (Motwani et al., 2004) .

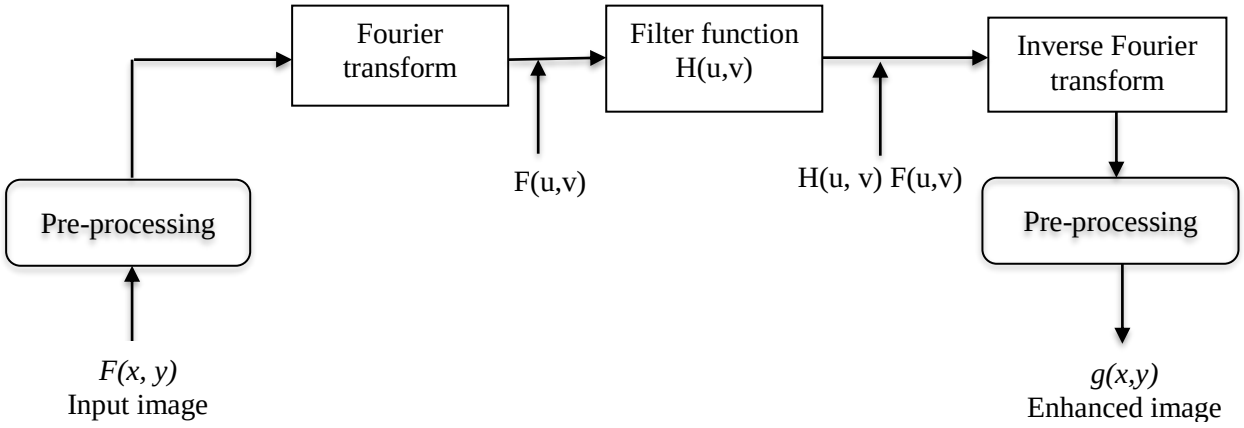

Figure 2-4: Basic steps of filtering in frequency domain.

Also, wavelets can offer a better performance in image de-noising because of properties for example multiresolution structure and sparsity. in the last two decades several algorithms for de-noising in wavelet domain was introduced. The first efforts involved very simple ideas such as thresholding of the orthogonal wavelet coefficients of the noisy data, after that reconstruction. Later efforts found that considerable improvements in perceptual quality may be gained by translation invariant approaches based on thresholding of an undecimated wavelet transform. Furthermore, several researchers have experimented with variants on the basic schemes— adjustments of thresholding functions, block thresholding, adaptive choice of threshold, level-dependent thresholding, and so on (Starck et al., 2002). Furthermore, the Discrete Cosine Transform (DCT) can be applied for image de-noising application. The DCT based filters could have better performance among currently existing groups of filters, in case of pictures corrupted by speckle noise and, Gaussian additive. Also different from wavelet filters, DCT based filters works as sliding blocks. This could offer more information about spatial correlation properties of noise in an easier method (Ponomarenko *et al.*, 2008). Lukin *et al.* (2010) claimed that DCT filter could be

simply adapted to a priori known or pre-estimated noise statistics. Finally, DCT-based filters have demonstrated good efficiency for eliminating different types of noise such as Poisson and film-grain that contaminate the signal through an additive or a multiplicative rule.

2.7 Conclusion

In this chapter, the most generally exploited discrete transforms are described for additional use in image forensics in the next chapters. Such transforms can offer a better energy distribution of the signal and considerably decrease the redundancy exhibited in the spatial domain. The DCT could be seen as a variant of the DFT in which the transform coefficients are real values. In addition, the DWT can provide extra flexibility in the range of the wavelet basis adaptively with signal content and depending on the application concerned.

CHAPTER 3 IMAGE FORENSICS AND SECURITY: REVIEW

3.1 Introduction

The demand for digital imaging devices has recently dramatically increased due to their unquestionable advantages. Although such digital devices can offer an easy way to save digital images of daily activities, these images can easily be amended without cost using free editing software. This in turn could lead to serious problems, especially when a video or digital image is treated as evidence of a crime or images are used for purposes of extortion. Digital image forensics could be defined as the science that attempts to analyse a specific digital asset in order to provide an assessment of such an image's content and estimate information that may be valuable to support an investigation by linking a digital document to a specific digital device. The fundamental idea behind multimedia forensics depends on the features that may exist due to the image acquisition process and any post-processing procedures. Such features may leave a distinctive mark on the data, as a kind of digital fingerprint. This fingerprint could be used to define the origin of the image and to determine the authenticity of the digital content. Image forensics technologies can introduce novel approaches for analysis and offer support in decision making in criminal investigation. Multimedia forensics researchers aim to assist human investigators by providing mechanisms for the authentication and analysis of multimedia documents. For example, we can imagine a situation in which the very action of creating a photograph involves an illegal action linked to the content represented in the data, such as child

pornography. In such a scenario, tracking the digital device that captured that digital asset could provide evidence of this issue and may lead the court to blame the owner of the digital device for that crime. Multimedia forensics methods could help in identifying the source of a digital image, making the digital content a silent witness in the courtroom. Other methodologies could be utilized in different circumstances in which a forensics analysis would assist the investigator in discovering whether the multimedia content is authentic or has been tampered with and stored using photo-editing software (Amerini, 2010). In multimedia forensics, many approaches could be used to verify the integrity and/or authenticity of multimedia documents. Based on the concepts involved, these methodologies can be categorised into two main approaches: extrinsic or proactive techniques and passive techniques using device characteristics. This chapter discusses the fundamentals and the motivations of digital forensics, and illustrates the major approaches proposed so far in order to answer two basic questions: a) what is the source of a multimedia document? and b) is such a multimedia document genuine or not? This chapter is organized as it follows. Section one discusses various application scenarios for digital image forensics technologies. Several kinds of digital fingerprint which could be used in image forensics are introduced in the second section. Proactive techniques such as watermarking and hashing schemes are then discussed in the third section. The fourth section discusses passive technologies and methodologies based on PRNU estimation are evaluated in section five. After that, a number of de-noising approaches which could be used during the PRNU estimation process are discussed. Finally, approaches which focus on similarity/dissimilarity among the PRNU signals are introduced in section seven.

3.2 Application scenarios

This section considers a number of application scenarios for digital forensics technologies and which problems they could provide solutions for. Although digital forensics tools have been used in many fields, the two major usage categories are the detection of forgeries and the identification of sources, and the relevant approaches are discussed in more detail in the following sections. In first case, it could be necessary to establish if an individual picture is authentic or has been tampered with. The target of such tampering could vary widely, ranging from commercial aims such as perpetrating an incorrect journalistic scoop or realizing a quasi-realistic advertisement, or for more important purposes such as, changing the judgement in a courtroom where digital photographs could be accepted as evidence. For the identification of the source, forensics processes are designed to determine the origin of the image, which can be split into two categories. The first aims to identify the type of digital device that created the multimedia document, if it was produced by a digital camera, scanner or computer. Several methods exist to achieve this objective, and the basic idea is that a search is conducted of the multimedia document for traces of a particular acquisition process and for the absence or presence of unique characteristics inside the digital data. The second category is concerning with individuation, among a particular set of digital devices. For instance, for images captured by a certain scanner or digital camera, the aim is to determine which model and brand has taken that image. The achievement of this aim could require the previous extraction of certain information from every digital device in order to create a sort of identifying fingerprint during the analysis of a set of multimedia documents called a training set captured by each device (Amerini, 2010).

In the next section, a number of digital fingerprints for image forensics are discussed in more detail.

3.3 Intrinsic digital fingerprints

Digital image forensics rely on digital fingerprints, which are characteristic traces left behind in a multimedia document during the generation stage and any other successive procedure (Swaminathan *et al.*, 2008). This kind of digital fingerprint relies on analysing the characteristic traces, with no embedding of additional data and without any knowledge about the linked original multimedia document (passive approach). Forensic experts could expose these traces by analysing some data on digital imaging mechanisms. The tasks for digital forensics fingerprint can be classified into:

1. Digital device identification: determining that a given digital video or image was captured by an identified individual device.
2. Source classification: classifying digital images according to their origin, such as scanned versus digital camera images, or based on camera model for instance Canon versus Samsung.
3. Processing history recovery: to recover the chain of processing that was applied to the multimedia document; for example, filtering, contrast/brightness adjustment and lossy compression.
4. Integrity verification: a procedure to determine malicious attacks, for instance, removing or inserting objects. (Chen et al., 2008).

A number of types of digital fingerprints can be taken into consideration for forensics analysis purposes. These fingerprints can be categorised in three classes: unique traces

which may be left by in-camera processing, traces left through out-camera processing, and digital fingerprints linked to the features of the framed scene.

3.3.1 In-camera digital fingerprints

Every component of a digital device can modify the input and leave intrinsic digital fingerprints in the final multimedia document caused by the particular optical system, colour filter array, sensors and some camera software. Additionally, natural pictures can have common characteristics unrelatedly to the content; for instance, inherent noise or a luminance behaviour that could be used as an inherent fingerprint (Amerini, 2010).

3.3.2 Out-camera digital fingerprints

Every process applied to a multimedia document (e.g. geometrical or statistical, or other) could lead to adjust their properties leaving particular indications accordingly to the processing itself.

It is worth noting that the first two types of fingerprints are independent of the content of the analysed data. This means that a trace left by a given camera device would be the same even if different contents are captured (Amerini, 2010).

3.3.3 Scene digital fingerprints

This kind of digital fingerprint can involve features related to the content of the picture itself. Some features relying on the content include lighting properties, which could be used to distinguish the reproduced scene.

The common procedure after selecting a particular fingerprint is to choose some feature of the fingerprint considered and then to find optimal parameters before

making a decision based on either estimation or classification procedures. For instance, in case of source device identification, usually certain traces can be obtained which are next compared with a number of available fingerprints, in order to identify a model, kind or brand of acquisition device (Amerini, 2010). The following sections discuss approaches of acquisition device identification and integrity verification based on the above kinds of digital fingerprints

3.4 Extrinsic methods

In extrinsic forensics approaches, additional visible information can be added to the output of multimedia documents for many reasons; for instance, source identification, copy detection, document tracking and tampering detection. Digital watermarking and hashing schemes are examples of extrinsic forensics approaches (Dirik, 2010).

3.4.1 Digital image watermarking

A digital watermark is described as a part of data that is hidden in a multimedia document. The principal advantage of this technique is that the hidden data cannot be separated from the multimedia content. Watermarks could be either added into digital content during its creation or inserted later using specific software. In forensically secure digital cameras, the watermark is applied inside the digital camera. Watermarking could be applied in several applications of watermarking, for owner identification, broadcast monitoring, transactional watermarks, and authentication (Langelaar *et al.*, 2000). In recent years, digital watermarking has been applied to identify and authenticate tampered regions in digital images. Methods of watermarking which are frequently used for image authentication are so-called “fragile” and “semi-

fragile" digital watermarking. The former could be exploited to detect any minor manipulations of a digital image and consequently any attacks that change the pixel values of the image will be determined. However, the main disadvantage of this technique is that it could be hard to discriminate between non-malicious and malicious attacks, and so for instance most of fragile techniques would judge a lossy compressed digital image to be a forged image. Semi-fragile watermarking techniques are applied to identify authentic image content, because these techniques are more robust against attack. The basic idea of this technique, as demonstrated in

figure 3-1, requires that features are first obtained from the digital image, and these are hidden within a robust and invisible watermark. Next, to test whether or not a digital image has been modified, it is essential to match its features with those of the original image which are retrieved from the watermark. The digital image has not been tampered with, if the features are matching; otherwise the dissimilarity will point to amended regions (Rey and Dugelay, 2002).

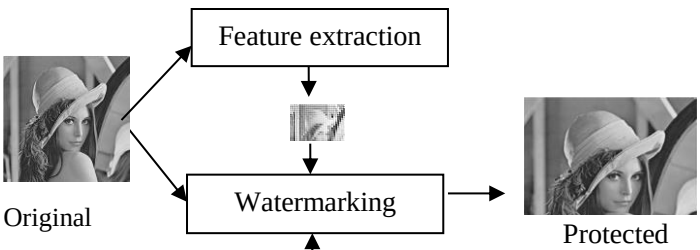

Figure 3-1 watermarking semi-fragile technique: (a) image security, (b) authenticity verification, (Source: Rey and Dugelay, 2002).

3.4.2 Digital image hashing

Frequently, the issues of data integrity can be solved using cryptographic hashes or message authentication functions, which are sensitive and key-dependent to every bit of the input message. As a result, the integrity of the message could be confirmed if every bit of the message is unchanged. Nonetheless, multimedia data can permit for lossy representations with small modification. Information carried by media data is commonly retained even after suffering geometric distortion, level of filtering, or noise corruption. Consequently, bit-by-bit verification is not a suitable technique to authenticate multimedia data (Swaminathan *et al.*, 2006). One scheme that might be useful for digital multimedia authentication is the multimedia hash. This approach is a content-based digital signature for the media data. In order to generate a multimedia hash, a private key is utilized to obtain specific features from the data. The hash can be transferred with the media either by embedding within it or by adding it to the main media data. In the testing phase as shown in

figure 3-2 , the authorised customer must have the same key to create the hash values, which will be compared to the ones transferred along with the data to validate its authenticity. The hash function could be applied in numerous applications, for instance identification/searching for images in large databases, content authentication, watermarking, and anti-piracy searches (Yang and Rhee, 2010). The fundamental

techniques for creating image hashing could be categorised into approaches based on statistics information, low-level image feature extraction, relations and preservation of coarse image representation (Monga and Evans, 2006). A robust hash function could be a method for identifying multimedia content. This technique may have same purpose as some watermarking technology, however Monga and Mihçak (2007) reported that, the key difference among a watermark and a digital signature is that the embedding procedure of the watermarking technology requires the content of the media to change. Nevertheless, for content authentication, both the watermark and the multimedia hash methods could be sensitive to any malicious modification of the media while being able to allow incidental modifications, for example image enhancement or JPEG compression. In other words, the hash is necessary to be robust to perceptually insignificant modifications to the image. The hash function could also be applied to improve the security of watermarking schemes in the case of a copy attack. This type of attack targets at estimating a watermark in marked content and transplanting the estimated mark in unmarked content (Celiktutan et al., 2007).

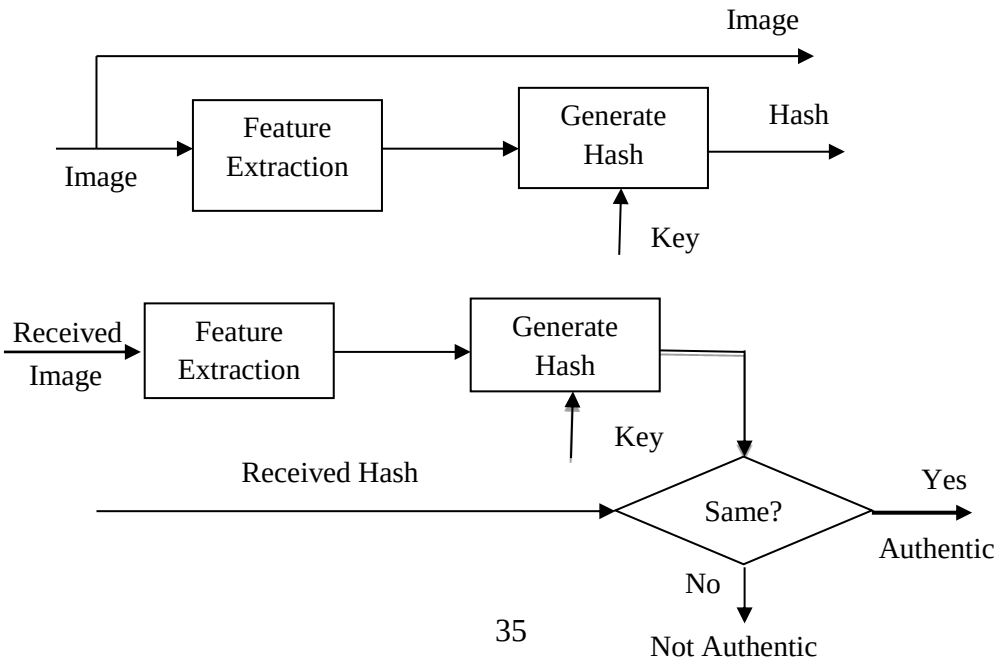

Figure 3-2: Hash functions for Image Authentication. Adopted from (Swaminathan et al., 2006).

3.5 Device characteristics methods

Many people can share their digital content through the Internet for example using an image published on a newspaper web-site, or a video posted on YouTube without adding any secure information. In this situation, active technologies such as watermarking and hashing cannot be applied to prove the content's authenticity or source tracking. In order to overcome the previous issues, recently, novel techniques for authenticating the contents of digital images called passive technologies are developed quickly, that does not require any prior information about the image. These passive methods can rely on the observation at each stage of the image history, from the acquisition process, to its storing in a compressed format, to any post processing process, which may leave a distinctive trace on the data, as a kind of digital fingerprint. For more simplicity, the original digital video or image could have distinguishable patterns because the devices used may have different characteristics due to the specific physical apparatus with different parameters being applied inside these devices which might then make possible diverse patterns in the output. These patterns would remain in all other digital content, which are captured by the same digital devices, or they could be modified after tampering. The passive methods can be used in applications of

image authentication by detecting modifications of the digital image and also as proof of ownership by identifying of the image's source (Zimba and Xingming, 2011).

3.5.1 Techniques for identifying the origin of the image

Generally, most approaches of device identification are concentrated on evaluating the origin of digital media (videos or images).

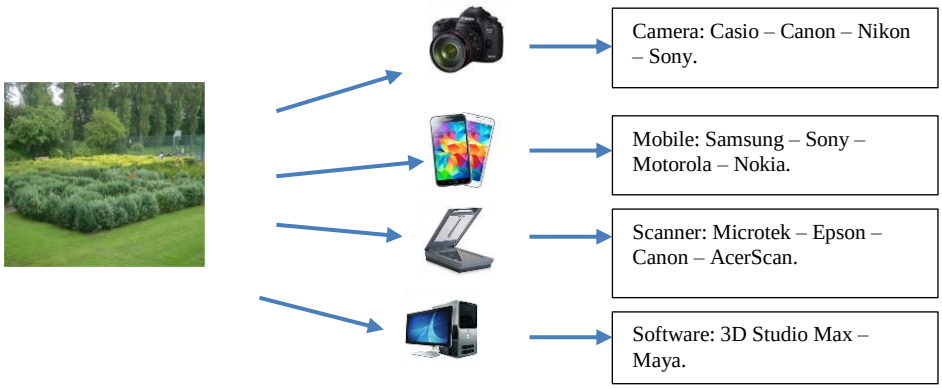

Figure 3-3 The source identification problem.

As shown in figure 3-3 , such an identification can be performed in two main stages. The purpose of the first stage is to determine which type of digital device has produced those digital media (e.g. a digital camera, a cell-phone, a scanner and so on) and the second stage then determines the model and brand of a scanner or camera that was used to acquire the image. Several techniques for source camera identification are discussed in the following sections.

3.5.1.1 Exchangeable image file

Digital images could be saved in several formats, for example JPEG, GIF, PNG, TIFF, and RAW, which may include useful information. For instance, JPEG files may include a specific feature that contains metadata such as quantization tables for lossy compressed data and image compression (Cohen, 2007). One of the simplest solutions to identify the source of a digital image is by checking the Exchangeable Image File (EXIF) header. This is a standard that classifies the formats of video images and includes information in the header of the image such as the model of digital camera, the manufacturer, the size of the image and exposure time. If the settings of an enquiry image do not match those of a given camera, it can be determined that the image did not come from that camera or that did not produce the original image. However, it is not possible to discriminate among images from instances of the same model of camera, since these images contain the same header information. Furthermore, the header information could be simply changed by JPEG recompression or any other image editing software (Luo *et al.*, 2007). This may limit the use of this approach in image source identification and forgery detection. Furthermore, such an editable information cannot be accepted in the courtroom as evidence.

3.5.1.2 Colour filter array and demosaicing artifacts

Generally, the sensor is the key element in a digital camera, and, due to cost considerations, many manufacturers set up a single sensor rather than using multiple sensors. In order to capture a colour scene, the CFA is permanently utilized in front of the sensor. As each sensor pixel obtains only a colour value, the other two pixels need to be estimated from other pixels. This estimation procedure is known as interpolation or demosaicing. Based on CFA demosaicing, numerous image forensics approaches

are applied for both source identification and forgery detection problems. Such colour interpolation could present correlations among the samples of a colour image, while the non-interpolated would be unlikely to be correlated in a similar manner as the interpolated samples. In other words, the main idea is that the CFA filter design and the interpolation algorithm for every manufacturer may be slightly dissimilar; this may lead to unique correlation structures in captured images (Bayram *et al.*, 2005). Another approach which relies on the observation that the demosaicing algorithm and the size of interpolation kernel can differ from one digital camera model to another has been suggested by (Bayram *et al.*, 2005) and (2006). Identification the source of a digital image is based on the estimation of the colour interpolation parameters applied by the camera. Such an approach could be limited to pictures that are not highly compressed because the compression artifacts can remove and suppress correlation among the pixels which are generated by the CFA interpolation. As no a priori knowledge could be available about the size of the interpolation kernel, probability maps could be used to obtain different sizes of kernels. Once observed in the frequency domain, these probability maps can show peaks at different frequencies with differing magnitudes representing the structure of correlation among the spatial samples. A support vector machine (SVM) classifier was then applied to test the efficiency of the proposed approach. The SVM classifier relied on two sets of features: the peak locations and magnitudes in the frequency spectrum, and the set of weighting coefficients used for interpolation (Khanna, 2009). A related method based on a linear model for the periodic correlations presented by CFA interpolation was proposed by Popescu and Farid (2005). They hypothesised that every interpolated pixel can be correlated with a weighted sum of pixels by using a small neighbourhood concentrated around itself.

While perhaps exceedingly simplistic when compared to the highly nonlinear nature of CFA interpolation procedures, this simple model can be easy to parameterize and could reasonably estimate the CFA interpolation algorithms. It is worth noting that the majority of CFA algorithms estimate a missing colour sample from neighbouring samples from all colour channels (Swaminathan *et al.*, 2007). However, Khanna (2009) reported that this method disregards these inter-channel correlations and considers each colour channel separately. In practice, neither the particular form of the correlations (that is, the parameters of the linear model) nor which samples are correlated to their neighbours is known. In order to approximate both of these concurrently, the Expectation Maximization (EM) algorithm is utilized as proposed by Dempster *et al.* (1977) .

3.5.1.3 Lens Aberration

As a result of the design and manufacturing process, lenses could produce diverse kinds of aberrations in pictures; therefore, the output picture could be distorted to a certain degree. In other words, the characteristics of optical distortions in digital output from most digital cameras may not change by usage and time. Two of these aberrations have been used in source camera identification: chromatic aberration and lens radial distortion. Examples of such distortions are shown in figure 3-4. With the aim to decrease manufacturing cost, the majority of digital cameras are provided with lenses may have nearly spherical surfaces which create radial distortions.

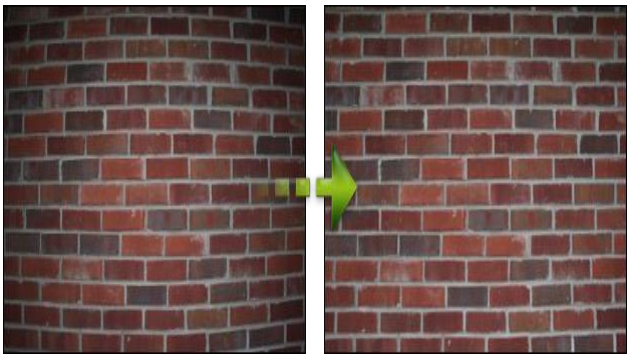

(a) (b)

(a) barrel distortion; (b) after removing the barrel distortion

(c) (d)

(c) chromatic aberration; (d) after removing the chromatic aberration

Figure 3-4 Lens distortion

Radial distortion can cause straight lines in the object space to be rendered as curved lines on the sensor. This happens after changes in transverse magnification with rising distance from the optical axis; this type of distortion is also known as barrel distortion (San Choi *et al.*, 2006). The amount and order of compensation of the radial distortion can be different from one manufacturer to another. Consequently, lenses from different camera model may leave unique traces on the captured pictures. The key idea of this forensics methodology is based on obtaining the distortion parameters of a specific camera, and then evaluating the error among the distorted line segments and the corresponding straight lines. The estimated parameters can be applied to train a classifier to distinguish between digital images captured by different cameras (San Choi *et al.*, 2006). Another kind of optical distortion, that of chromatic aberration, has been used to detect image tampering and in camera identification applications (Johnson and Farid, 2006); (Dirik *et al.*, 2007); (Van *et al.*, 2007). This distortion can be produced by various refractive indications of a lens to different colours (wavelengths of the incident light). As a result of such differences, every colour in the incident light could focus on a dissimilar point on the camera's lens axis, producing

colour edges and minor shifts among colour channels. Because diverse kinds of lenses could cause dissimilar distortions in images, source camera identification could be achieved by estimating the distorted parameters from images with lens aberrations (Johnson and Farid, 2006). Nevertheless, this approach might be failed for computing radial distortion, in case of a non-appearance of straight lines in the image; also as shown in figure 3-4, it is likely to correct any radial distortion on pictures using some editing software. Moreover, this approach has not been assessed using two cameras of same camera model (Dirik, 2010).

3.5.1.4 Image features

Several image features can be applied to classifying a camera according to a model, such as: wavelet domain statistics, colour features, and image quality metrics. The image feature approach has been utilized for *N* images from two different cameras models, where a number of images were used for training and testing the classifier. The accuracy for such algorithm reaches 98.73% for uncompressed images and dropped to 93.42% for compressed images. When five digital cameras were used, the identification rate has been reduced to 88% (Kharrazi *et al.*, 2004) . Nonetheless, this approach could fail with cameras sharing the same CCDs and is not very useful for identifying images captured from cameras of the similar models. Furthermore, the use of this approach requires that all images should be captured at the same resolution with same content, which will usually not be possible in practice (Tran Van *et al.*, 2007). Moreover, the large sample of pictures required in order to train a classifier for every digital camera is unlikely to available (Khanna, 2009) .

3.5.1.5 Sensor imperfections

Additional approaches for source camera identification are based on characterising the imaging sensor. Geradts *et al.* (2001) considered that some pixels in the CCD sensor could be defective especially in low-cost digital cameras. These defects could include point defects, hot point defects, dead pixels, pixel traps, and cluster defects. These defect pixels might be in different places of the CCD sensor relying on the diverse sensors; consequently, such pixel defects can be considered to be unique evidence to identify the digital cameras. Nevertheless, according to Tran Van *et al.* (2007) the pixel defects may be visible only in darker regions of images and might also depend on temperature. Moreover, a number of post-processing processes such as gamma correction, JPEG compression and enhancement might remove or suppress these defective pixels. Besides, there may not be any visible defective pixels in digital cameras with high CCDs; thus, this technique cannot be applied with all digital cameras. Lukas *et al.* (2006) developed a source camera identification system based on a unique sensor pattern noise. This PRNU is unique for both CCD and CMOS imaging sensors. There are several sources of noise and imperfections that occur at different stages of the image acquisition procedure. Even if the image sensor takes an image of a completely evenly lit scene, the digital image may include slight alterations in intensity between pixels. This is partly caused by random factors, such as, readout noise or shot noise, and partly as a result of pattern noise. Imaging sensor noise could normally be considered as random noise and pattern noise. The former can be named by statistical models, as it changes from frame to another and is temporally random in nature. In contrast, pattern noise can generate a pattern in the spatial domain and does not alter

from one frame to another to any great extent. Therefore, pattern noise may not be suppressed by frame averaging, whereas the random noise would be. As illustrated in figure 3-5, sensor pattern noise can consist of two parts, which are fixed pattern noise (FPN) and photo-response non-uniformity noise (PRNU). The FPN is a result of dark currents and normally occurs with sensors where specific pixels are exposed to give brighter intensities rather than the common noise. The FPN could rely on exposure and hotness and denotes to pixels-to-pixels differences. PRNU, on the other hand, is the key component of the pattern noise of standard images, and is based primarily on pixel non-uniformity (PNU), which can be defined as the dissimilar sensitivity of pixels to light. PNU is the result of imperfections caused by the manufacturing process due to the lack of homogeneity of the silicon area in the imaging sensor (Janesick, 2001). The origins and characteristics of PNU noise make it unlikely that even sensors from similar wafers would exhibit similar PNU patterns. PNU is more likely to be stable over time and may not depend on temperature. The PNU is a main characteristic (fingerprint) for both CMOS and CCD sensors and it is the basis of powerful methods to check the integrity of images and for camera identification. Furthermore, several low-frequency components such as light refraction and zoom settings, as well as optical surfaces may contribute to PRNU noise. These components are not characteristic of the sensor (Lukas *et al.*, 2006). Fridrich (2009b) reported that PNU could include significant properties which are necessary in order to treat a PRNU as a unique sensor fingerprint. Firstly, dimensionality which means that the fingerprint include a massive amount of information content making it dissimilar to all sensors.

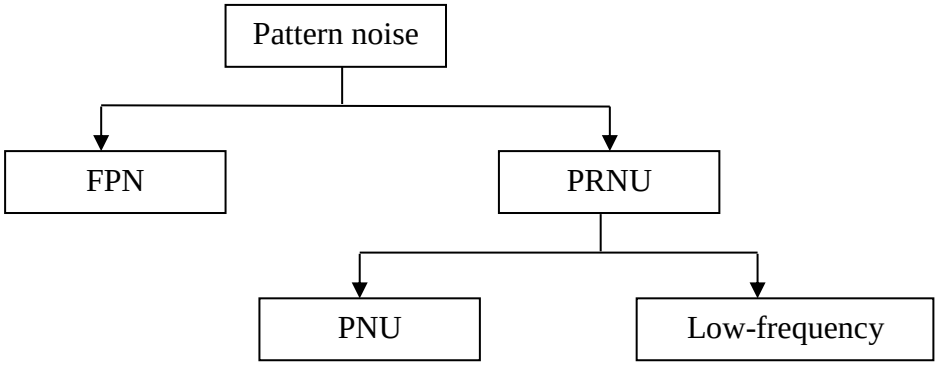

Figure 3-5 Pattern noise in CCD sensor.

Additionally, PRNU could exist in most pictures regardless of the digital camera settings, camera lens, or scene content. Furthermore, PRNU is stable over time under a variety of environmental conditions and finally, it is not affected by gamma correction, lossy compression or other post-processing procedures. Fridrich (2009b) suggested that PRNU may be utilized in image forensics tasks in numerous ways. Firstly, it could be applied in order to verify the presence of an individual digital camera's fingerprint in the image. Furthermore, there is possibility of identifying forged objects by determining the non-appearance of the PRNU in specific regions of the digital image. Additionally, certain aspects of the processing history of an image might be reconstructed; for instance, the digital camera fingerprint can be applied as a template in order to estimate geometrical processing such as scaling or rotation. Finally, PRNU is beneficial for determining the particular make of camera or differentiating among a scanned and digital camera images (Fridrich, 2009a). The issue of image origin based on PRNU has been addressed in the literature using different techniques, for instance in the works of (Lukas *et al.*, 2006), (Chen *et al.*, 2007), (Sutcu *et al.*, 2007), (Li, 2010), (Kang *et al.*, 2011), and (Hu *et al.*, 2015). Moreover, Dirik *et al.* (2008) suggested another type of sensor imperfection which could be used to identify the source digital

camera. This approach relies on traces of sensor dust in digital single lens reflex (DSLR) which permit customers to exchange camera lenses. In such kind of cameras, lens interchangeability may lead to a major issue that the environmental dust or dirt might attract in front of the sensor and generate a unique pattern which degrades the image quality. Such a natural sensor dust pattern could be used for unique source device identification. Dust specks can be detected by measuring intensity variations and shape features to form the dust pattern of the DSLR camera. Their experimental results illustrated that the dust pattern could be applied to identify the source camera model with low false positive rates. However, this approach strongly depends on the lens settings and image content, which means that these device characteristics are less suitable for general purpose forensics analysis. Moreover, this method could anyway have limited use in image forensics since this dust could be removed by cleaning the sensor surface. In addition, this approach would only be suitable for images captured from DSLR cameras and it has not yet been assessed using two of the same camera model. In addition, PRNU has been also applied in scanner identifications in (Gloe *et al.*, 2007) and (Khanna *et al.*, 2007b).

3.5.2 Techniques for assessing image integrity

Even though digital cameras can offer a simple and efficient way of taking and saving digital image of daily activities as digital images, such images may be simply amended by using some image editing software such as Photoshop, GIMP, and Paint Shop. Tampering with digital images without leaving any clear trace might no longer be difficult job. In general, picture modification may not display evidence of malicious tampering as in cases of contrast or colour correction to enhance the image and file

format adaptation in order to save storage space. Such manipulations would generally not amend the content of the image, while a malicious attack can change the meaning of the image, for instance by modifying, removing or inserting an object (Redi *et al.*, 2011). Numerous techniques can be exploited for image forgery detection. For instance, Hany (2006) applied JPEG quantization tables for forgery detection. Digital cameras normally usage JPEG compression in order to encode images; such types of lossy compression can use a quantization table to control the degree of compression. Many companies construct their digital devices with different compression parameters and levels, and such modifications can be applied in order to authenticate images by obtaining the JPGE quantization table from an image and comparing it with a database of identified digital camera models. This procedure can lead to identify the source of the image; similarly; a comparison could be conducted with a database of photo-editing software to recognize the integrity of the image. Therefore, by identifying the presence of JPEG quantization tables unique for particular photo-editing software, one could determine whether the image is authentic or has been modified and saved using particular photo-editing software (Farid, 2008). Another technique which can be used for integrity verification based on illuminating light was offered by Johnson and Farid (2005). This method discovers inconsistencies in the direction of the illuminating light source for each object in an image using a two dimensional model. The method can test three different states which are local, infinite and multiple light sources to identify the error in the estimated direction linked to the actual direction. This approach would be effective for determining contradictory evidence in light directions. Nevertheless, analysis using this method could be very complex in case of indoor images with several light sources, due to multiple occluding boundaries. Moreover, it may be

expected that such an algorithm would be more successful for outdoor images since the sun is normally the only light source. Further technique proposed by Fridrich *et al.* (2003) relies on the detection of a copy-move attack which is a specific type of forgery where an object in an image can be duplicated in another area in the same image. This idea was used for uncompressed images, matching between blocks of size $B \times B$ in order to detect precise replicas. A robust matching method using quantized DCT is applied to enhance the method for the JPEG format, instead of direct matching of the pixel representation for every $B \times B$ block. While experiments are more likely to perform well with the copied and pasted areas, the algorithm could fail to identify some areas which are flat, uniform areas, such as the sky (Swaminathan *et al.*, 2009). Other techniques can be applied for forgery detection by reviewing the inconsistency of lateral chromatic aberrations throughout a digital image. The lateral chromatic aberration is considered as the contraction of a colour channel in relation to each other, which results in a colour channel's misalignment. The technique's parameters are designed to readjust the colour channels dependent on shared data which is applied for quantifying the alignment. Johnson and Farid (2006) reported that, one of the disadvantages of this technique is that it could be difficult to estimate chromatic aberration from a block which has a little or no spatial frequency content. This suggests that the method may be doubtful to discover areas of the image that have little spatial frequency. One further possible technique for identifying image forgery is based on the camera response function (CRF) and geometry invariants. The idea behind the technique of Hsu and Chang (2006) is to detect image splicing by examining for irregularities in the CRFs. This system was examined only for BMP or RAW image formats. The accuracy of such a technique is probable to be highest for

just the uncompressed images. Furthermore, spliced images generated from the same digital camera may not be recognized as forgeries (Van Lanh *et al.*, 2007) . Moreover, the PRNU has been used as a camera fingerprint in order to detect forged areas with an image. The idea is that the tampered areas could destroy or change position of the PRNU(Chen *et al.*, 2008). There are several Image forgery detection techniques in the literature which rely on PRNU such as the works of (Lukáš *et al.*, 2006), (Chen *et al.*, 2008), (Chierchia *et al.*, 2010), (Chierchia *et al.*, 2013) and (Chierchia *et al.*, 2014), each one has its theory, based on type of manipulation. More recently, the PRNU has been applied to detect forgeries produced by Hue modification (Hou and Lee, 2016).

3.6 Methodologies based on PRNU estimation

Many researchers have verified the reliability of PRNU as a unique component for digital image forensics analysis, In particular, Goljan *et al.* (2009) conducted an extensive experiment examining over one million digital images covering 6896 cameras and 150 camera models. Due to the promising outcomes with PRNU fingerprints, many research groups have paid attention in the past decade for improving PRNU estimation. Nevertheless, the effectiveness of PRNU in forensics applications relies heavily on the quality of the estimation of such weak signal. In this section, all the techniques proposed in the literature based on PRNU estimation procedure are reviewed. Lukas *et al.* (2006) was the first to develop a common technique to estimate a camera's reference PRNU in order to resolve the problem of source camera identification. In order to obtain a trustworthy estimation of PRNU (K), the digital camera itself or a number of images taken by the camera sensor is required. Let us assume that N denotes the number of available images. As demonstrated in

figure 3-6 , the first step is to separate each original image from its noise, by obtaining a de-noised version of the original image (**I**). According to Lukáš *et al.* (2005), the best performance is achieved when a wavelet de-noising filter, as proposed in the work of Mihcak *et al.* (1999), is used to obtain a filtered version of (**I**). After that, the residue noise is calculated by subtracting the original image from denoised version of the image$F(\mathbf{I})$:

$$\widehat{\mathbf{R}} = \mathbf{I} - \mathrm{F}(\mathbf{I}) \qquad 3.1$$

It is worth noting that, the residue noise as shown in equation 3.1 could include random noise from other sources and image content contamination, which cannot be exploited in source camera identification. Therefore, with the purpose of improving the purity of the estimated PRNU, the estimated residue signals ($\widehat{\mathrm{R}}$) of a number of images taken by the same camera sensor are averaged as shown in equation 3.2. This technique is referred to as "basic-PRNU" in the rest of this thesis.

$$\mathbf{K} = \frac{\sum_{i=1}^{N} \hat{R}}{N} \qquad 3.2$$

In the detection stage, in order to determine if the camera fingerprint (K) is present in tested image (I), the residue signal is estimated as shown in equation 3.1 for each image. Then, a similarity measurement such as normal correction can be applied, for instance to assess the similarity between the sensor fingerprint for camera *C* and the residue signal of the tested image.

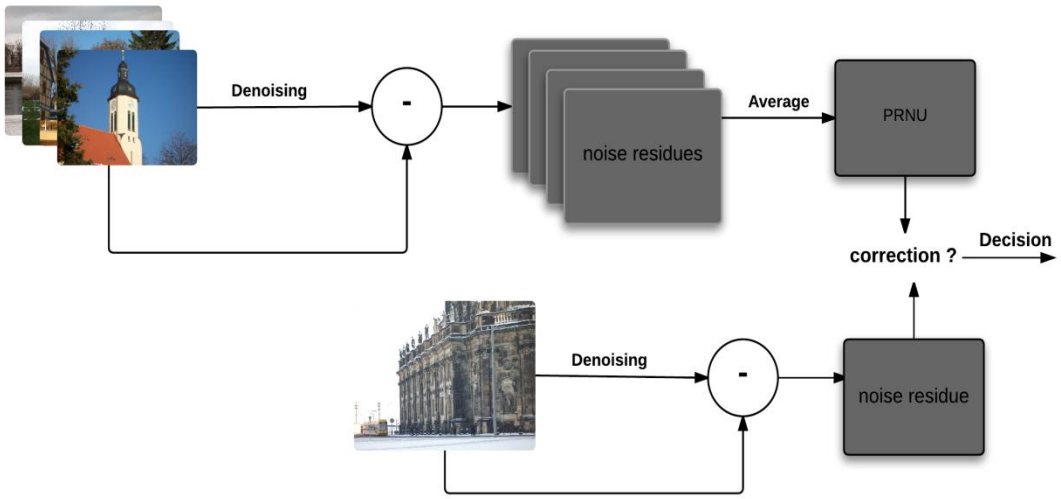

Figure 3-6 PRNU estimation process.

The final step is to compare the value of similarity (p) with a threshold (t) for this camera. If $p > \mathrm{t}$, the system will identify that the query image was taken by camera C. Chen *et al.* (2007) introduced the maximum likelihood estimator (MLE) to estimate the camera's reference PRNU. The authors demonstrated the residue noise as $\hat{\mathrm{r}} = \mathrm{I}_0\mathrm{K} - \Theta$, where Θ is a combination of image contamination and random noise. Such noise could be non-stationary in textured regions; and hence digital images with smooth areas (blue sky images) can help to achieve better PRNU. This method is based on the assuming that $\theta_\mathrm{i}(\mathrm{m},\mathrm{n})$, $i = 1, \ldots, L$, is white Gaussian noise with a fixed variance. The maximum likelihood estimator of the PRNU can be written as:

$$\widehat{K} = \frac{\sum_{i=1}^{N} \mathbf{R}_i . \mathbf{I}_i}{\sum_{i=1}^{N} (\mathbf{I}_i)^2} \qquad 3.3$$

Even if the PRNU is unique to the sensor, there are some components that could be shared between cameras with the same sensor design or those of a similar brand. Therefore this similarity might lead to an increase in false identification rates and some

detection errors in integrity verification. Therefore, enhancement operations is proposed in the work of Chen *et al.* (2008) to remove particular systematic patterns, in order to improve the quality of PRNU estimation. The steps in removing shared components (RSC) can be summarized as follows. Firstly, a zero-mean operation is applied, which could be done by subtracting the column average from each pixel in the column and after that the row average is subtracted from every pixel in the row. These two steps aim to reduce the effect of colour interpolation, row-wise and column-wise operations of processing circuits and sensors. The final step is to transform the signal into the Fourier domain, filter it with the Wiener filter, and retain only noise component. This approach is referred to as MLE-PRNU in rest of this thesis. However, according to evaluation of Liu *et al.* (2015), there is no great difference among using by MLE-PRNU and constant basic PRNU is case of using flat field images (images of almost constant intensity). Moreover, another enhancement technique was proposed by Kang *et al.* (2012), who assumed that the camera's reference PRNU is a white noise signal to remove non-unique components in PRNU. The noise residue is extracted from an image as illustrated in equation 3.1. In order to clear the noise residue from the image contents and colour interpolation, and sensor design, as shown in equation 3.4 and 3.5, the noise residue R_j is whitened first in the frequency domain and it has constant Fourier magnitude coefficients, except that its direct current Fourier coefficient equals zero. Next, they obtained the phase-only component:

$$\mathbf{R}_j = \mathrm{DFT}(\mathbf{R}_j) \tag{3.4}$$

$$\mathbf{R}_{\varphi j} = \mathbf{R}_j / |\mathbf{R}_j| \tag{3.5}$$

In this technique, the camera reference PRNU is computed by:

$$\widehat{K} = \text{real}\left(\text{IDFT}\left(\frac{\sum_{j=1}^{N} R_{\varphi j}}{N}\right)\right) \qquad 3.6$$

In the rest of this thesis the approach of Kang *et al.* (2012) will be called phase-PRNU. Li (2010) pointed out that the PRNU gained from a picture may be contaminated by the image content; for example, with a periodic structure and texture. This idea is based on the fact that less trustworthy components are the stronger components of the signal in a PRNU, and therefore these components should be attenuated. Combined with a wavelet filter, this proposal offers an improved PRNU by allocating lower weighting factors to the strong components of *R* in the wavelet domain, with the intention of suppressing contamination by scene details. Nonetheless, attenuating strong components from a signal can lead to an attenuation of the beneficial PRNU components as well (Kang *et al.*, 2012). Moreover, Hu *et al.* (2009) proposed another improved technique based on the assumption that the large components of a camera's PRNU is more trustworthy and consequently should be utilized in correlation detection, whereas other elements should be discarded. The authors sorted the PRNU pixels in a descending order, and then only the first largest components are used while ignoring the rest of the reference PRNU. At the same time, the positions of those large components are saved in order to be used with the estimated noise residue of the tested image. Another technique relying on the pairwise magnitude relations of cluster pairs was proposed by Tomioka *et al.* (2013). This approach aims to suppress the random noise contamination in the PRNU, and is achieved by calculating the PRNU as shown in equation 3.2. After that, the PRNU pixels are sorted a descending/ascending order. Next, every set of pixels is simply averaged. With the clustered PRNU, a record of the positions of the clustered pixels is saved and used in the noise residue of the tested

image. Theoretically, such a procedure might generate a higher quality reduced-size PRNU, which may lead to a more trustworthy PRNU than the original full-size counterpart (Tomioka and Kitazawa, 2011). Furthermore, the principal component analysis (PCA) technique was employed by Li *et al.* (2014) in order to decrease the dimensionality of the PRNU noise and reduce the effect of scene details during the filtering process. The idea underlying this technique is that the energy of the noise residues characterizing the reference PRNU could be concentrated in a small subspace of the entire eigenspace, while the remaining energy represents undesirable (image-dependent) noise components. Hence, by maintaining only the most significant subspace, characterized by the eigenvectors which are linked to the most significant eigenvalues, and then conducting the inverse PCA transform, the image-dependent noise could be significantly decreased. With the aim to reduce the burden some aspects of storage and computation of the PRNU signal, particularly with a large size of images, Valsesia *et al.* (2015) indicated that the usage of random projections could considerably decrease the dimensionality of PRNU without any effect on camera identification performance. The PRNU signal may not be compressed with regular approaches, for example JPEG, due to the signal's lack of redundancy. Valsesia *et al.* (2015) applied a compressive sensing technique to represent the sensor fingerprint space using a dictionary. This technique starts by representing the PRNU in a binary-quantization form, which may lead to a considerable reduction of the matching process. An additional universal study in fingerprint compression linked to random projection can be found in the work of (Donoho, 2006). Moreover, Chang-Tsun and Yue (2012) suggested a colour decoupling process before the filtering stage in order to decrease colour interpolation noise which was presented by the CFA. This process is based on

the fact that the artificial colours gained during the demosaicing process could not be physically captured from the scene by the sensor. Consequently, Chang-Tsun and Yue (2012) claimed that the PRNU obtained from the physical components would be more trustworthy. This can be achieved by decomposing every image into sub-images and after that extracting the PRNU from each sub-image. Finally, the PRNU of the sub-images can be combined in order to gain the final PRNU. This technique is called CD PRNU in the rest of this thesis. Another novel pre-processing technique, namely spectrum equalization algorithm, was suggested by Lin and Li (2016) in order to reduce the false identification rate. The authors equalize the magnitude spectrum of the PRNU by detecting and suppressing notable peaks according to the local characteristics, since peaks in the spectrum could be created by periodic artifacts which are unlikely to be linked to the true PRNU. Then, the similarity measure with the tested noise residue is applied. Moreover, three colour combination schemes were proposed by Hu *et al.* (2010) in order to obtain the final PRNU using the red, green and blue channels. The key idea is based on extracting the PRNU from each colour channel separately and then selecting the pixel with the largest magnitude.

3.7 PRNU de-noising techniques

A number of de-noising techniques have been reported in the literature in the PRNU estimation stage. This section examines the strengths and weaknesses of some of these denoising methods in estimating the PRNU. Lukas *et al.* (2006) firstly utilized a wavelet-based filter for identifying the source of digital images based on PRNU, and this filter had initially been suggested by Mihcak *et al.* (1999). Lukas *et al.* (2006) assessed a number of de-noising filters and their experimental results have shown that

wavelet-based filter can outperform other filters, such as Wiener filters and median filters. For image restoration and enhancement applications, it is common to use criteria such as the mean squared error or peak signal-to-noise ratio, in order to examine a filter's noise reduction performance. Wavelet-based denoising performs well by using the above criteria and it has been recommended by researchers for better PRNU extraction (Cooper, 2013). This filter can be divided into two phases. Firstly, the variance in local image is estimated; and secondly, a local wiener filter is applied in order to obtain an estimation of the denoised images in wavelet domain. The wavelet de-noising filter operates as follows. First of all, the fourth-level wavelet decomposition of the noisy image is analysed by a breakdown of the noisy images into 8-tap Daubechies mirror filters. The diagonal, horizontal, and vertical subbands are dented as $d(i,j), h(i,j), v(i,j)$ where $(i,j) \in J$, and J is the set of the wavelets coefficient, which could depend on the level of decomposition. The de-noised wavelet coefficients could be obtained using the Wiener filter as follows

$$h_{den}(i,j) \coloneqq h(i,j)\frac{\hat{\sigma}^2(i,j)}{\hat{\sigma}^2(i,j)+\sigma_0^2} \qquad 3.7$$

where $\hat{\sigma}^2(i,j)$ respresents the estimated local variance for the wavelet coefficient of the original image $\mathbf{I}^{(0)}$ (the sensor output in the absence of the PRNU noise), which could be estimated by using the maximum a posteriori probability (MAP) method for each subband:

$$\hat{\boldsymbol{\sigma}}^2{}_W(i,j) = \max\left(0, \frac{1}{w^2}\sum_{(i,j)\in N} h^2(i,j) - \sigma_0^2\right) \qquad 3.8$$

where $w \times w$ is the size of the window, and it is suggested that w should be a set of (3, 5, 7, and 9). After that, the minimum of the four variances can be applied in equation 3.7. Lukas *et al.* (2006) pointed out that the value of σ_0 may have a slight effect on the performance of the filter in PRNU estimation, and the authors found that the best filter performance was achieved when σ_0 is equal to 5. Another filter based on a four neighbour context adaptive interpolation (CAI4) algorithm was proposed by Guangdong *et al.* (2012). The same authors (2014) extended their algorithm so as to be based on an eight-neighbours (CAI8) to better suppress the interference of the image edge and for less prediction error. This approach targets the identification of edges and to generate a pure sensor pattern noise. In this technique, the local regions have been classified into six classes: smooth, vertically edged, horizontally edged, right-diagonal edge, left-diagonal edge, and others. A mean filter can be applied to estimate the centre value pixel of the eight neighbouring pixels in the smooth regions.

wn	***n***	***En***
w	***P***	***E***
ws	***s***	***Es***

Figure 3-7 Neighbourhood of the centre pixel to be predicted.

In edge regions the centre pixel is predicted along the edge. In other regions, median filtering could be used. Assuming that P is the centre-pixel value and as shown in figure 3-7, $\mathrm{T} = [\mathrm{n}, \mathrm{s}, \mathrm{e}, \mathrm{w}, \mathrm{en}, \mathrm{es}, \mathrm{wn}, \mathrm{ws}]'$ to be a vector of the eight-neighbouring pixels. The centre pixel value is given by:

$$\hat{p} = \begin{cases} mean(\acute{T}) & (\max(\acute{T}) - min(\acute{T}) \leq 20 \\ (n+s)/2 & (|e-w| - |n-s| > 20) \\ (e+w)/2 & (|n-s| - |e-w| > 20) \\ (es+wn)/2 & (|en-ws| - |es-wn| > 20) \\ (en+ws)/2 & (|es-wn| - |en-ws| > 20) \\ median(\acute{T}) & (otherwise). \end{cases} \quad 3.9$$

After that the Weiner filtering operation at the pixel domain is used in order to remove the influence of the image scene. However, this technique could be unsuccessful for PRNU estimation with small natural images, and Guangdong *et al.* (2012) recommend the use of more than 150 blue sky images for efficient PRNU extraction. Consequently, the usage of such a technique in image forensics may be limited. An additional novel filtering strategy based on a combination of adaptive and median filtering applied in the spatial domain was suggested by Cooper (2013). The author divided the approach to two stages. In the first stage, adaptive Weiner filtering as proposed by Jong-Sen (1980) is applied in the spatial domain:

$$\mathrm{F}(\mathrm{I_{ij}}) = \mathrm{u} + \frac{\sigma^2}{\sigma^2 + \mathrm{v}^2}(\mathrm{I_{ij}}) - \mathrm{u} \quad 3.10$$

where $\mathrm{v}^2, \mathrm{u}, \sigma^2$ denotes the noise variance ,mean , and the variance around the local neighbourhood of each pixel respectively.

$$\mathrm{u} = \frac{1}{NM} \sum_{ij \in B} I_{ij} \quad 3.11$$

$$\sigma^2 = \frac{1}{NM} \sum_{ij \in B} I_{ij}^2 - u^2 \quad 3.12$$

where $N \times M$ is the pixel-size of the window B, which is recommended to be a window of 9×9 pixels. After that, the output of the Wiener filter is subtracted from the image. In the second stage, the PRNU noise residue is further filtered by two 2×2

median filters in cascade. The median filtering could lead to an increase the correlation magnitude with matching data and decrease the correlation bias for non-matching data (Cooper, 2013). This suggested filtering technique is followed by an enhancement strategy where only pixels with high probabilities of significant PRNU noise residue bias are retained. Nonetheless, smaller digital images frequently have less PRNU data, and therefore identification performance for small digital images needs to be improved further. In this technique no experimentation is applied with small images, and also its effectiveness is based on small a sample of data with just three reference cameras. Dabov *et al.* (2007) suggested an image denoising approach relies on an improved sparse representation in the transform domain, and this filter has been applied in PRNU estimation by Chierchia *et al.* (2010) , (2011). The improvement in sparsity can be realised by grouping alike 2D image blocks into 3D data arrays. This filter contains of three successive stages: the 3D transformation of the group, shrinkage of the transform spectrum, and inverse 3D transformation. The outcome is a 3D estimate that contains of the jointly filtered grouped image blocks. By attenuating the noise, the collaborative filtering can detect even the finest details shared by grouped blocks and it also preserves the important features of every block. After that, the filtered blocks can be returned to their original locations. Since these blocks are overlapping, many different estimates can be gained, for each pixel and these should be combined. Combination is a specific averaging process which is used in order to take benefit of this redundancy. van Houten and Geradts (2012) proposed another novel filter to be adopted in PRNU estimation. This filter was originally suggested by Perona and Malik (1990) and it based on the anisotropic diffusion equation. In their discrete form of equation 3.13, $I(m, n, t)$ can be a de-noised version of the original image at iteration

step t while $\mathrm{I}(\mathrm{m},\mathrm{n},0)$ is the original image, and the diffusion coefficient which is chosen to preserve edges and textures could be defined as

$$\frac{\partial \mathbf{I}(\mathrm{m},\mathrm{n},\mathrm{t})}{\partial \mathrm{t}} = \mathrm{I}(\mathrm{m},\mathrm{n},\mathrm{t}+1) - \mathrm{I}(\mathrm{m},\mathrm{n},\mathrm{t}).\,\mathrm{c}(|\nabla \mathbf{I}(\mathrm{m},\mathrm{n},\mathrm{t})|) \qquad 3.13$$

Modern digital cameras can have high sensor pixel density, and it could be expected that two neighbouring pixels may have very close values in images. Al-Ani *et al.* (2015) propose a 2-pixel technique filtering. This technique takes advantage of this observation in spatial domain filtering. It involves as little as one neighbouring pixel during the estimation of the PRNU at a pixel location in order to suppress the unwanted pixel-wise correlation in the estimation stage. An additional filter, called total variation minimization, has been used for PRNU estimation by Gisolf *et al.* (2013). Such a filter can preserve edges while smoothing away noise in flat areas, even at low signal-to-noise ratios (Rudin *et al.*, 1992). The work of Gisolf *et al.* (2013) relied on a simplified version of the total variation filter. The authors applied the unconstrained total variation technique as proposed by Rudin and Osher (1994) and used the gradient-decedent optimization. Moreover ,Qu *et al.* (2013) offered a novel PRNU noise extraction system based on homomorphic filtering. The PRNU is extracted by simply averaging a huge number of pictures, without any de-noising step. This methodology contains three stages: Firstly all natural images are averaged together to obtain one average image. Next, the logarithmic value is taken of each pixel of the average image, and finally the Wiener filter is used to estimate the reference PRNU. The advantage of this process is that it only one image needs to be denoised, while the other approaches require the application of denoising for every image (*N* times). However, when the sample of images is small, such as *N* being less

than or equal to 20, the estimation of the reference PRNU could be deteriorated which may lead to reduced source identification performance compared with the existing state-of the- art systems.

3.8 PRNU similarity measures

Most PRNU-based forensics applications commonly depend on measuring the similarity or dissimilarity among PRNU signals for decision-making. In this section, several similarity measures applied in PRNU-based forensics are outlined due to its close relationship to the techniques studied here. One of the basic measures is the normalized cross-correlation, which is normally conducted between the reference PRNU (K) and the noise residue of the query image (R). The normal correlation is defined as:

$$p(\mathbf{K},\mathbf{R}) = \frac{\sum_m \sum_n (\mathbf{K}_{mn} - \bar{\mathbf{k}}).(\mathbf{R}_{mn} - \bar{\mathbf{R}})}{\sqrt{(\sum_m \sum_{\boldsymbol{n}} (\mathbf{K}_{mn} - \bar{\mathbf{K}})^2)\,(\sum_m \sum_n (\mathbf{R}_{mn} - \bar{\mathbf{R}})^2)}} \qquad 3.14$$

where $\bar{K}$, $\bar{R}$ refer to the means of K, R respectively. Then, with the target of decreasing the effect of periodic noise contamination and hence enhancing the false positive rate in SCI, the peak-to-correlation energy (PCE) was suggested by Goljan (2008). The key idea behind the PCE is to consider the correlations between the PRNU and shifted versions of the noise residue in order to decrease the similarity which could exist between the PRNU of a particular camera and the noise residue of an image taken by a different camera (Goljan, 2008) and (Goljan *et al.*, 2009). As shown in equation 3.15, the PCE ratio is defined as the squared correlation divided by the sample variance of the circular cross-correlations:

$$PCE(x,y) = \frac{c_{xy}^2 \quad (0,0)}{\frac{1}{\omega \times \nu - |A|}\sum_{m_1,m_2 \notin A} c_{xy}^2 \quad (m_1,m_2)} \qquad 3.15$$

where A is a small neighbour area typically of size 11 $\times$ 11 around the central point at (0,0), $|A|$is the number of pixels in A, and $c_{xy} \quad (m_1,m_2)$ represents the circular cross-correlation expressed as

$$c_{xy} \quad (m_1,m_2) = \frac{\sum_{i=0}^{\omega-1}\sum_{j=0}^{\nu-1} x(i,j)y(i \oplus m_1, j \oplus m_2)}{\omega \times \nu} \qquad 3.16$$

where $\oplus$ is the modulo addition.If x and y are contaminated by similar periodic noise which might not be unique for a specific digital camera (Goljan, 2008), the circular cross-correlation $c(m)$ can peak at numerous m values, and hence increase the denominator of PCE and PCE drops, this and may avoid generating a false positive identification. Kang *et al.* (2012) pointed out that, despite the fact that PCE has the benefit to suppress periodic noise; it also may increase the false positive rate due to the squaring operation for $c_{xy}^2 \quad (m_1,m_2)$. Such a squaring operation could convert a negative correlation into a positive PCE value. In order to improve the performance of PCE, Kang *et al.* (2012) suggested the use of correlation over the circular cross-correlation norm (CCN), which can achieve lower false positive rates by as much as a half compared to PCE. The CCN could be expressed as:

$$CCN(x,y) = \frac{c_{xy} \quad (0,0)}{\sqrt{\frac{1}{\omega \times \nu - |A|}\sum_{m_1,m_2 \notin A} c_{xy}^2 \quad (m_1,m_2)}} \qquad 3.17$$

An additional flexible, pixel-wise weighting technique relying on similar features was offered by Chan *et al.* (2013). The calculation of the correlation to identify the source camera could be affected by the image content left behind in the noise residue. To

solve this issue, Chan *et al.* (2013) proposed the application of a nonlinear regression model in order to determine the effect of image content. The impact of image content was considered in block-based manner. Next a confidence map is generated which could be utilized to measure the reliability of every pixel in the PRNU estimation. The aim of using a confidence map in correlation calculations is to decrease the effect of image content since a lower weighting would be given to saturated regions or highly textured regions, while a larger weighting is given to reliable regions. A different similarity measure was proposed by Chen *et al.* (2008) for both camera identification and forgery detection. The authors started by presenting a pixel-wise multiplicative shaping factor $\mathrm{T} \in \mathbb{R}^{\mathrm{M}\times\mathrm{N}}$ and updated their model for $\widehat{\mathrm{R}}$ of the tested image to:

$$\hat{\mathbf{r}}_q = \mathbf{TIK} + \boldsymbol{\theta}, \tag{3.18}$$

where θ is coloured Gaussian noise (a sequence of independent Gaussian variables with unequal variances). In this work the authors divided the noise residue signal into *M* non-overlapping blocks. The pixels (m,n) for every block, $\mathrm{b} = 1, \dots, M$ were assigned a fixed (m,n), and their noise $\theta(\mathrm{m},\mathrm{n})$ was assumed to have a fixed variance σ_{c}^2. A further novel, pixel-wise weighting method based on related features was proposed by Liu *et al.* (2010). The idea of this method based on using only the significant regions of the tested noise residue. The significance of a block can then be measured based on its signal-to-noise ratio (SNR). Other researchers such as Çeliktutan *et al.* (2007),Khanna *et al.* (2007a),Celiktutan *et al.* (2008) and Costa *et al.* (2014) have applied SVM classification systems, instead of using correlation methods in order to identify the source of a digital image.

3.9 Conclusion

The essentials and motivations of digital forensics techniques have been considered in this chapter. The differences between the proactive and passive methodologies are considered, and it is concluded that a passive methodology could be a more efficient approach even if the images are shared through the internet without applying any authentication system. PRNU could be seen as a unique component of images produced by both CCD and CMOS imaging sensors. The key use of PRNU is the detection of forgeries and identification of the source device of an image.

CHAPTER 4 IMAGE SHARPENING for PRNU ESTIMATION

4.1 Introduction

Image enhancement is one of the key areas in the digital image processing field, and involves methods to provide alterations of the pixel intensity of an input image, so that the output picture could subjectively appear to be better (Ibrahim and Kong, 2009). Jain (1989) pointed out that the primary purpose of image enhancement is to improve the visual appearance of digital images by the sharpening of features for instance boundaries and edges. Image sharpening could be useful in many different areas, for example in military, electronic printing and medical imaging system. Enhancement approaches could be applied in the pixel domain by controlling the pixel data or in the frequency domain by adjusting the spectral components. Types of enhancement approaches include: point operations, where every pixel may be amended according to a specific equation which is not dependent on other pixel values; mask operations, where each pixel can be changed based on the values of its neighbours (convolution masks); or global processes where all the pixel values in the image (or sub-image) could be taken into consideration. Image enhancement may involve grey level and contrast manipulation, noise reduction, edge sharpening, filtering, interpolation and magnification, and other operations (Schalkoff, 1989). This chapter examines the performance of Unsharp Masking (UM) technique in order to enhance the source camera identification rate. Edge detectors are discussed in section two, and one of the common methods of image enhancement (UM) is introduced in section three. The

fourth section presents the pre-processing technique proposed in this study, and the relevant data collection and experimental work will be in section five and six respectively. The conclusion is made in section seven.

4.2 Derivative operators

Edge detectors could be seen as a collection of very significant local image pre-processing approaches used to detect changes in the intensity function (Sonka *et al.*, 1999). Several types of operators can be applied for edge detection. Chen *et al.* (1987) reported that based on how the picture has been filtered by image filtering techniques, edge detectors can be categorised in two broad classes, which are first order derivative (gradient) operators and second order derivative operators. Trichili *et al.* (2002) pointed out that derivative operators are the most effective approaches for detecting local intensity variations, where edges could be gained either by extracting the local maximas of the first derivative, or by extracting the zero cross of the Laplacian or the directional second derivative (Trichili *et al.*, 2002). However, such operators may require more computational time, which limits their use in real-time applications (Bhardwaj and Mittal, 2012).

4.2.1 First order derivative

For a first order derivative, an image could be convolved by an adapted mask to produce a gradient image. Most popular operators such as Robert, Sobel, and Prewitt are gradient operators. These operators consider the maximum and minimum intensity values in order to identify edges. As a result of images being two-dimensional, it is essential to take into account the changes in the levels of the x and y directions;

consequently, partial derivatives of the image should be used. Estimating the edge direction can be calculated using the derivatives in x and y, and computing the vector sum. If an image is a function of two variables *A(x, y)* then the gradient is defined as:

$$\nabla A(x,y) = \left(\frac{\partial A}{\partial x} \quad , \quad \frac{\partial A}{\partial y}\right) \tag{4.1}$$

The gradient is a vector which has a magnitude $|grad\ A(x,y)|$ indicating edge strength and gradient direction φ. The gradient magnitude and direction can be calculated respectively as follows:

$$|grad\ A(x,y)| = \sqrt{\left(\frac{\partial A}{\partial x}\right)^2 + \left(\frac{\partial A}{\partial y}\right)^2} \tag{4.2}$$

$$\varphi = \tan^{-1}\left(\frac{\partial A}{\partial y} \Big/ \frac{\partial A}{\partial x}\right) \tag{4.3}$$

As a result of a digital image's discrete function, equations 4.2 and 4.3 are approximated according to differences instead of using derivatives. The first differences of image *A* in the horizontal and vertical directions are shown in equations 4.4 and 4.5

$$\nabla_x A(x,y) = A(x,y) - A(x-n,y) \tag{4.4}$$

$$\nabla_y A(x,y) = A(x,y) - A(x,y-n) \tag{4.5}$$

where n is a small integer, normally equal to 1 (Sonka et al., 1999).

4.2.2 Second order derivative (Laplacian operator)

In the second order derivative, a pixel is indicated as an edge at the location where the second derivative becomes zero. The commonly used operator for the second order derivative is the Laplacian operator ∇^2, which gives the magnitude of gradient only (Kumar and Saxena, 2013). The Laplacian operator is defined in a 2D image *A(x, y)* as:

$$\nabla^2 \mathrm{A(x,y)} = \frac{\partial^2 A(x,y)}{\partial \mathrm{x}^2} + \frac{\partial^2 A(x,y)}{\partial \mathrm{y}^2} \quad 4.6$$

where the second differences of $\frac{\partial^2}{\partial \mathrm{x}^2}$ and $\frac{\partial^2}{\partial \mathrm{y}^2}$ are defined respectively as:

$$\frac{\partial^2}{\partial x^2} = A(x, y+1) - 2A(x,y) + A(x, y-1) \quad 4.7$$

$$\frac{\partial^2}{\partial y^2} = A(x+1, y) - 2A(x,y) + A(x-1, y) \quad 4.8$$

According to equation 4.7 and 4.8 , the discrete approximation of Laplacian can be represented as follows:

$$\nabla^2 A(x,y) = -4A(x,y) + A(x,y+1) + A(x,y-1) + A(x+1,y) + A(x-1,y) \quad 4.9$$

Trichili *et al.* (2002) claimed that the Laplacian approach is more accurate than the gradient approach and it offers additional detail in providing edges. Moreover, it does not depend on direction, and as a result edges will be identified independently of their orientation. Additionally, although the Laplacian technique may respond even more to some edges in the image, it delivers much better performance than gradient operators.(Baxes, 1994)

4.3 Unsharp masking (UM) method.

Popular approaches for image enhancement can generally be cast in two groups: pixel domain and frequency domain techniques. In the former, the gray value of every pixel is modified based on statistical information of the digital image. In the second group, the high frequency components of the image are separated from the low frequency content in two different signals. Each signal is then processed independently, and finally combined to reconstruct the sharpened signal. Unsharp masking (UM) belongs to the second class (Badamchizadeh and Aghagolzadeh, 2004). An unsharp mask is a

technique used to sharpen an image, in contrast to what its name might imply. Unsharp masking could be one of most common types of sharpening and it has been used in the printing industry for making edges more crisp (Jain, 1989). The basic idea behind the unsharp mask is to add a fraction of the high-pass filtered version of the input signal to the original signal itself as shown in figure 4-1. Unsharp masking can powerfully enhance the darker regions of images more than the lighter regions. Nonetheless, it is sensitive to noise since it generally amplifies the high frequency components of the input image which contain a proportion of noise in noisy images (Guillon *et al.*, 1998). Figure 4-2 illustrates the main processes in unsharp masking. Based on this process unsharp masking can be defined as

$$y(m,n) = x(m,n) + \lambda\ z(m,n) \qquad 4.10$$

where $\lambda > 0$ and $z(m,n)$ denote the high pass function. The Laplacian filter is a normally used high pass filter in unsharp masking (Jain, 1989).

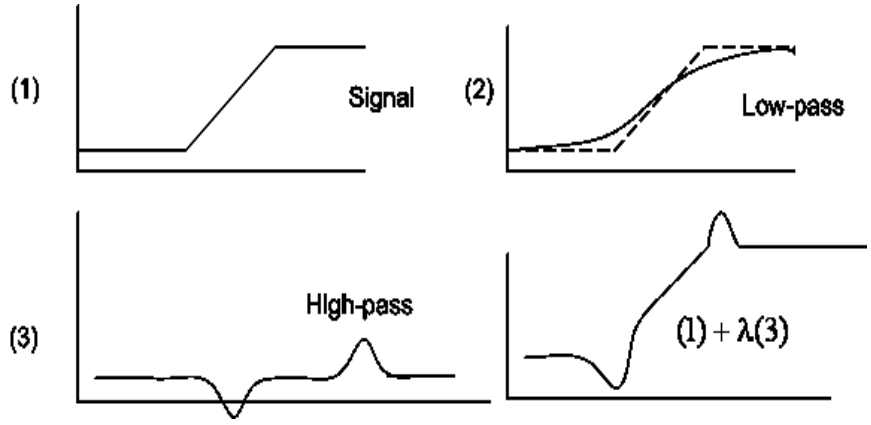

Figure 4-1 Unsharp masking (UM) method (Source: Li, Jain, 1989).

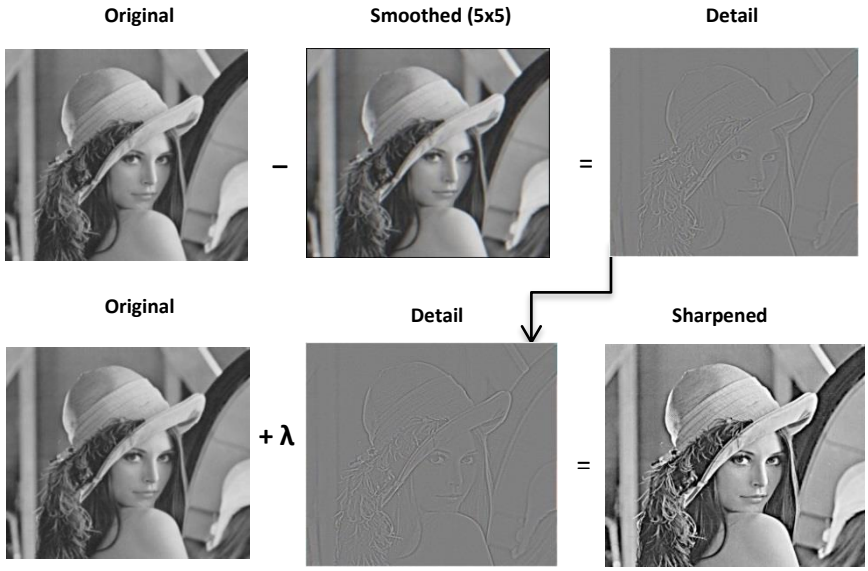

Figure 4-2 Unsharp masking process for image ‘Lena’.

Figure 4-3 shows another example to examine the effect of unsharp masking, on a blurry image (a; b) along with how the unsharp masking can increase noise on noisy images in (c;d).

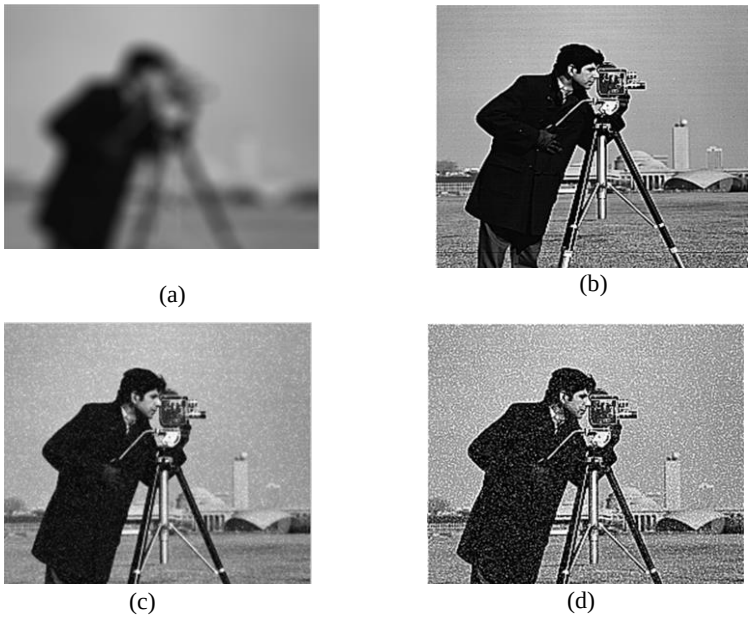

Figure 4-3 Effects of unsharp masking: (a) blurry image; (b) sharpened version of (a); (c) noisy image; (d) sharpened version of (c).

4.4 Proposed pre-processing technique

PRNU estimation depends on the differences among a set of digital images and their smoothened versions in order to capture the characteristics of the sensor. Consequently, such a procedure can use a part of the content of the sensor noise, which is concentrated in the high frequency range, and present in contours, edges and textured regions of the digital images. In this thesis, the unsharp masking method is applied in order to amplify the high frequency content of the PRNU; hence, strengthening its presence in the sample images in order to facilitate efficient source camera identification (Lawgaly et al., 2013). It is worth mentioning that the UM may also amplify a portion of the undesirable noise (i.e. the noise that is different from PRNU) and this may increase the false identification rate. However, note that the undesirable noise changes from an image to another for the same camera because it does not represent the imaging sensor. Under the assumption that the undesirable noise is centred (i.e. with zero mean), the averaging process, described by Equation (3.2), tends to suppress it and keep only the PRNU components.

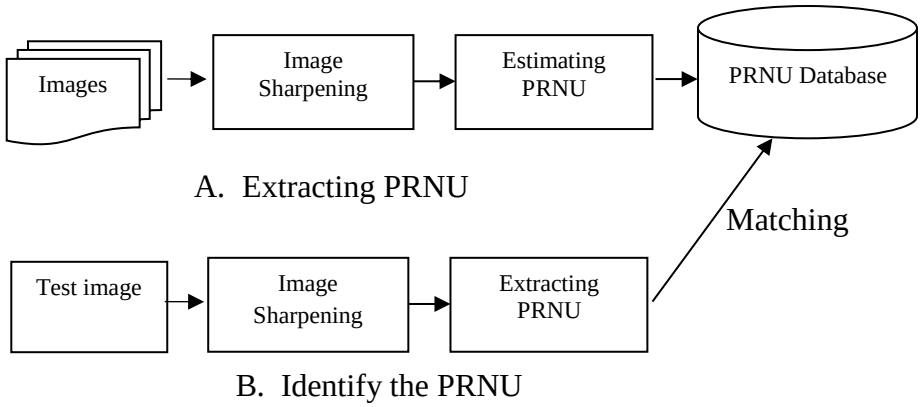

Figure 4-4 High-level of the proposed algorithm.

Figure 4-4**Error! Reference source not found.** demonstrates a diagram of the p roposed scheme. Initially, the image sharpening is exploited with the aim to increase the high frequency content of PRNU noise in digital images. This procedure could

ensure a strong presence of PRNU before estimation. At the matching stage, the same sharpening procedure is carried out for accurate source camera identification.

4.5 Data collection

In order to examine the performance of the proposed technique in this thesis, the evaluation has been conducted using two different datasets: our dataset and the Dresden database (Gloe and Böhme, 2010). Our dataset includes digital images captured from thirteen digital cameras. It should be noted that some digital cameras of the same brand such as Canon IXUS115HS and Fujifilm S2950, numbered 1 and 2 are used to differentiate between them. The technical specifications of these digital cameras are given in Table 4.1. Samples of natural indoor and outdoor scenes in our dataset are shown in figure 4-5. Table 4.2 shows the technical properties of digital cameras used for the Dresden database. From this, the ten digital cameras which have the largest numbers of images are chosen to provide a greater number of images in the testing stage. In this chapter and the following chapters, the available images for both image datasets are grouped into two sub-sets. The first set is used to estimate the camera reference PRNU, and the second is used to test the performance of source camera identification. All proposed techniques are assessed with differently sized blocks from 64×64 to 512×512. Image blocks are directly cropped from the centre of the full size images without affecting their content. It is worth noting that, the Dresden dataset is divided into two subsets, i.e. uncompressed and compressed images. In this thesis, only uncompressed images are used.

Camera brand	Symbol	Native resolution	Sensor [inch or mm]	Number of images
Canon IXUS115HS-1	C1	4000 x 3000	1/2.3", CMOS	250
Canon IXUS115HS-2	C2			250
Canon G10	C3	4416 x 3312	1/1.7", CCD	250
Fujifilm S2950 - 1	C4	4288 x 3216	1/2.3", CCD	250
Fujifilm S2950 - 2	C5			250
Nikon Coolpix L330-1	C6	5152 x 3864	1/2.3" , CCD	250
Nikon Coolpix L330-2	C7			250
Panasonic DMC TZ20-1	C8	4320 x 3240	1/2.33" CMOS	250
Panasonic DMC TZ20-2	C9			250
Samsung pl120 - 1	C10	4320x3240	1/2.33" , CCD	250
Samsung pl120 - 2	C11			250
Samsung L301	C12	4000 x 3000	1/2.3" CCD	250
Sony DSC HX200V	C13	4896 x 3672	1/2.3" BSI CMOS	250

Table 4.1 Digital cameras in our image dataset.

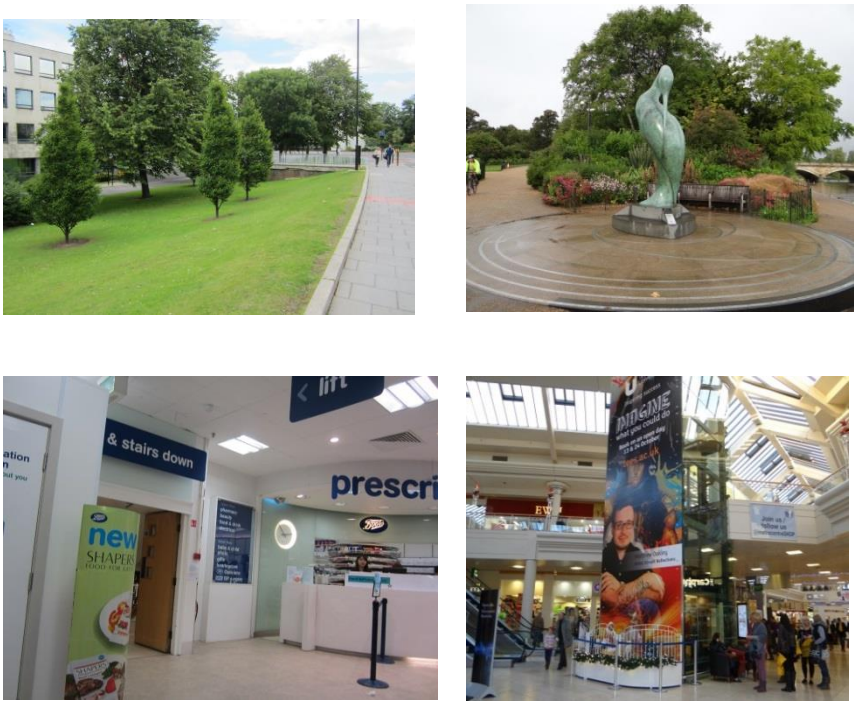

Figure 4-5 Examples of natural indoor and outdoor scenes in our dataset.

Camera brand	Symbol	Native resolution	Sensor [inch or mm]	Number of images
AgfaPhoto DC-733s	DC1	3072 × 2304	1/2.5" , CCD	281
AgfaPhoto DC-830i	DC2	3264 × 2448	1/1.8" , CCD	363
Kodak M1063_0	DC3	3664 × 2748	1/2.33", CCD	464
Kodak M1063_1	DC4			458
Nikon D200_0	DC5	3872 × 2592	23.6 × 15.8 mm, CCD	372
Nikon D200_1	DC6			380
Panasonic DMC-FZ50_0	DC7	3648 × 2736	1/1.8", CCD	265
Panasonic DMC-FZ50_1	DC8			415
Sony DSC-H50_0	DC9	3456 × 2592	1/2.33", CCD	284
Sony DSC-H50_1	DC10			257

Table 4.2 Digital cameras in the Dresden dataset.

4.6 Experimental work

The main aim in this chapter and the following chapters is to identify the particular digital camera that was used to capture each image. The camera identification problem can be viewed as the following; the enquiry image contains the PRNU characteristics. Therefore, the PRNU estimated from a camera should exhibit high similarity when compared to the noise residue extracted from the image. The proposed pre-processing technique is evaluated using two common camera identification techniques which are basic-PRNU as proposed in the work of Lukas *et al.* (2006) and phase-PRNU as explained in Kang *et al.* (2012). In this experimental work all of the above 23 digital cameras are applied to examine the performance of the proposed technique. It is worth noting that a wavelet based de-noising filter is used in the proposed technique. The query image PRNU and the camera reference PRNU are extracted from the green channel, which could include more physical PRNU components (Kang *et al.*, 2012),

For each digital camera, the camera reference PRNU is extracted from 50 original digital images for both data sets, as described in the basic-PRNU and Phase-PRNU techniques. Then, for our data set, 200 test images obtained by the same sensor are selected to calculate the false negative rate (FNR), while 2400 digital images captured by the other twelve digital cameras (200 photos for every camera) are selected in order to compute the false positive rate (FPR). From the Dresden dataset, as mentioned above, 50 images are used for estimating the PRNU and the other available image are used to calculate the false negative and false positive rates. The FNR for a camera C represents the proportion of test images taken by C but incorrectly assigned to a different camera. On the other hand, the FPR for C is the proportion of test images assigned to C but taken by a different camera. The results show that the unsharp masking technique achieves greatly superior performance compared to that of the basic-PRNU technique and phase-PRNU techniques for all different image sizes. Table 4.3 illustrates the overall results for false negative rate and overall false positive rate with our dataset. It is worth noting that in most cases the proposed technique reduces the overall false negative rate by more than 4% compared to basic-PRNU and phase-PRNU, when image sizes are equal to 64×64. With images of 128×128 the overall false negative rate is downgraded by about 10% and 5% compared to basic-PRNU and phase-PRNU techniques respectively. A small improvement is visible in sizes of 256×256 and 512×512. As shown in table 4.3, using the unsharp masking technique leads to a reduction in the overall false positive rate regardless of the size of the image. Moreover, a clear enhancement is shown with the Dresden dataset, for instance the overall false negative rate have been reduced compared with basic-PRNU

from 52.22% to 49.32 %, 30.48 % to 28.07 %, 11.40% to 10.05% and from 2.75% to 2.32% depending on the image size used (see table 4.4).

Technique	FNR (%)				FPR (%)			
	Image size 64×64	Image size 128×128	Image size 256×256	Image size 512×512	Image size 64×64	Image size 128×128	Image size 256×256	Image size 512×512
basic-PRNU	48.04	24.96	12.15	7.08	4.01	2.10	1.06	0.61
Proposed basic-PRNU with sharpening	45.35	22.35	11.35	6.62	3.65	1.86	0.89	0.55
Phase-PRNU	45.81	23.27	11.00	6.31	3.82	1.94	0.92	0.53
Proposed Phase-PRNU with sharpening	43.77	22.08	10.50	5.27	3.65	1.82	0.87	0.41

Table 4.3 Overall FNR and FPR for each technique with our dataset.

Technique	FNR (%)				FPR (%)			
	Image size 64×64	Image size 128×128	Image size 256×256	Image size 512×512	Image size 64×64	Image size 128×128	Image size 256×256	Image size 512×512
basic-PRNU	52.22	30.48	11.40	2.75	5.80	3.37	1.20	0.37
Proposed basic-PRNU with sharpening	49.32	28.07	10.05	2.32	5.19	2.81	0.92	0.27
Phase-PRNU	49.66	28.45	10.10	2.03	5.52	3.16	1.12	0.23
Proposed Phase-PRNU with sharpening	45.80	25.75	8.12	1.88	5.01	2.71	0.90	0.20

Table 4.4 Overall FNR and FPR for each technique with the Dresden dataset.

Another improvement is shown in the overall false negative rate compared with Phase-PRNU, where the reduction in the overall false negative rate reach to 7%, 9%, 19% and 7% with image sizes of 128×128, 256×256 and 512×512 respectively (see table 4.4). The results in more detail for our dataset and the Dresden dataset showing the false negative and false positive rates for each digital camera are shown in table 4.5 to table 4.12. With regards to the improvement to the basic-PRNU, note that the unsharp masking technique improves the results for the majority of digital cameras. For example, in table 4.5 the unsharp masking technique reduces the false negative rate from 54.50% to 50.50%, 25.50% to 23.00% and 4% to 3.5% with image size of

64×64, 128×128 and 256×256 respectively for images taken by C1 (Canon IXUS115HS-1 digital camera). Meanwhile small improvements in the false positive rate are apparent for most digital cameras as shown in table 4.6. However, in a few cases, the false negative rate marginally increases when utilizing the proposed technique; for instance, in C3 with image size of 128×128 and 512×512 , the false negative rate rises from 17% to 17.50% and from 5.50 % to 6.00% and on improvement with image size of 64×64. In addition, the false positive rate slightly rises with same camera (C3) from 3.63% to 3.67% with image size 64×64. This is justified by the fact that the C3 camera includes a tiny sensor (1/1.7"), which may create much undesirable noise affecting the estimation of the PRNU noise (kenrockwell, 2008). Moreover, in C7 with image size of 256×256, the false positive rate increases from 0.00% to 0.50% .The reason for such a result is that the cameras C7 and C8 are of the same brand (inter-class PRNU) which may lead to an increase in similarity between the two PRNUs. For the same reason, the false positive rate also increases in C11 from 3.92% to 4.38% and in C6 from 0.71% to 0.88%, with image size of 64×64 and 512×512 respectively (see table 4.6). As for the Dresden dataset, the same observation can be made regarding the cameras DC7/ DC8 and DC9/ DC10 (see table 4.7, 4.8 and 4.9).

Image size	Techniques	C1	C2	C3	C4	C5	C6	C7	C8	C9	C10	C11	C12	C13
64×64	basic-PRNU	54.50	48.50	45.00	54.00	71.50	37.50	17.50	81.50	70.50	50.00	43.00	11.00	40.00
	Proposed basic-PRNU with sharpening	50.50	47.00	45.00	54.00	64.50	35.50	13.00	82.50	74.50	46.50	37.50	8.5	30.50
128×128	basic-PRNU	25.50	20.00	17.00	31.50	44.00	6.00	2.00	67.00	60.50	20.00	21.00	1.00	9.00
	Proposed basic-PRNU with sharpening	23.00	16.00	17.50	28.50	41.50	4.50	2.00	63.00	57.50	15.00	14.00	1.50	6.50
256×256	basic-PRNU	4.00	2.50	7.50	17.00	10.50	1.50	0.00	50.00	47.50	8.50	7.00	0.00	2.00
	Proposed basic-PRNU with sharpening	3.50	2.00	7.00	17.00	9.50	1.00	0.50	47.50	45.50	7.00	5.50	0.00	1.50
512×512	basic-PRNU	0.50	0.00	5.50	9.50	0.50	0.00	0.00	35.50	28.00	5.00	4.00	0.00	3.50
	Proposed basic-PRNU with sharpening	0.50	0.00	6.00	9.00	0.00	0.00	0.00	33.00	26.00	4.00	4.00	0.00	3.50

Table 4.5 False negative rate (%) of basic PRNU and proposed basic PRNU with sharpening for our dataset.

Image size	Techniques	C1	C2	C3	C4	C5	C6	C7	C8	C9	C10	C11	C12	C13
64×64	basic-PRNU	4.50	3.88	3.63	4.67	3.42	3.75	5.71	3.42	4.04	3.67	3.92	3.17	4.29
	Proposed basic-PRNU with sharpening	4.13	3.79	3.67	3.88	2.71	3.25	5.00	3.08	3.75	3.13	4.38	2.42	4.29
128×128	basic-PRNU	2.42	1.71	2.46	1.96	1.33	2.75	2.88	1.96	1.96	1.58	2.04	1.46	2.63
	Proposed basic-PRNU with sharpening	2.38	1.58	2.46	1.63	1.17	2.00	2.46	1.92	1.54	1.42	1.63	1.38	2.63
256×256	basic-PRNU	1.04	0.88	1.50	0.92	1.04	1.21	1.17	0.96	1.17	0.88	1.21	0.79	0.96
	Proposed basic-PRNU with sharpening	1.04	0.83	1.42	0.75	0.67	1.13	1.00	0.75	0.96	0.71	0.71	0.79	0.79
512×512	basic-PRNU	0.92	0.46	0.75	0.33	0.54	0.71	1.04	0.58	0.33	0.63	0.54	0.63	0.50
	Proposed basic-PRNU with sharpening	0.79	0.42	0.54	0.33	0.46	0.88	1.04	0.38	0.17	0.50	0.54	0.63	0.50

Table 4.6 False positive rate (%) of basic PRNU and proposed basic PRNU with sharpening for our dataset.

Image size	Techniques	C1	C2	C3	C4	C5	C6	C7	C8	C9	C10	C11	C12	C13
64×64	phase-PRNU	52.50	42.00	40.50	54.00	69.00	31.00	19.50	80.50	71.50	46.50	39.50	10.50	38.50
	Proposed phase-PRNU with sharpening	50.00	43.00	42.50	50.00	67.50	33.50	18.00	78.00	68.50	41.50	36.50	9.00	31.00
128×128	phase-PRNU	24.00	15.00	13.50	32.00	43.00	6.50	4.00	64.00	57.00	17.50	15.50	1.00	9.50
	Proposed phase-PRNU with sharpening	23.00	13.00	13.50	32.00	41.50	4.50	4.50	61.50	55.50	15.50	14.50	1.00	7.00
256×256	phase-PRNU	3.50	1.50	8.00	14.50	10.50	0.50	0.00	46.50	40.50	9.00	6.50	0.00	2.00
	Proposed phase-PRNU with sharpening	3.50	1.50	8.00	14.50	8.00	0.50	0.00	45.50	40.00	8.50	5.50	0.00	1.00
512×512	phase-PRNU	0.00	0.00	4.50	5.50	0.00	0.00	0.00	34.00	27.50	3.50	3.50	0.00	3.50
	Proposed phase-PRNU with sharpening	0.00	0.00	6.00	3.50	0.00	0.00	0.50	26.50	25.00	3.00	2.00	0.00	2.00

Table 4.7 False negative rate (%) of phase-PRNU and proposed phase-PRNU with sharpening for our dataset.

Image size	Techniques	C1	C2	C3	C4	C5	C6	C7	C8	C9	C10	C11	C12	C13
64×64	phase-PRNU	4.04	3.42	3.54	4.00	3.21	4.33	5.00	3.54	3.54	3.50	4.38	2.63	4.50
	Proposed phase-PRNU with sharpening	4.08	3.38	4.08	3.96	2.54	3.46	4.58	3.25	3.50	3.38	4.54	2.58	4.08
128×128	phase-PRNU	2.33	1.58	2.38	1.38	1.54	2.25	2.58	1.92	1.79	1.79	1.92	1.58	2.17
	Proposed phase-PRNU with sharpening	2.58	1.79	1.96	1.46	1.33	2.04	2.50	1.83	1.63	1.63	1.29	1.46	2.17
256×256	phase-PRNU	1.29	1.00	1.38	0.79	0.88	1.00	0.79	0.58	0.67	0.96	0.75	0.83	1.00
	Proposed phase-PRNU with sharpening	1.25	1.00	1.29	0.63	0.96	1.04	0.83	0.50	0.58	0.75	0.71	0.79	1.00
512×512	phase-PRNU	0.63	0.46	0.79	0.17	0.50	0.67	1.08	0.58	0.38	0.46	0.46	0.38	0.29
	Proposed phase-PRNU with sharpening	0.63	0.25	0.50	0.38	0.21	0.58	0.71	0.38	0.25	0.33	0.58	0.17	0.38

Table 4.8 False positive rate (%) of phase-PRNU and proposed phase-PRNU with sharpening for our dataset.

Image size	Techniques	DC1	DC2	DC3	DC4	DC5	DC6	DC7	DC8	DC9	DC10
64×64	basic-PRNU	63.29	52.17	62.32	57.00	59.90	51.69	51.69	52.66	28.50	43.00
	Proposed basic-PRNU with sharpening	54.59	48.79	51.21	50.72	50.24	56.52	56.04	54.11	29.47	41.55
128×128	basic-PRNU	35.27	25.60	44.44	43.00	45.89	28.50	32.85	27.05	8.70	13.53
	Proposed basic-PRNU with sharpening	32.85	24.15	35.27	36.23	45.89	30.43	30.43	27.05	4.83	13.53
256×256	basic-PRNU	13.04	6.28	21.74	22.22	17.87	10.63	11.11	8.70	0.97	1.45
	Proposed basic-PRNU with sharpening	11.11	5.8	18.36	15.46	18.84	10.63	9.18	8.7	1.45	0.97
512×512	basic-PRNU	4.35	1.93	4.35	4.35	4.35	0.48	2.90	4.83	0.00	0.00
	Proposed basic-PRNU with sharpening	5.80	1.93	2.90	0.97	2.42	1.45	2.90	4.83	0.00	0.00

Table 4.9 False negative rate (%) of basic PRNU and proposed basic PRNU with sharpening for the Dresden dataset.

Image size	Techniques	DC1	DC2	DC3	DC4	DC5	DC6	DC7	DC8	DC9	DC10
64×64	basic-PRNU	4.35	5.21	4.88	5.64	4.78	5.69	6.66	8.11	6.12	6.60
	Proposed basic-PRNU with sharpening	3.97	3.86	3.92	3.76	4.78	4.67	6.28	8.64	6.17	5.80
128×128	basic-PRNU	2.68	3.49	2.90	3.22	3.22	3.97	3.60	3.38	3.81	3.44
	Proposed basic-PRNU with sharpening	2.31	2.63	2.04	1.66	3.11	2.58	3.60	4.46	3.54	2.15
256×256	basic-PRNU	0.91	0.97	1.13	1.18	1.18	1.29	0.91	0.91	1.77	1.72
	Proposed basic-PRNU with sharpening	0.54	0.59	0.59	0.48	1.66	1.29	0.91	1.07	1.02	1.02
512×512	basic-PRNU	0.21	0.32	0.32	0.38	0.16	0.54	0.21	0.16	0.75	0.64
	Proposed basic-PRNU with sharpening	0.00	0.00	0.00	0.21	0.16	0.54	0.27	0.86	0.38	0.27

Table 4.10 False positive rate(%) of basic PRNU and proposed basic PRNU with sharpening for the Dresden dataset.

Image size	Techniques	DC1	DC2	DC3	DC4	DC5	DC6	DC7	DC8	DC9	DC10
64×64	phase-PRNU	58.94	46.38	57.97	59.42	55.07	48.79	51.21	51.69	26.57	40.58
	Proposed phase-PRNU with sharpening	57.00	46.86	53.62	54.11	44.44	48.79	51.21	41.06	24.64	36.23
128×128	phase-PRNU	34.30	21.26	38.65	38.65	37.68	28.99	34.78	29.95	5.80	14.49
	Proposed phase-PRNU with sharpening	29.95	20.77	38.16	38.16	29.95	28.99	29.47	23.19	4.35	14.49
256×256	phase-PRNU	11.59	4.83	18.36	20.29	14.98	7.73	11.59	10.63	0.48	0.48
	Proposed phase-PRNU with sharpening	10.14	3.38	18.36	18.84	9.66	4.35	8.70	7.25	0.00	0.48
512×512	phase-PRNU	3.38	1.45	3.86	1.45	4.35	0.00	1.45	4.35	0.00	0.00
	Proposed phase-PRNU with sharpening	2.90	1.45	2.90	1.93	1.45	0.48	5.31	2.42	0.00	0.00

Table 4.11 False negative rate (%) of phase-PRNU and proposed phase-PRNU with sharpening for Dresden dataset.

Image size	Techniques	DC1	DC2	DC3	DC4	DC5	DC6	DC7	DC8	DC9	DC10
64×64	phase-PRNU	5.21	4.88	5.37	5.10	4.35	4.56	5.96	6.87	6.44	6.44
	Proposed phase-PRNU with sharpening	4.46	4.03	3.49	3.22	3.54	4.62	6.49	7.62	6.17	6.44
128×128	phase-PRNU	2.90	2.74	2.90	3.06	2.84	2.84	2.95	3.65	4.19	3.54
	Proposed phase-PRNU with sharpening	2.25	2.52	1.99	1.99	2.68	2.42	2.79	3.22	4.08	3.17
256×256	phase-PRNU	0.86	0.91	1.34	1.13	1.13	1.13	1.23	0.75	1.23	1.50
	Proposed phase-PRNU with sharpening	0.48	0.86	0.75	0.75	0.91	0.97	0.97	0.75	1.13	1.40
512×512	phase-PRNU	0.05	0.11	0.16	0.27	0.11	0.48	0.16	0.16	0.48	0.27
	Proposed phase-PRNU with sharpening	0.05	0.00	0.00	0.16	0.11	0.32	0.11	0.64	0.38	0.27

Table 4.12 False positive rate (%) of phase-PRNU and proposed phase-PRNU with sharpening for the Dresden dataset.

4.7 Conclusion

PRNU may be weak for smaller images or those with areas that contain a saturated background with dark areas (Chen *et al.*, 2008). Furthermore, it would often be contaminated in the frequency domain by image content, non-unique artefacts, colour interpolation and sensor design. Consequently, the performance of source camera identification for small images needs to be further improved. In this chapter, an image sharpening technique has been proposed in order to enhance the source camera identification based on PRNU estimation. The proposed image sharpening technique, namely Unsharp masking, aims to amplify the PRNU noise present in the digital image in order the accuracy of its estimation. Extensive experiments on two different data sets have demonstrated that the proposed sharpening technique achieves considerable improvements between two recent state-of the-art source camera identification schemes with different sizes of images. In the future, it would be sensible to consider the improvement of unsharp masking by applying the confusion matrix, which contains information about actual and predicted classifications done by a classification system.

CHAPTER 5 **WEIGHTED AVERAGING**

5.1 Introduction

Noise could be described as an unwanted signal affecting the original signal. The presence of interference could be associated with the technique or sensor used for acquiring the signal. One of the common techniques for obtaining a useful signal and to reduce noise is averaging the signal, which could be achieved by a simple arithmetic average (John *et al.*, 2001). Averaging signals in the time domain could be one of the major procedures of noise reduction in biomedical signal processing where some systems generate cyclic patterns such as in electrocardiographic (ECG) acquisition systems (Momot, 2009; Pander *et al.*, 2013). However, traditional averaging techniques may require particular assumptions (for instance, alignment signals of equal shape, uncorrelated and zero mean) in order give optimal performance. Basically, the assumption of stationarity cannot always be achieved. Variance in noise could change on some beats based on, for example, muscle tone or deviations in the acquisition environment (Bataillou *et al.*, 1995). Motivated by this, in this chapter the generalised form of averaging namely weighted averaging (WA) has been applied for source camera identification, and to the best of the author's knowledge, this technique has not been used in the PRNU estimation process. The traditional technique for estimating the PRNU uses a set of digital images where the pattern residue signal can be extracted from each image. The extracted residue signals are then averaged in order to determine the sensor pattern noise. Such a procedure is referred to as constant averaging in the

rest of this thesis. This chapter is organized as follows: the problems with the constant averaging technique will be discussed in section two. The weighted averaging technique is then introduced in section three. Next, the effectiveness of weighted averaging is evaluated in section four, and the conclusions are presented in section five.

5.2 Problem formulation

The constant averaging technique has been used for PRNU estimation in many studies (Chen *et al.*, 2007; Chen *et al.*, 2008; Goljan *et al.*, 2009; Hu *et al.*, 2010; Kang *et al.*, 2012; Li, 2009; Liu *et al.*, 2010; Lukas *et al.*, 2006). The assumption made is usually that every residue signal is a noisy observation of the sensor pattern noise. This hypothesis is well justified in practice because digital images can be obtained in various conditions, creating the corresponding residue signals which are different from each other. For example, bright digital images may provide better PRNU estimation than dark digital images. Moreover, saturated pixels can raise the estimation errors in residue signals (Lukas *et al.*, 2006). Because every residue signal could carry undesirable image-dependent noise, as mentioned earlier, constant averaging may not give optimal results. In fact, treating all of the PRNU residue signals similarly through constant averaging can be an optimal solution only if they contain undesirable noise of similar power (variance). Based on this observation, the weighted averaging technique is suggested for effective PRNU estimation. The weighted averaging technique for PRNU estimation depends on the principle of the estimation of unknown signal from noisy observations (Laciar and Jane, 2001; Momot, 2011). As discussed earlier, the PRNU is estimated using N images I_i, $i = 1, 2 \cdots, N$. Denote by L the number of

samples of each image rearranged in one direction (i.e. vertically or horizontally). In view of (1.3) and (3.1), the corresponding noise residue can be expressed as:

$$r_i(j) \approx I_i^0(j)K(j) + \Phi_i(j) \ , i = 1,2,..,N \ ; \ j = 1,2,\dots,L \tag{5.1}$$

where Φ_i is an independent noise. For the sake of demonstration, let us assume that the images used for estimating the PRNU represent smooth regions describing the same color information such as blue-sky content (i.e., the variance of I_i^0 is extremely small $\sigma^2_{I^0_{i(j)}} \ll 1$). This may not be true in practice but the development given below remains valid to some extent as will be shown in experiments on natural images of various content. Let ξ be a constant so that $\xi = \frac{1}{NL}\sum_{i=1}^{N}\sum_{j=1}^{L} I_i^0\,(j)$. it follows:

$$\begin{aligned} r_i(j) &\approx \xi K(j) + \Psi_i(j) \\ &= s(j) + \Psi_i(j) \end{aligned} \tag{5.2}$$

where $s(j) = \xi K(j)$ and

$$\begin{aligned} \Psi_i(j) &= \Phi_i(j) - K(j)(\xi - I_i^0(j)) \\ \Psi_i(j) &\approx \Phi_i(j) \end{aligned} \tag{5.3}$$

Here we are mainly interested in the sensor pattern noise K. In view of (5.2) and (5.5), the problem of estimating the PRNU from a set of N images can be seen as an estimation of an unknown signal s(j) with $j = 1; 2 \cdots ;L$ in a noisy environment, i.e., using *N* noisy observations. The i^{th} observation r_i is the sum of a signal *s* and a random noise Ψ_i with zero mean and a variance for each observation equal to σ_i^2 . The conventional method to estimate *s* consists of averaging the observations (Van Drongelen, 2006).

$$\hat{s}(j) = \frac{1}{N}\sum_{i=1}^{N} r_i(j) \tag{5.4}$$

This technique will be referred as the constant averaging technique since each observation is multiplied by the same constant factor 1/N. Theoretically, the constant averaging technique is optimal if the noise variance is constant in all observations (Bataillou *et al.*, 1995; Laciar and Jane, 2001). The procedure of estimating ŝ by the constant averaging technique is shown in figure 5-1. If the noise variance changes from one observation to another, then the weighted averaging technique may offer the closest estimation to the actual signal in terms of the mean squared error (Bataillou *et al.*, 1995; Laciar and Jane, 2001). Figure 5-2 illustrations the procedure of weighted averaging which could be described as:

$$\hat{s}(j) = \sum_{i=1}^{N} w_i \, r_i(j) \qquad 5.5$$

where w_i is a weight corresponding to the i^{th} noise residue r_i.

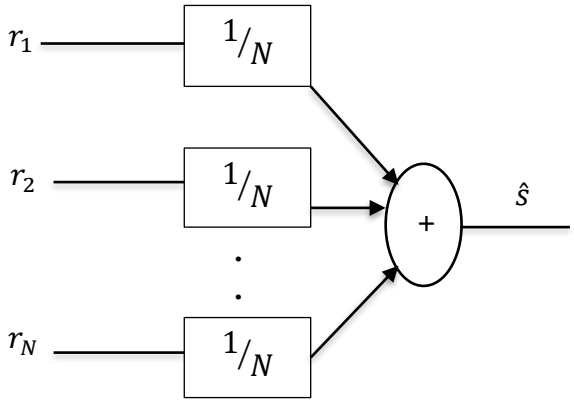

Figure 5-1 The concept of constant averaging.

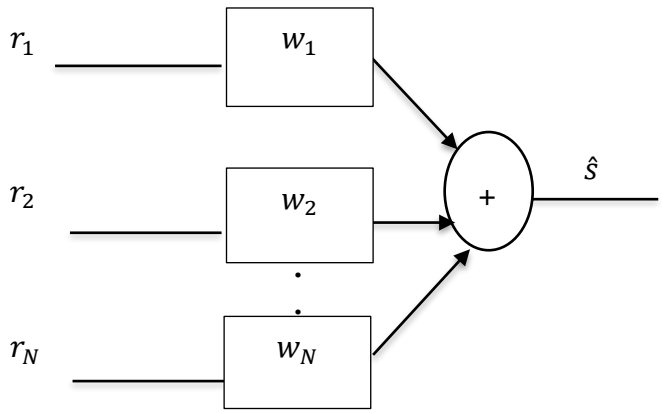

Figure 5-2 The concept of weighted averaging.

The optimal weight for the i^{th} observation can then be defined by:

$$w_i = \frac{1}{\sigma_i^2}\left(\frac{1}{\sum_{k=1}^{N}\frac{1}{\sigma_k^2}}\right) \tag{5.6}$$

w_i is optimal since it based on minimizing the Mean Square Error (MSE). The proof of equation (5.14) can be summarised as:

First, to obtain an unbiased estimation, the weights are assumed to sum up to 1 (Bataillou *et al.*, 1995)

$$\sum_{i=1}^{N} w_i = 1 \tag{5.7}$$

Let us define the MSE as:

$$e = \frac{1}{L}\sum_{i=1}^{L}(\hat{s}(j) - s(j))^2 \tag{5.8}$$

where $\hat{s}$ is the estimated version of s as given by (5.5). In a matrix form, the MSE can be expressed as

$$e = E[\,(W^T X - s)^2\,]$$
$$= W^T E[XX^T]W + E[s^2] - 2W^T E[sX] \qquad 5.9$$

where T is the transpose operation. $X = [x_1, x_2, \ldots x_N]^T$ and $W = [w_1, w_2, \ldots, w_N]^T$. The gradient of the MSE in respect to W is

$$\Delta w(e) = 2E[XX^T]W - 2E[sX] \qquad 5.10$$

Minimizing the MSE leads to the following estimate

$$\Delta w(e) = 2E[XX^T]W - 2E[sX] \qquad 5.11$$

Under the assumption that the noise Ψ_i is centered (i.e., zero mean) and independent of the signal s, we obtain

$$E[XX^T] = U^T E[s^2]U + \begin{pmatrix} \sigma_1^2 & 0 & \cdots & 0 \\ 0 & \sigma_2^2 & \cdots & 0 \\ \vdots & \vdots & \ddots & \vdots \\ 0 & 0 & \cdots & \sigma_N^2 \end{pmatrix} \qquad 5.12$$

where $U = [1,1, ..., 1]$ and $E[sX] = E[s^2]U^T$. From (5.19) and (5.12), it follow

$$w_1 \sigma_1^2 = w_2 \sigma_2^2 = \cdots = w_N \sigma_N^2 \qquad 5.13$$

In view of (5.7) and (5.13), the weights can be deduced as shown in (5.6). Obviously, the weights depend on the variance of undesirable noise Ψ_i in each observation. As proposed in work of Laciar and Jane (2001) , the estimated noise variance can be computed as

$$\hat{\sigma}_i^2 = \frac{\sum_{j=1}^{L} (\hat{n}_i(j) - \bar{n}_i)^2}{L} \qquad 5.14$$

With

$$\hat{n}_i(j) = r_i(j) - \bar{r}(j), \qquad j = 1, \dots, L \tag{5.15}$$

where $\bar{r}$ denotes the mean of the estimated noise $\hat{n}_i$ and $\bar{r}(j) = \sum_{i=1}^{N} r_i(j)$ represents the average signal. The estimated PRNU term with WA can be computed as

$$PRNU(j) = \sum_{i=1}^{N} w_i \, r_i(j) \tag{5.16}$$

5.3 Proposed WA technique for PRNU Estimation

Most PRNU techniques estimated the PRNU using the constant averaging of residue signals extracted from a number of images. Such a technique could be optimal if every residue signal has the same quantity of undesirable noise with constant variance for all images. Nevertheless, this hypothesis may not hold since such noise depends heavily on the content of the image. The weighted averaging technique is suggested to enhance PRNU estimation for more efficient source camera identification (Lawgaly *et al.*, 2014). The next two sub-sections explain the usage of the weighted averaging technique with two recent state-of-the-art source camera identification schemes proposed in the work of Lukas *et al.* (2006) and Chen *et al.* (2008) respectively.

5.3.1 Weighted basic PRNU estimation

In the work of Lukas *et al.* (2006), the PRNU (K) is the outcome of the traditional averaging technique as illustrated in equation 5.4. In the proposed technique, the residue signal is extracted as described in the technique of Lukas *et al.* (2006); and then the theory of weighted averaging, as explained previously in 5.16, which assumes that every residue signal can be a noisy version of the PRNU, is applied.

5.3.2 Weighted maximum likelihood estimator

As describe in the work of Chen *et al.* (2008) the MLE-PRNU estimation technique can be defined as :

$$\widehat{K} = \frac{\sum_{i=1}^{N} \mathbf{r}_i . \mathbf{I}_i}{\sum_{i=1}^{N} (\mathbf{I}_i)^2} \qquad 5.17$$

The MLE-PRNU estimation technique can be seen as a technique using constant averaging as follows, when equation 5.17 could be written as:

$$\widehat{K} = \frac{N\left(\frac{\sum_{i=1}^{N} \boldsymbol{S_i}}{N}\right)}{\sum_{i=1}^{N} (\boldsymbol{I})^2} \ , \ \boldsymbol{S_i} = \boldsymbol{r_i I_i} \qquad 5.18$$

As seen above, the observations ***Si*** are averaged in order to estimate the PRNU. As opposed to constant averaging, the proposed modification, which will be called 'WA MLE-PRNU', uses a weighted averaging in order to estimate ***K***. This can then be expressed as:

$$\widehat{K} = \frac{N\left(\sum_{i=1}^{N} w_i \boldsymbol{S_i}\right)}{\sum_{i=1}^{N} (\boldsymbol{I})^2} \ , \ \boldsymbol{S_i} = \boldsymbol{r_i I_i} \qquad 5.19$$

where w_i is the weight corresponding to the i^{th} observation S_i .

5.4 Experimental Work

In this section, the effectiveness of the weighted averaging technique is examined with the formerly mentioned camera identification techniques as described in the work of Lukas *et al.* (2006) and Chen *et al.* (2008). Our dataset and the Dresden dataset have

been used in the experiments. Normally smaller images frequently provide less PRNU information and therefore the performance of source camera identification for small digital images may need to be improved further (Kang *et al.*, 2012). In this experimental work, several values of blocks sizes 64×64, 128×128, 256×256 and 512×512 are considered. The camera reference PRNU is extracted from 50 green images and the wavelet-based de-noising filter is utilized. The camera reference PRNU for each technique basic-PRNU, proposed WA basic-PRNU, MLE-PRNU and proposed WA MLE-PRNU is calculated as shown in equations, 5.4 , 5.16 , 5.17 and 5.19 respectively. The residue signals have been divided into two, four, eight and sixteen intervals to examine their impact on the performance of the weighted averaging technique. The results have shown that the proposed WA basic-PRNU and the WA MLE-PRNU techniques offer the most significant improvements compared to basic PRNU and MLE-PRNU when eight intervals are used.

5.4.1 Comparison with Constant basic PRNU Estimation

In this sub-section, the false negative rate and the false positive rate for each digital camera are calculated, and also to summarize the performance for each technique the overall false negative and false positive rates are considered. Figure 5-3- Figure 5-10 show the efficiency of WA basic PRNU compared to basic-PRNU. As can be seen, a clear improvement is demonstrated in an image sized 64×64 with a decrease in the false negative rate achieved for each digital camera in the Dresden dataset DC1 to DC10 of 21%, 9%, 19%, 18%, 29%, 6%, 18%, 33%, 1% and 25% respectively (see figure 5-3). With image size of 128×128 and 256×256, figure 5-4 and figure 5-5 have

shown that the false negative rate have been decreased in all available digital cameras. Moreover, a small improvement for the false negative rate is visible in images of 512×512. Regarding the improvement in false positive rate for Dresden dataset, a clear enhancement is illustrated by using the proposed weighted averaging technique in images size of 64×64, 128×128 and 256×256 as shown in figure 5-7-5.9 where the false positive rate goes down in all Dresden digital cameras. However, when applying the weighted averaging technique with the DC5 digital camera the false negative rate is increased from 4.35% with basic-PRNU to 5.80% (see figure 5-6). Also, in DC8 the false positive rate goes up to 0.64% compared to only 0.16% when using basic-PRNU (see figure 5-10) . Both cameras (DC5 and DC8) give undesirable results only when image size is equal to 512×512. The Interpretation of such results is that the WA interval size (8 intervals) may be in conflict with such size of DC1 and Dc8 cameras. The DC1 and Dc8 show some improvement compared to constant averaging when 16 intervals are used. Moreover, in specific cases such as DC5, DC6 and DC7, the WA gives the same performance as constant averaging (see figure 5.6 and 5.7). The reason for such performance could be that images are captured with deferent resolution and the DC5, DC6 and DC7 cameras have the highest resolution. In addition, the number of images, which are used for estimating the PRNU, could be small for such high-resolution cameras. Therefore, for further confirmation of the reliability of the algorithm, estimating the PRNU with a larger set of images should be conducted.

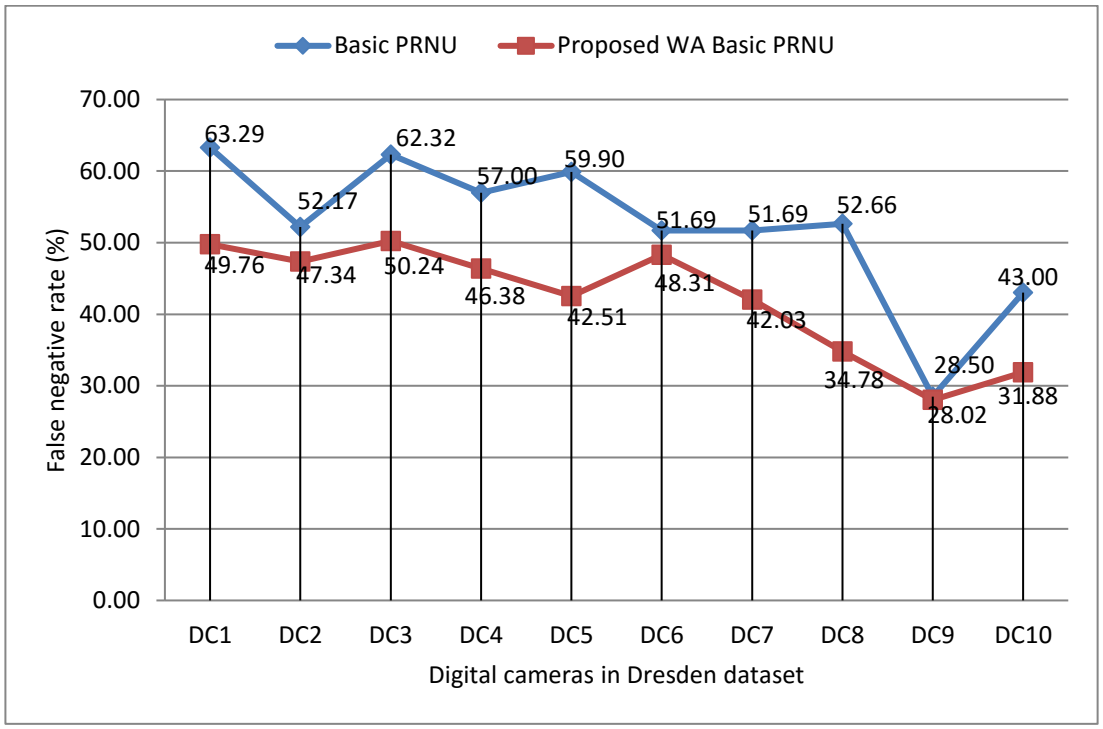

Figure 5-3 False negative rate (%) of Basic PRNU and proposed WA Basic PRNU for Dresden dataset (image size 64×64).

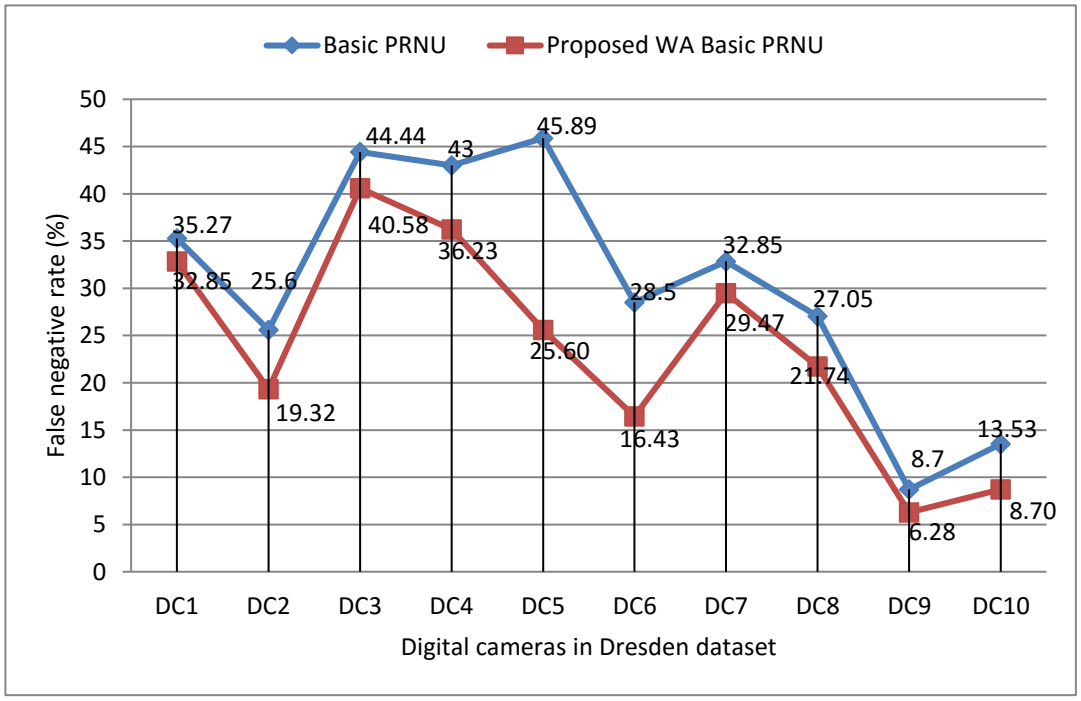

Figure 5-4 False negative rate (%) of Basic PRNU and proposed WA Basic PRNU for Dresden dataset (image size 128×128).

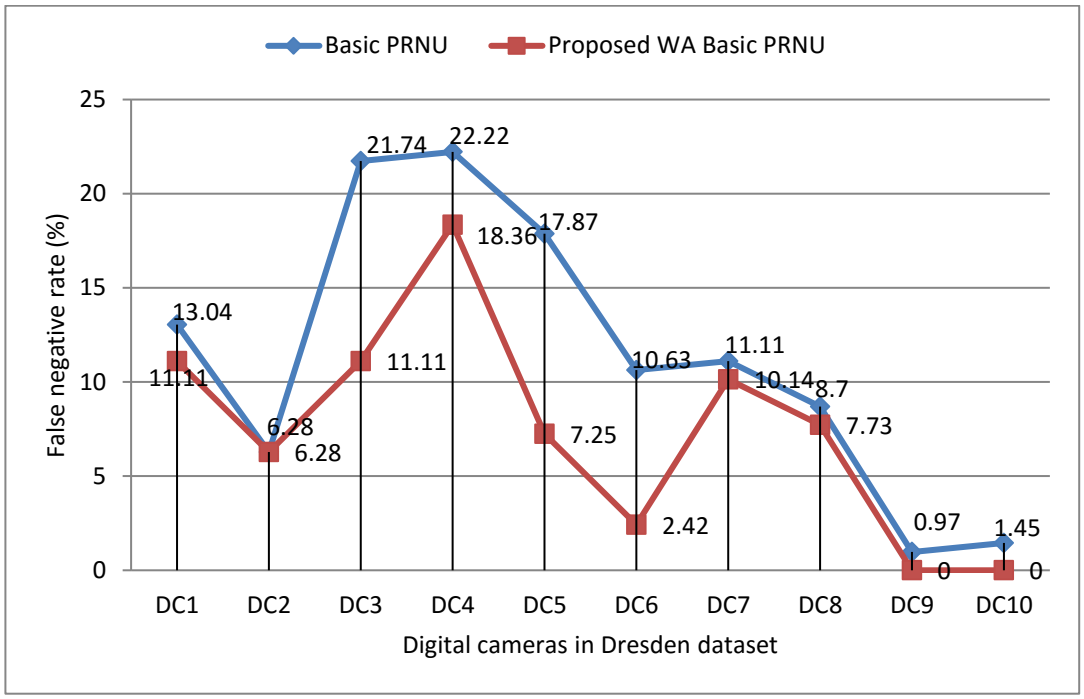

Figure 5-5 False negative rate (%) of Basic PRNU and proposed WA Basic PRNU for Dresden dataset (image size 256×256).

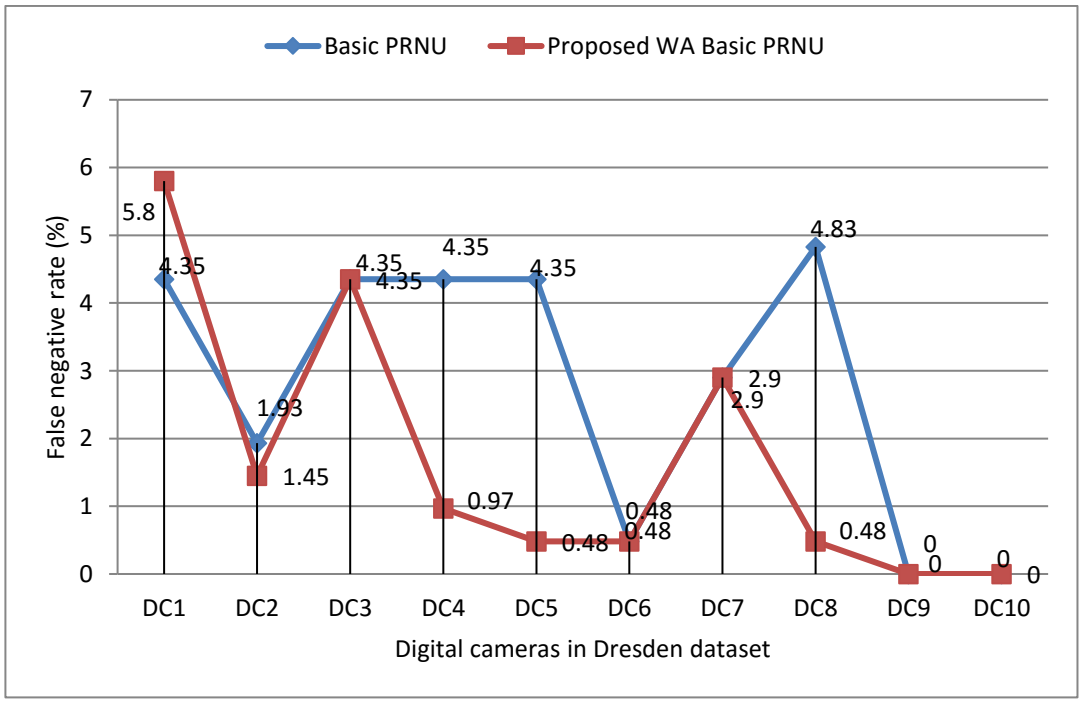

Figure 5-6 False negative rate (%) of Basic PRNU and proposed WA Basic PRNU for Dresden dataset (image size 512×512).

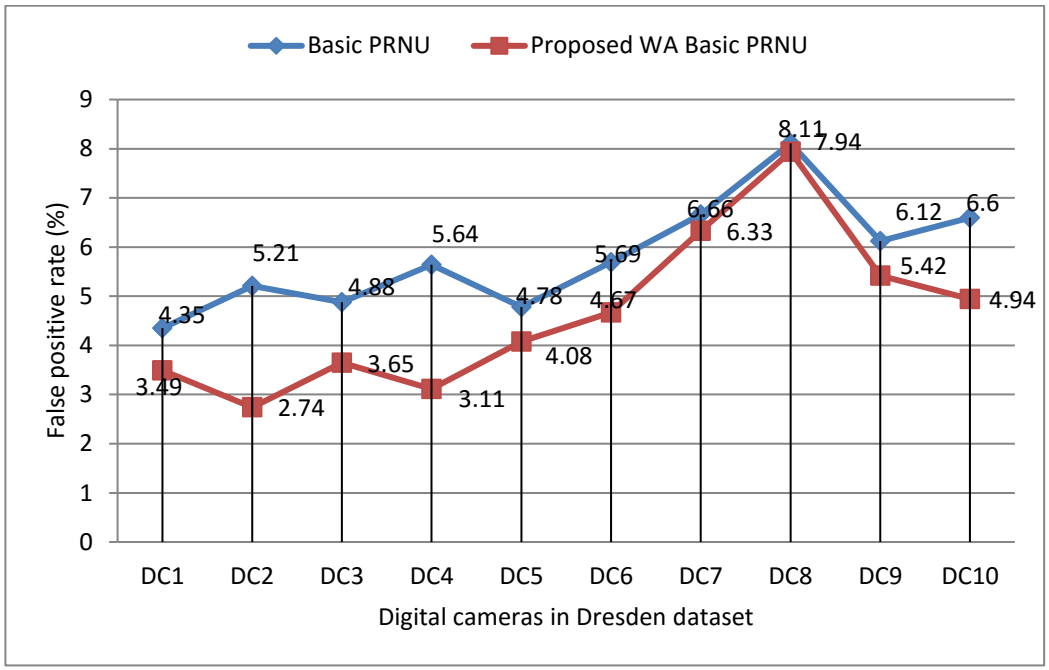

Figure 5-7 False positive rate (%) of Basic PRNU and proposed WA Basic PRNU for Dresden dataset (image size 64×64).

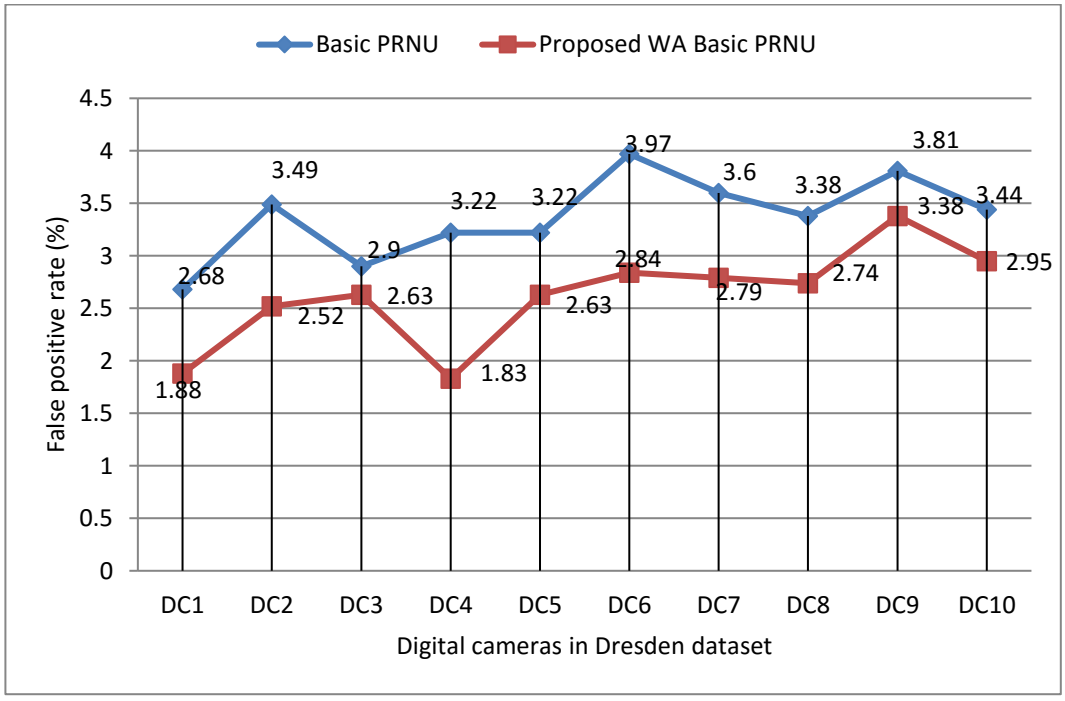

Figure 5-8 False positive rate (%) of Basic PRNU and proposed WA Basic PRNU for Dresden dataset (image size 128×128).

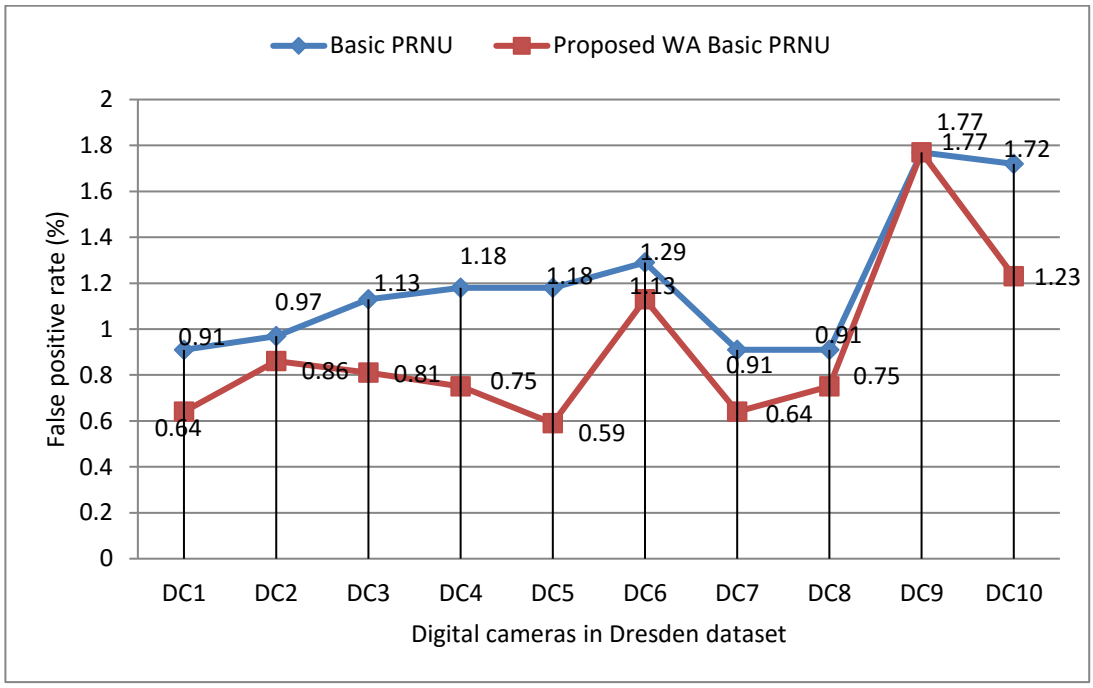

Figure 5-9 False positive rate (%) of Basic PRNU and proposed WA Basic PRNU for Dresden dataset (image size 256×256).

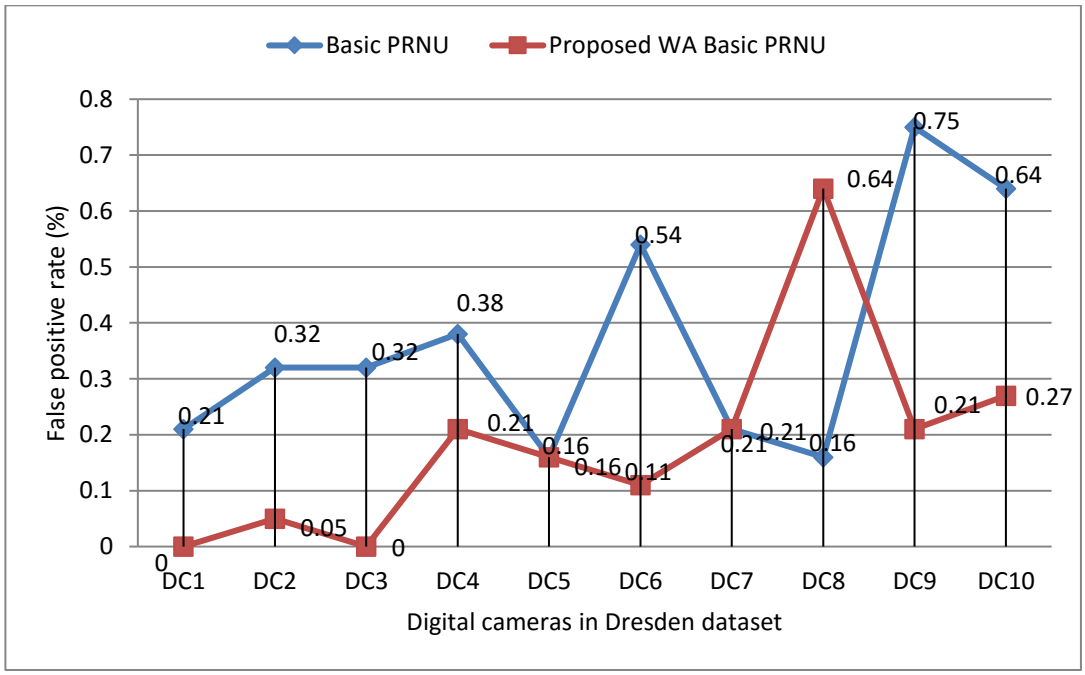

Figure 5-10 False positive rate (%) of Basic PRNU and proposed WA Basic PRNU for Dresden dataset (image size 512×512).

In our dataset with image sizes of 64×64 and 128×128, a clear improvement is shown in figure 5-11 and figure 5-12 where in C5 ,C7 ,C10 ,C11 ,C12 and C13, the proposed approach decreases the false negative rate up to 14%, 42%, 11%, 15%, 31% and 23% (see figure 5-11) and by more than 4 points less with image sizes of 128×128 as illustrated in C2, C4, C8, C9 and C11 (see figure 5-12). Nonetheless, a slight improvement in the false negative rate is shown for our dataset with image sizes of 256×256 and 512×512 (see figure 5-13 and figure 5-14). Concerning the false positive rate for our dataset, the proposed weighted averaging achieves better performance than Basic PRNU with different image sizes as shown in figure 5-15- figure 5-18. However, due to the inter-class similarity (C10 and C11), the proposed WA does not show good performance with FPR in C11 camera, where it increases form 2.04% to 2.29% (see figure 5.16). On the other hand, the WA remains an efficient approach for C11 by decreasing the error rate by 16% compared to basic constant averaging, if the overall FNR and FPR for this camera are considered

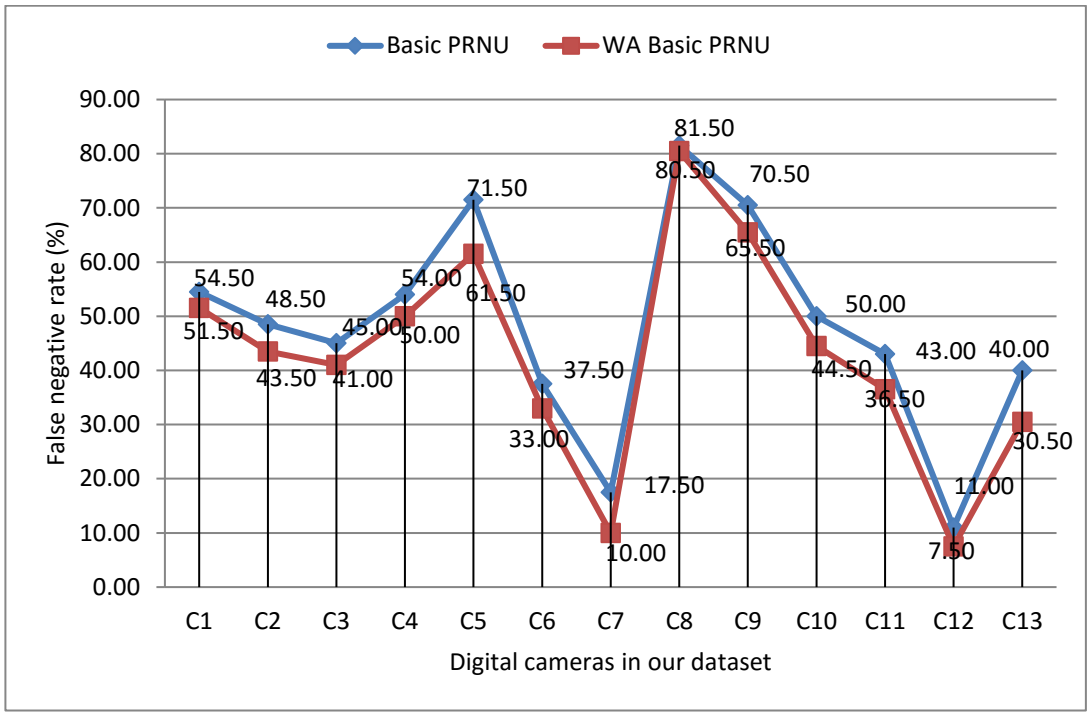

Figure 5-11 False negative rate (%) of Basic PRNU and proposed WA Basic PRNU for our dataset (image size 64×64).

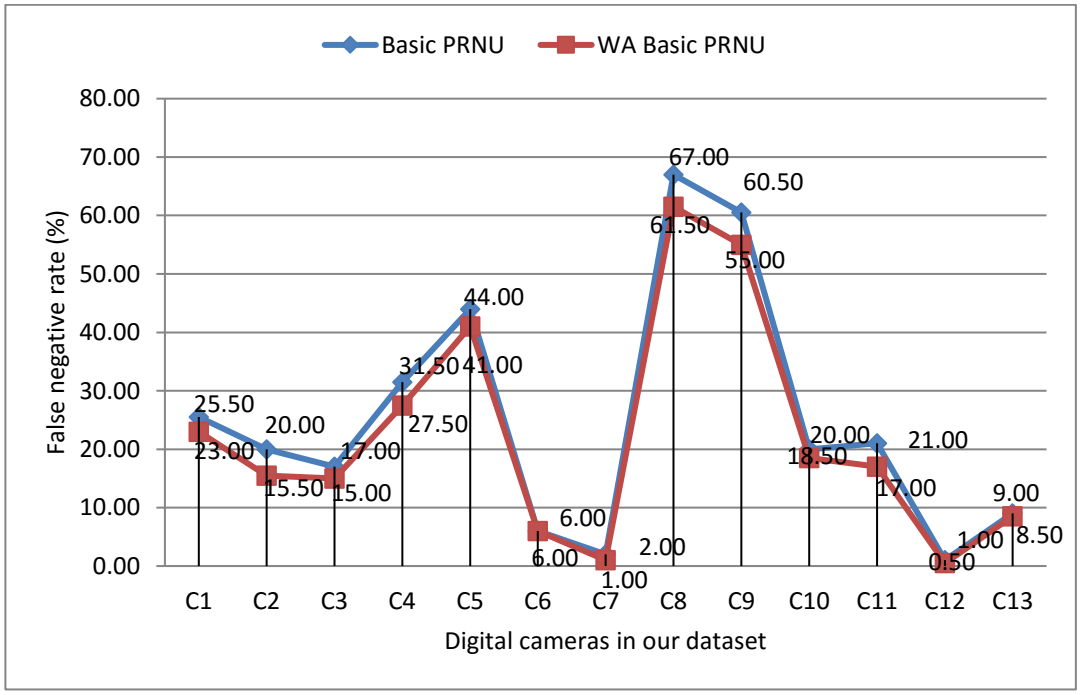

Figure 5-12 False negative rate (%) of Basic PRNU and proposed WA Basic PRNU for our dataset (image size 128×128).

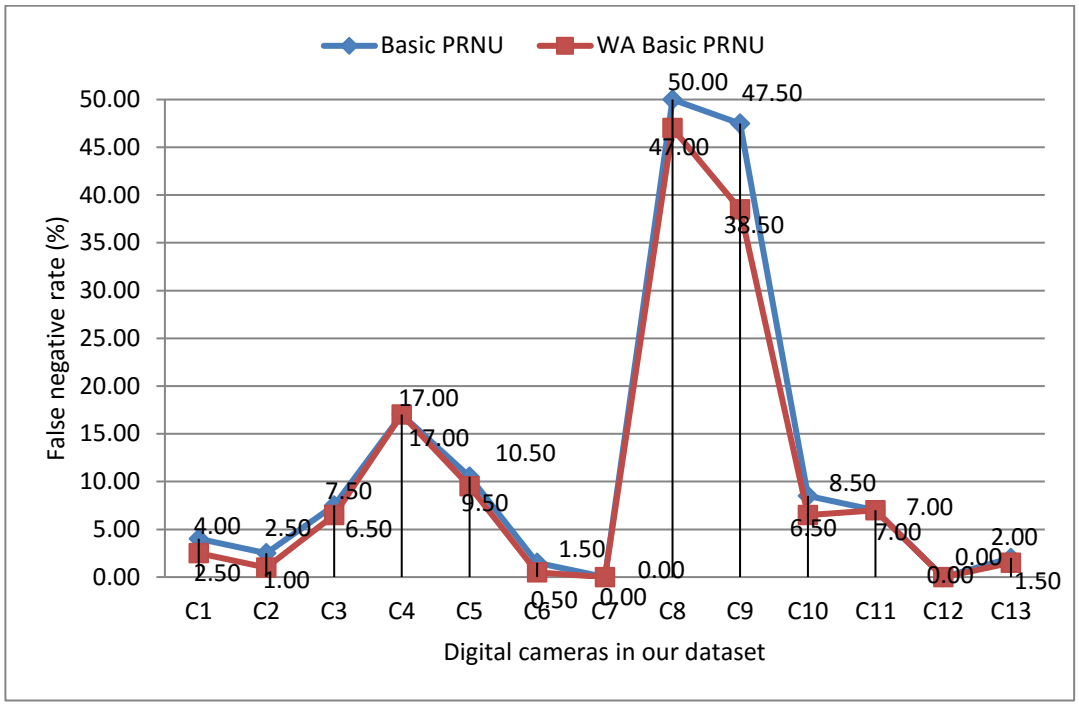

Figure 5-13 False negative rate (%) of Basic PRNU and proposed WA Basic PRNU for our dataset (image size 256×256).

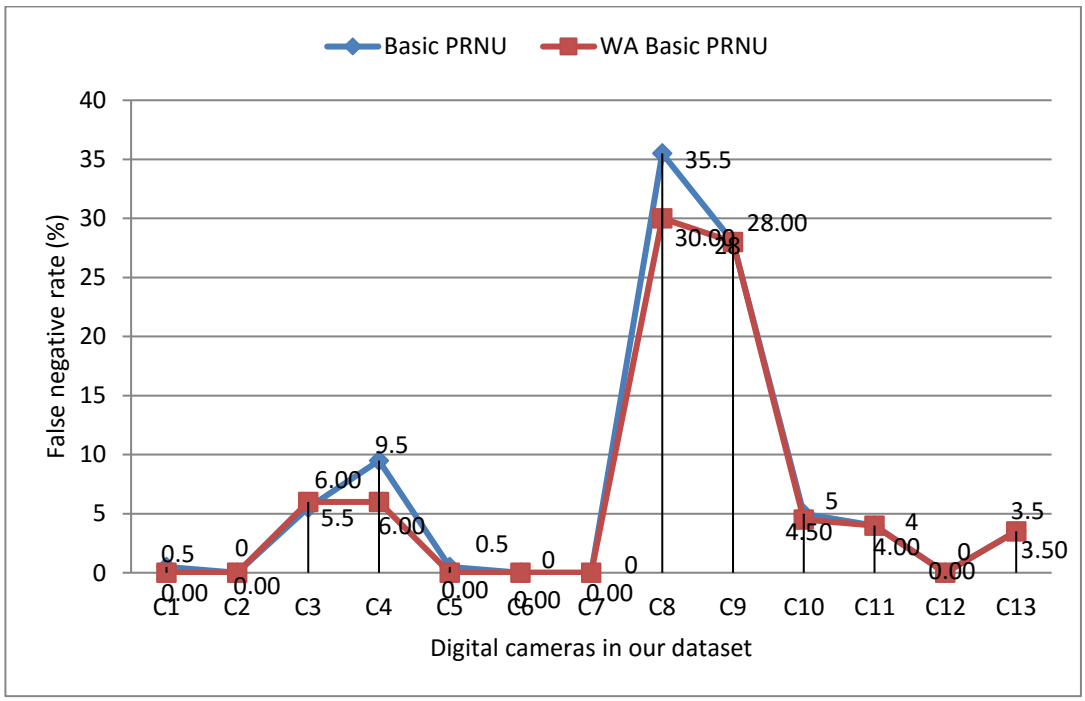

Figure 5-14 False negative rate (%) of Basic PRNU and proposed WA Basic PRNU for our dataset (image size 512×512).

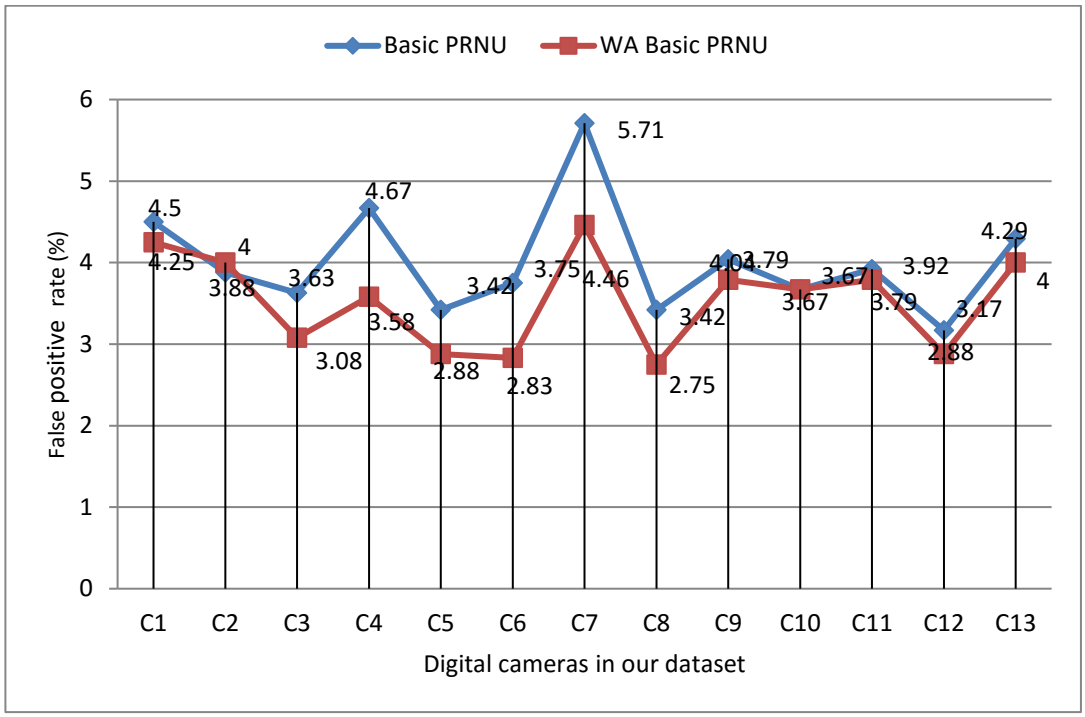

Figure 5-15 False positive rate (%) of Basic PRNU and proposed WA Basic PRNU for our dataset (image size 64×64).

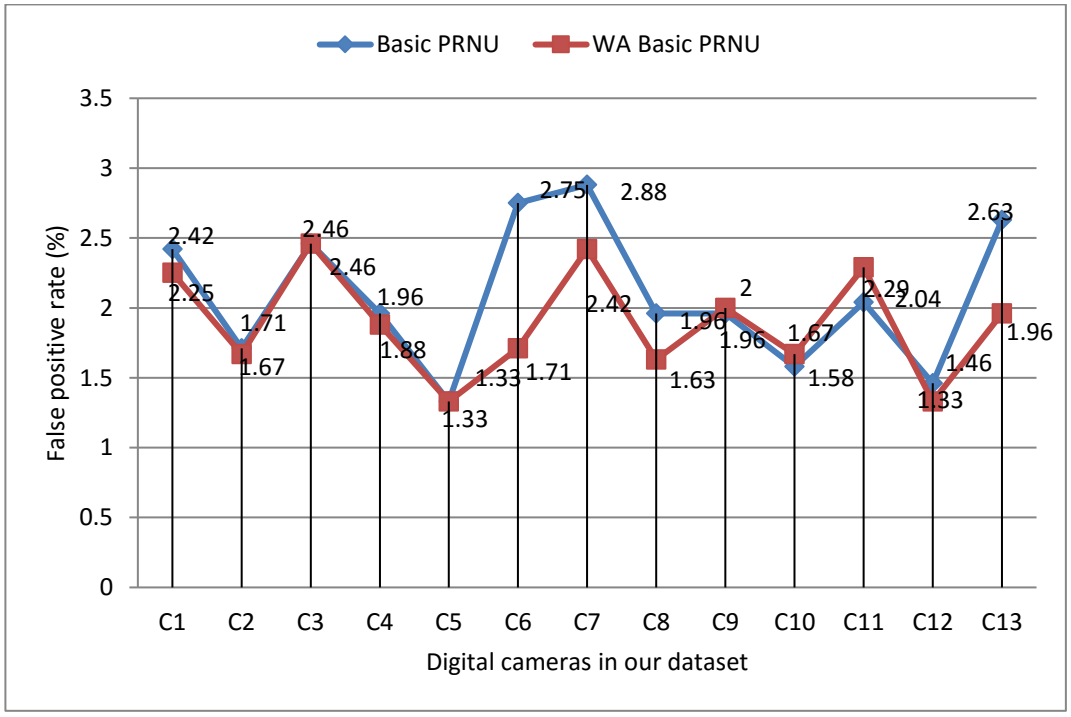

Figure 5-16 False positive rate (%) of Basic PRNU and proposed WA Basic PRNU for our dataset (image size 128×128).

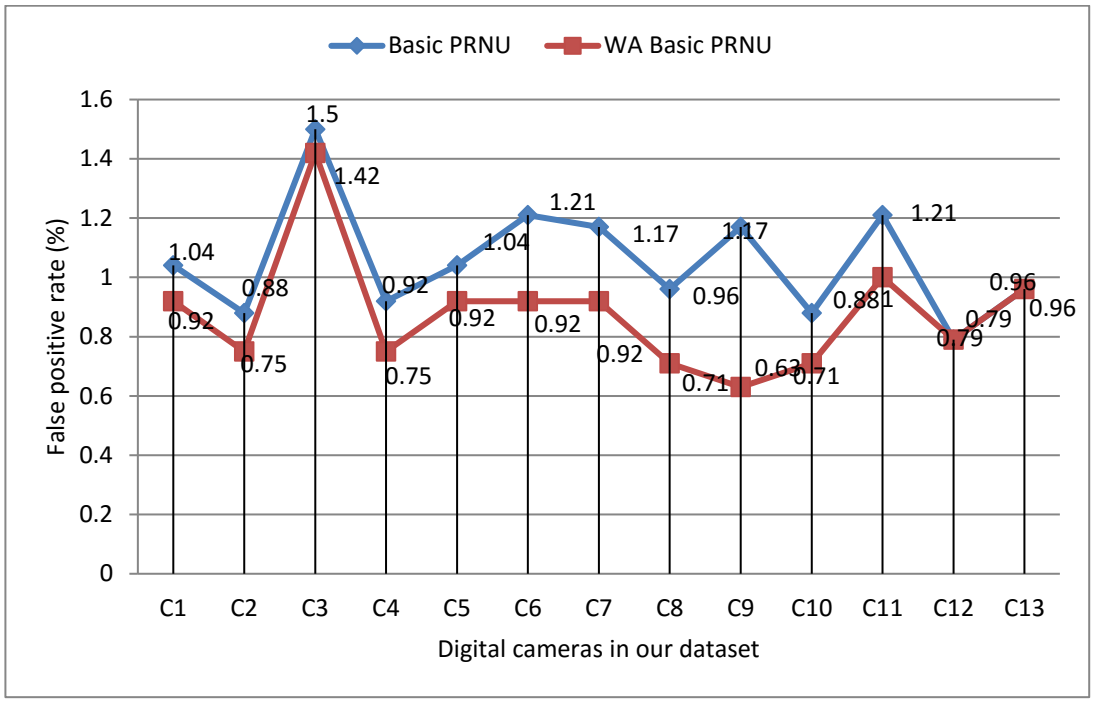

Figure 5-17 False positive rate (%) of Basic PRNU and proposed WA Basic PRNU for our dataset (image size 256×256).

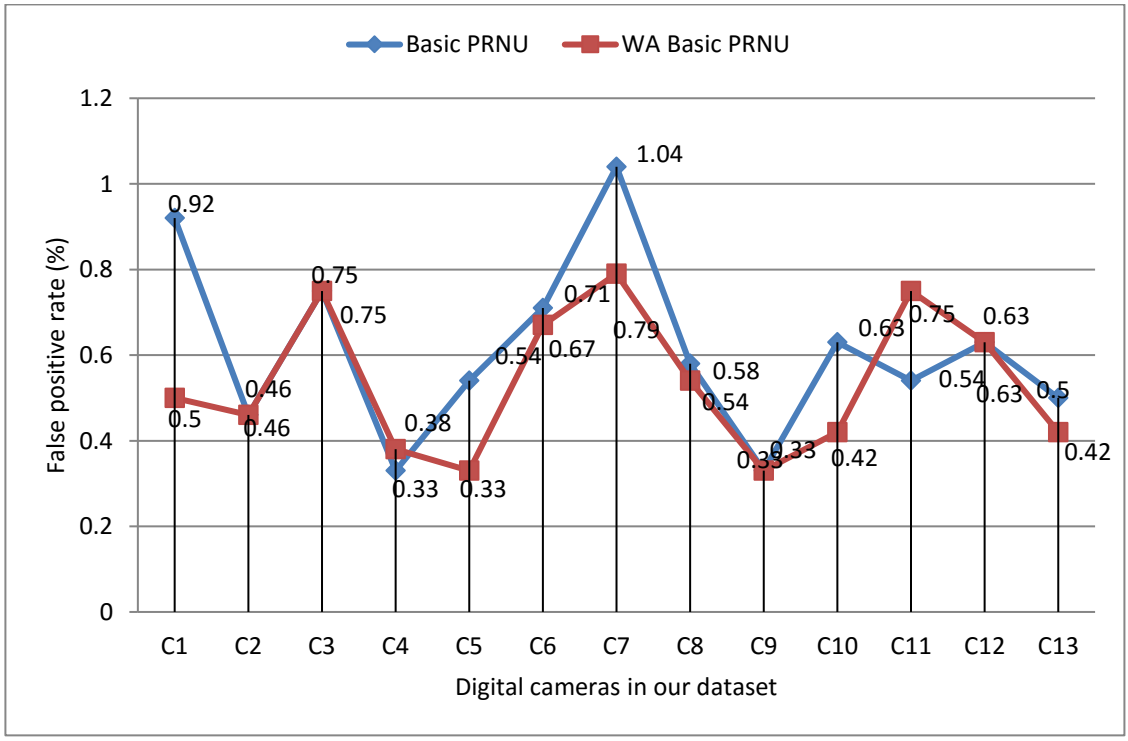

Figure 5-18 False positive rate (%) of Basic PRNU and proposed WA Basic PRNU for our dataset (image size 512×512).

Although the above figures indicate that the proposed weighted averaging does not always give an improvement for every digital camera, the overall false negative and false positive rates of the proposed WA basic PRNU technique exceeds that of the basic- PRNU. This is true for all image sizes as shown in table 5.1 and table 5.2.

Technique	FNR (%)				FPR (%)			
	Image size 64×64	Image size 128×128	Image size 256×256	Image size 512×512	Image size 64×64	Image size 128×128	Image size 256×256	Image size 512×512
basic-PRNU	52.22	30.48	11.40	2.75	5.80	3.37	1.20	0.37
WA Basic PRNU	42.13	23.73	7.44	1.69	4.64	2.62	0.92	0.20

Table 5.1 Overall FNR and FPR for each technique on Dresden dataset.

As can be observed, considerable improvements are obtained particularly with the Dresden dataset with images of sizes 64×64, 128×128, 256×256 and 512×512 where the decrease in overall false negative rate reaches 19%, 22%, 34% and 45% , while the decrease in overall false positive rate reaches 20%, 22%, 23% and 45% respectively (see table 5.1). Nonetheless, less significant improvements have been achieved with our dataset, where the overall false negative rate goes down to about 11%, 10%, 13% and 12% , and also the overall false positive rate has been reduced by approximately 11%, 10%, 15% and 11% with images of size 64×64, 128×128, 256×256 and 512×512 respectively (see table 5.2).

Technique	FNR (%)				FPR (%)			
	Image size 64×64	Image size 128×128	Image size 256×256	Image size 512×512	Image size 64×64	Image size 128×128	Image size 256×256	Image size 512×512
Basic PRNU	48.04	24.96	12.15	7.08	4.01	2.10	1.06	0.61
WA Basic PRNU	42.73	22.31	10.58	6.23	3.54	1.89	0.90	0.54

Table 5.2 Overall FNR and FPR for each technique on our dataset

5.4.2 Comparison with Constant MLE estimation

This section examines the performance of weighted averaging compared to the work of Chen *et al.* (2008). The camera reference PRNU for MLE-PRNU method is extracted as shown in equation 5.17, while the camera reference PRNU for the proposed WA MLE-PRNU method is estimated as shown in equation 5.19. For the Dresden dataset, a clear enhancement is displayed in image sizes of 64×64 and 128×128. For instance, with an image size of 64×64, the false negative rate for cameras DC1, DC3, DC5 and DC7 are decreased by 22%, 10%, 23% and 14% respectively. Furthermore, another example of a clear enhancement can be seen with the image size 128×128, especially for cameras DC1, DC7 and DC10 (see figure 5-20). Again, figure 5-21 and figure 5-22 confirm the same observation with regards to the performance of the proposed weighted averaging with image sizes of 256×256 and 512×512. For example with 256×256 the false negative rate goes down from 8.21% to 5.80%, 18.84% to 9.66%, and 13.53% to 8.21% in DC2, DC3 and DC5 respectively. In addition, with images of 512×512 improvements can be observed especially in DC3 and DC8 (see Figure 5-22). Figure 5-23-Figure **5-26** illustrate the performance of the proposed weighted averaging technique in terms of the false positive rate. A significant improvement is shown in camera DC2 with image sizes of 64×64, 128×128, 256×256, and 512×512 where the false positive rates decrease from 5.31% to 2.15, 3.22% to 0.81%, 0.91% to 0.70 % and 0.11% to 0% respectively. Additionally, with image size 128×128 the false positive rate is improved in digital cameras DC2, DC4 and DC6 to more than 50% less. However, the proposed weighted averaging technique increases the false negative rate for digital camera DC1 compared to the MLE-PRNU technique with image sizes

128×128. Also, in images of 512×512 the proposed weighted averaging technique gives unexpected results in the two digital cameras DC4 and DC7, where the false negative rate increases from 1.93% to 2.90% and 2.90% to 3.86% respectively. Another unexpected aspect of performance with an image size of 256×256 is shown in DC3 and DC7 (see figure 5-25).

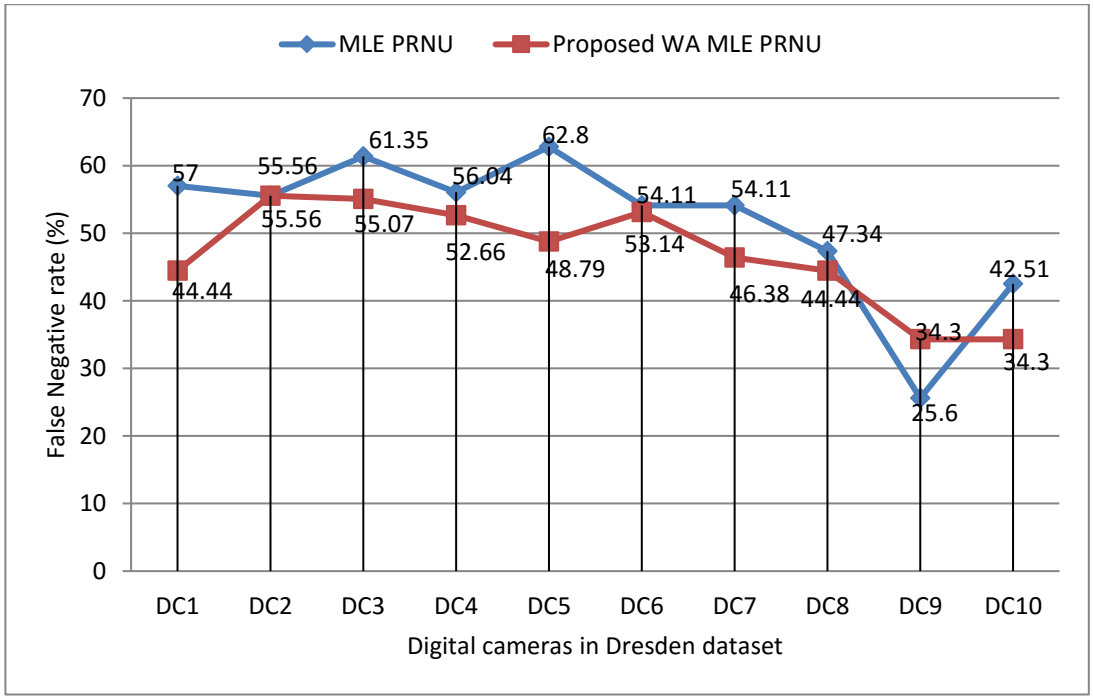

Figure 5-19 False negative rate (%) of MLE-PRNU and proposed WA MLE-PRNU for Dresden dataset (image size 64×64).

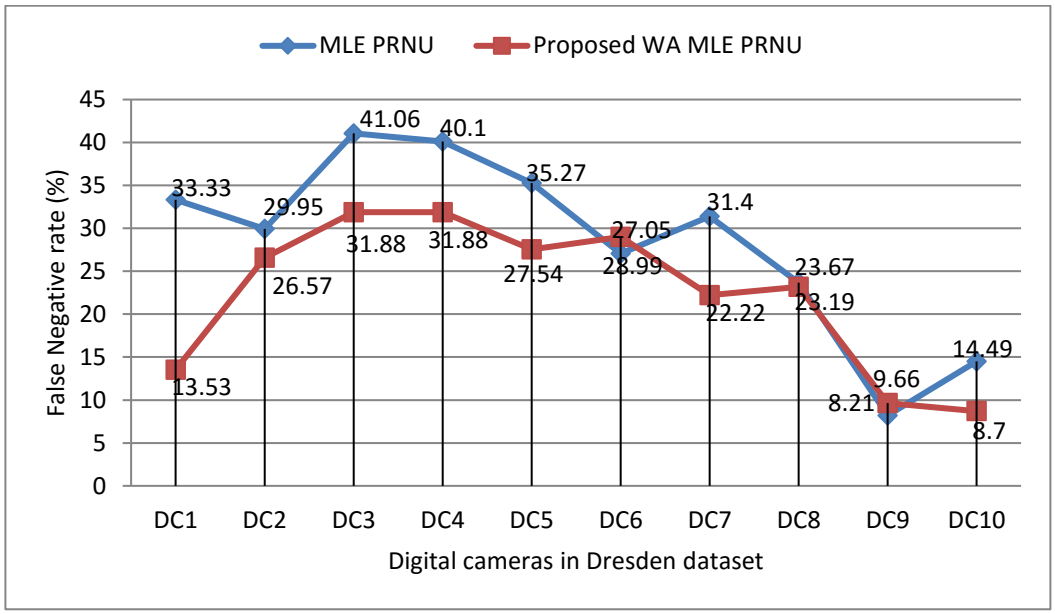

Figure 5-20 False negative rate (%) of MLE-PRNU and proposed WA MLE-PRNU for Dresden dataset (image size 128×128).

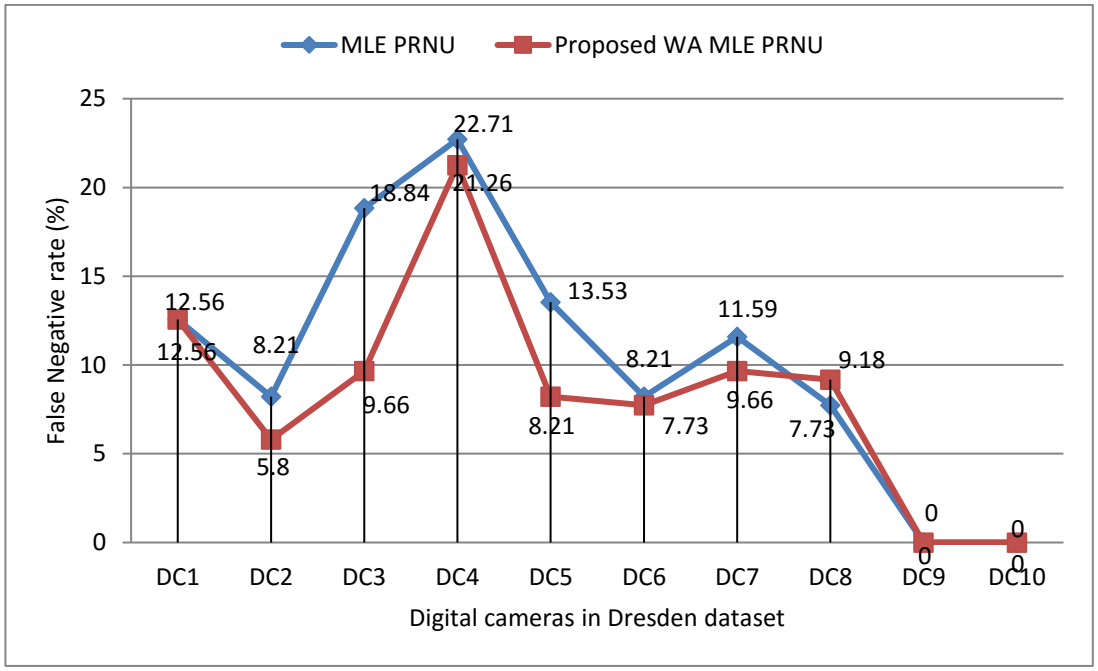

Figure 5-21 False negative rate (%) of MLE-PRNU and proposed WA MLE-PRNU for Dresden dataset (image size 256×256).

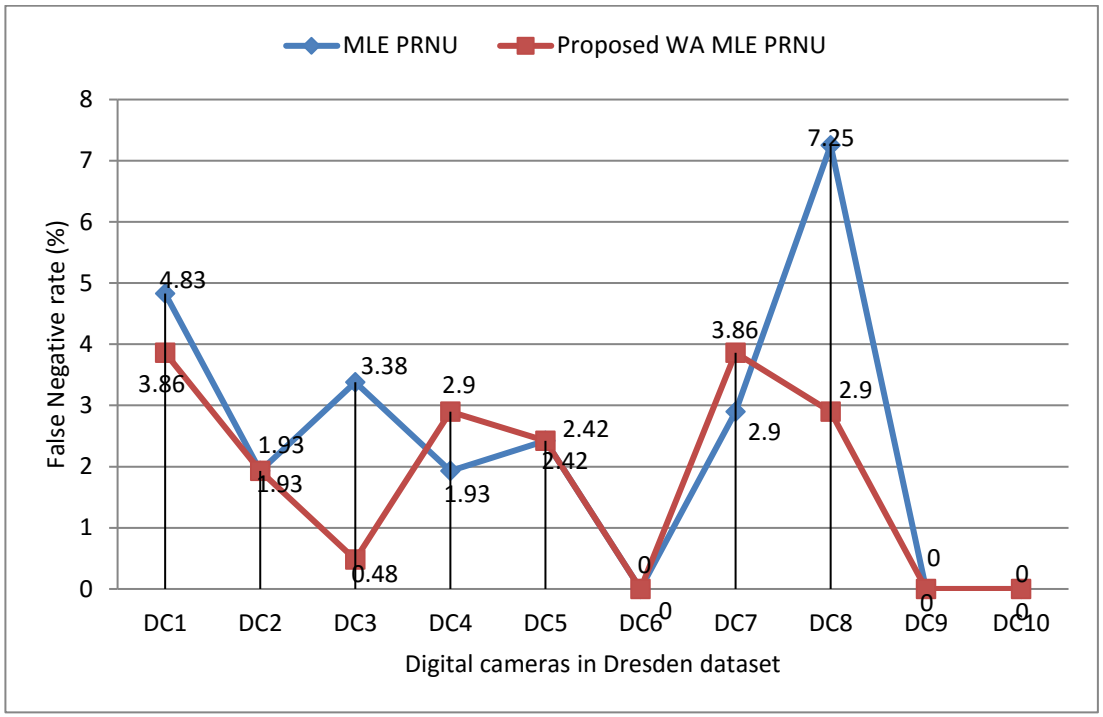

Figure 5-22 False negative rate (%) of MLE-PRNU and proposed WA MLE-PRNU for Dresden dataset (image size 512×512).

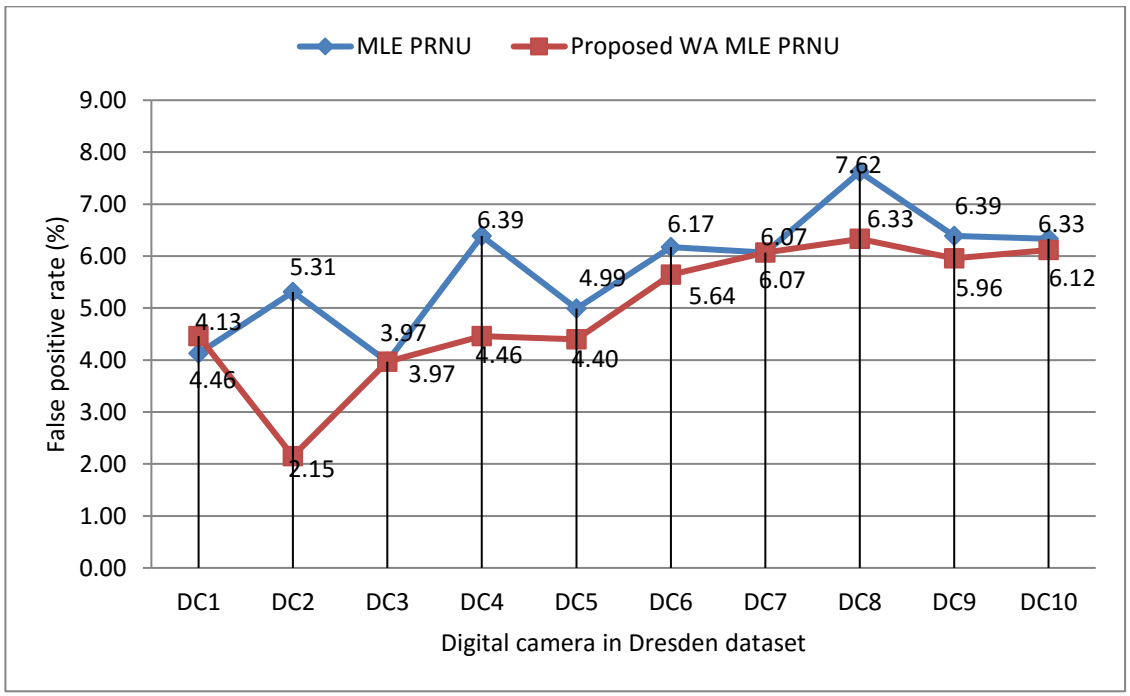

Figure 5-23 False positive rate (%) of MLE-PRNU and proposed WA MLE-PRNU for Dresden dataset (image size 64×64).

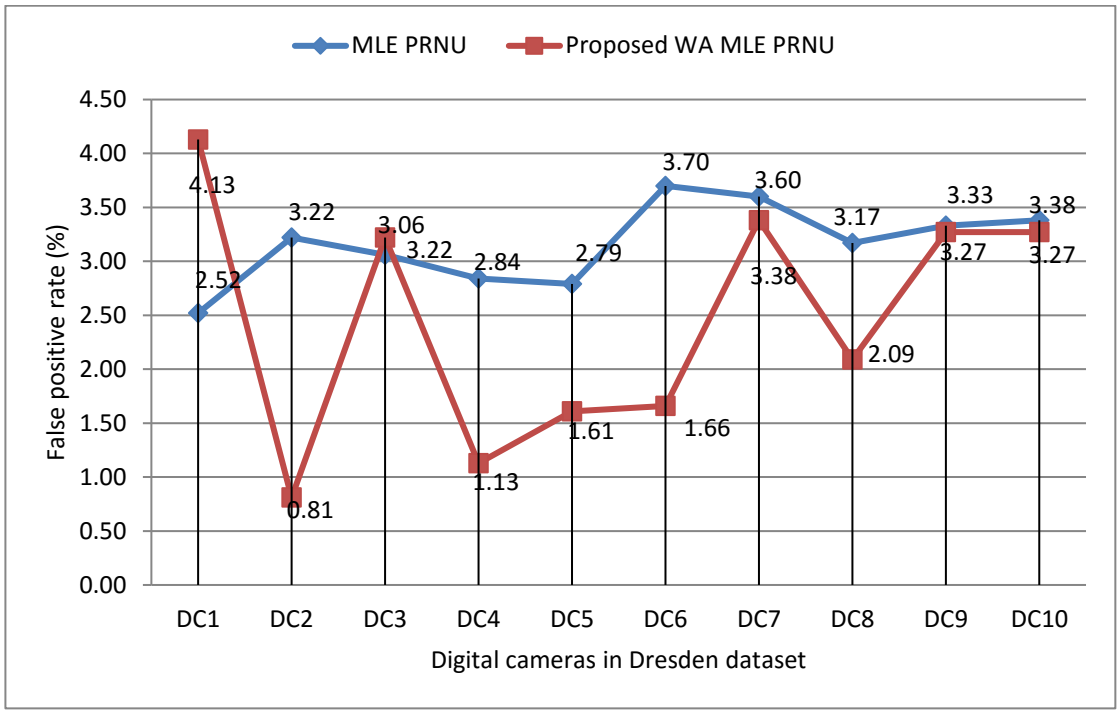

Figure 5-24 False positive rate (%) of MLE-PRNU and proposed WA MLE-PRNU for Dresden dataset (image size 128×128).

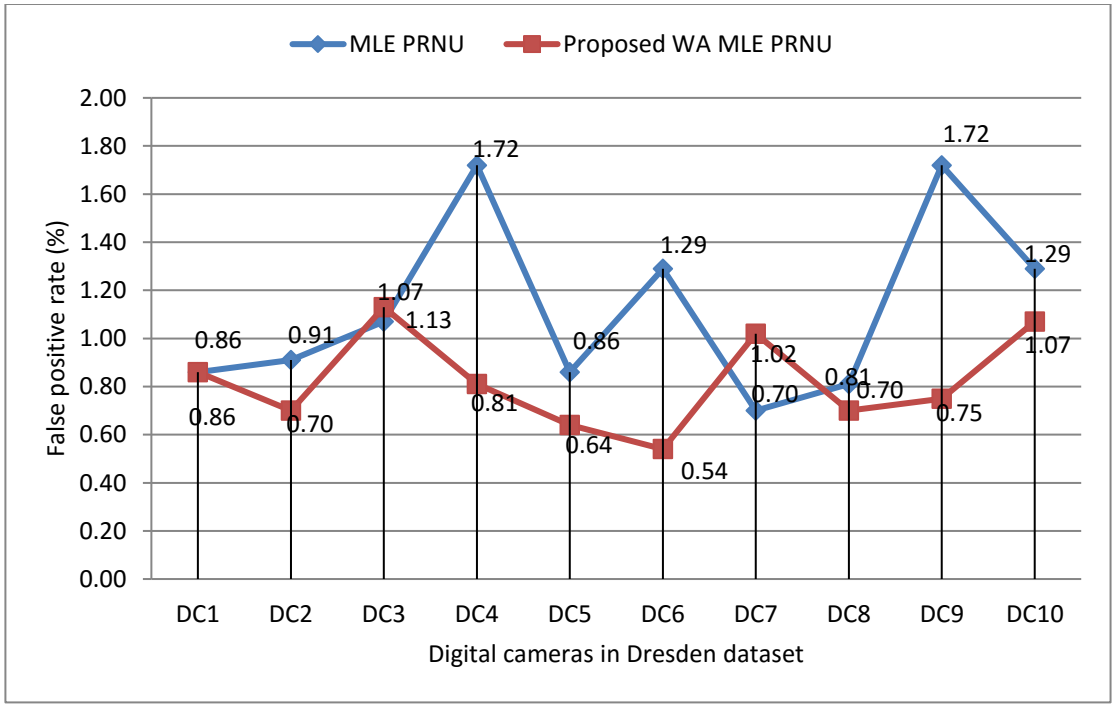

Figure 5-25 False positive rate (%) of MLE-PRNU and proposed WA MLE-PRNU for Dresden dataset (image size 256×256).

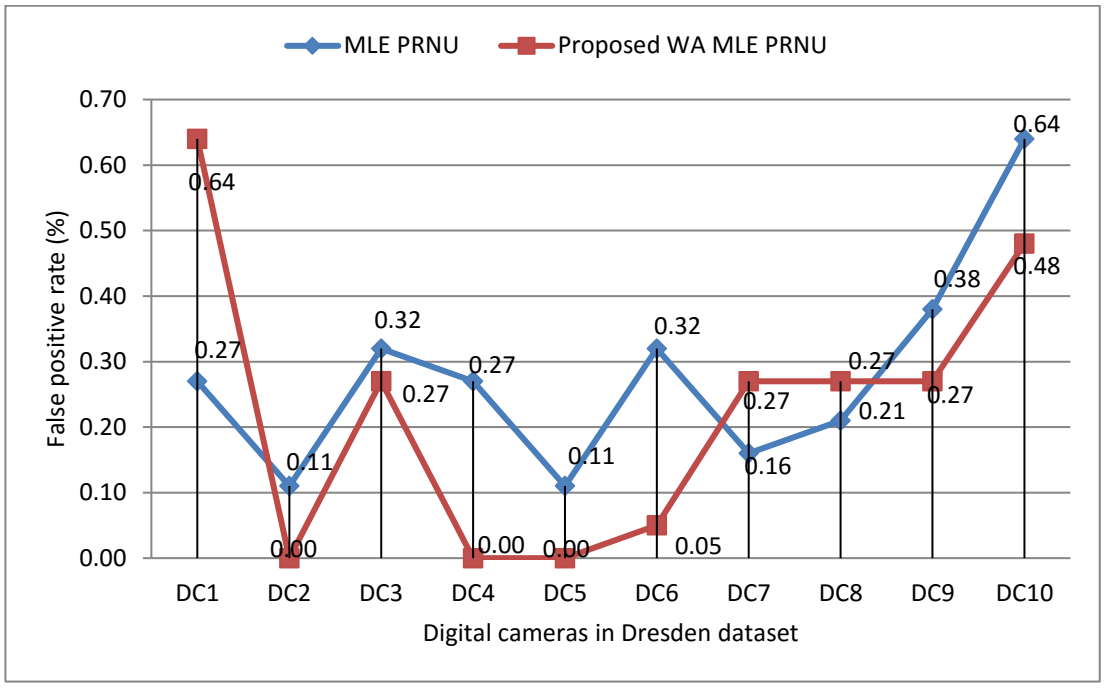

Figure 5-26 False positive rate (%) of MLE-PRNU and proposed WA MLE-PRNU for Dresden dataset (image size 512×512).

Once more, the proposed weighted averaging technique has shown some improvement with our dataset. The efficiency of the WA MLE-PRNU technique can be shown with the image size of 64×64, where the false negative and false positive rate are significantly improved in ten digital cameras out of thirteen digital (see figure 5-27 and figure 5-31). With the image size 128×128, a smaller improvement can be seen using the WA MLE-PRNU technique where the false negative and the false positive rates are decreased in many digital cameras such as in C2, C5, C6, C10 and C13 (see figure 5-28). With regards to the image size of 256×256, the results show that WA MLE-PRNU can reduce the false negative rate in the majority of digital cameras; for instance a good improvement is shown in C4, C5, C8 and C13 where the false negatives is decreased from 16.50% to 12%, 7% to 3.5%, 49.50% to 46.50%, and from

2.50% to 0.5% respectively (see figure 5-29). With the same image size of 256×256, the decrease in false positive rate reaches 10% in C1 while as shown in figure 5-33 the false positive rate decreases to more than 50% in C9, C11 and C12. Furthermore, in image size 512×512 the false positive rate is improved by using the proposed approach in most of our digital cameras (see figure 5-34). However, in limited cases the weighted averaging technique has increased the false positive rate for digital camera C3 compared to the existing MLE-PRNU technique for image sizes 64×64, 128×128 and 256×256 (see figure 5-27-figure 5-29). The interpretation could be that the C3 camera includes a tiny sensor (1/1.7"), which may lead to much undesirable noise, therefore more images should be used for PRNU estimation (kenrockwell, 2008). Beside this, in images sized 64×64 the WA MLE-PRNU technique shows a negative effect in the C2 and C4, where the increase in false positive rate reaches 5% and 7% respectively (see figure 5-31). Moreover, the C8 and C9 cameras do not show positive results in figure 5.27 and figure 5.28. The reason for such performance could be that the previous cameras belong to same model and brand camera and it includes CMOS sensor which may create more noise than the CCD (Li and Nathan, 2005)..

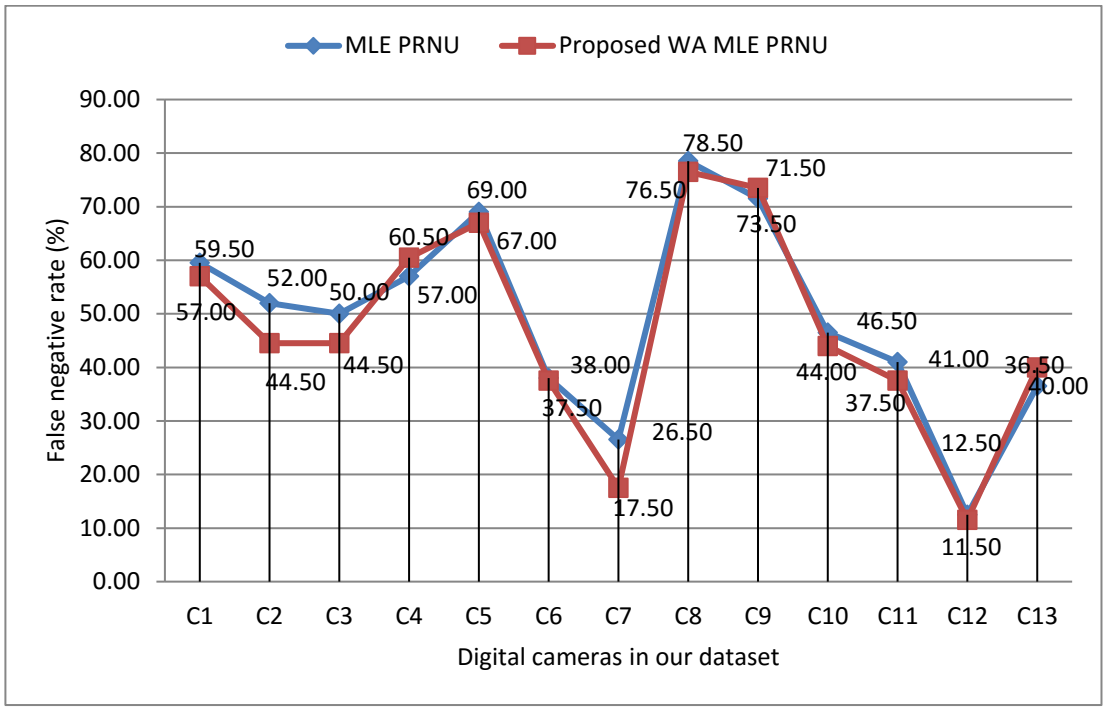

Figure 5-27 False negative rate (%) of MLE-PRNU and proposed WA MLE-PRNU for our dataset (image size 64×64).

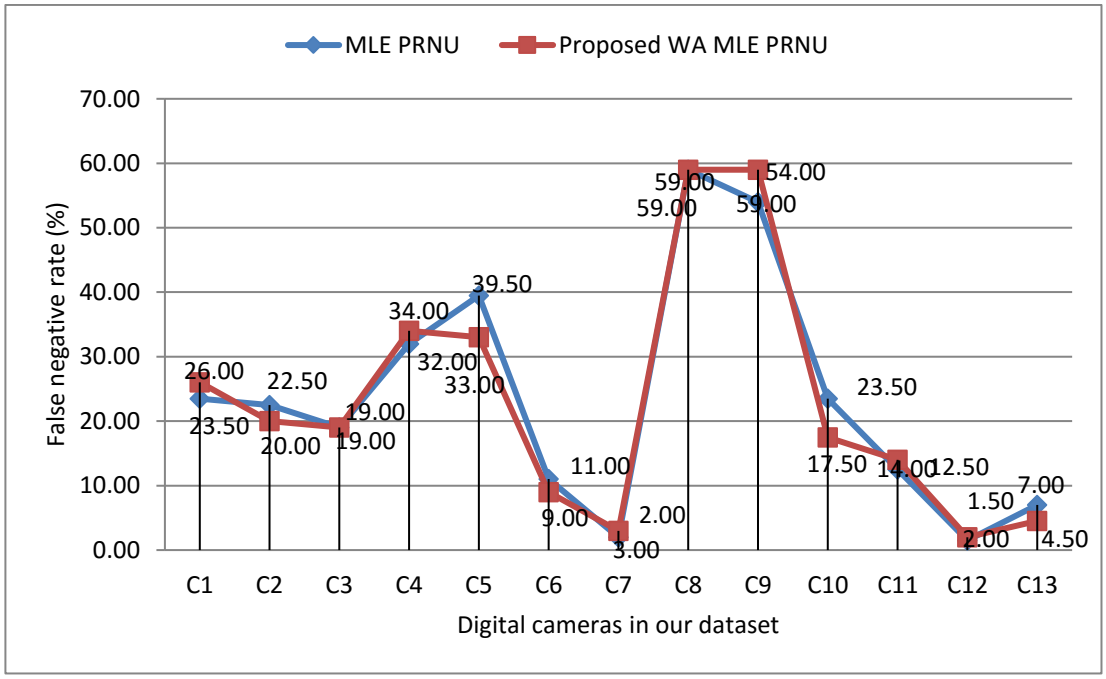

Figure 5-28 False negative rate (%) of MLE-PRNU and proposed WA MLE-PRNU for our dataset (image size 128×128).

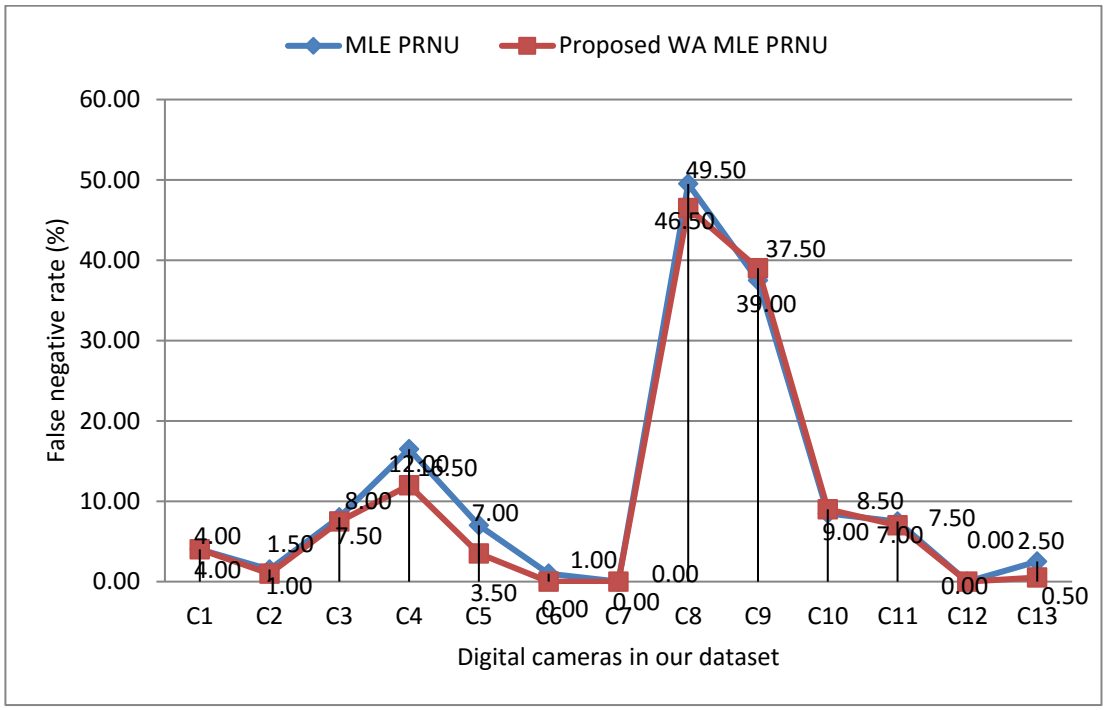

Figure 5-29 False negative rate (%) of MLE-PRNU and proposed WA MLE-PRNU for our dataset (image size 256×256).

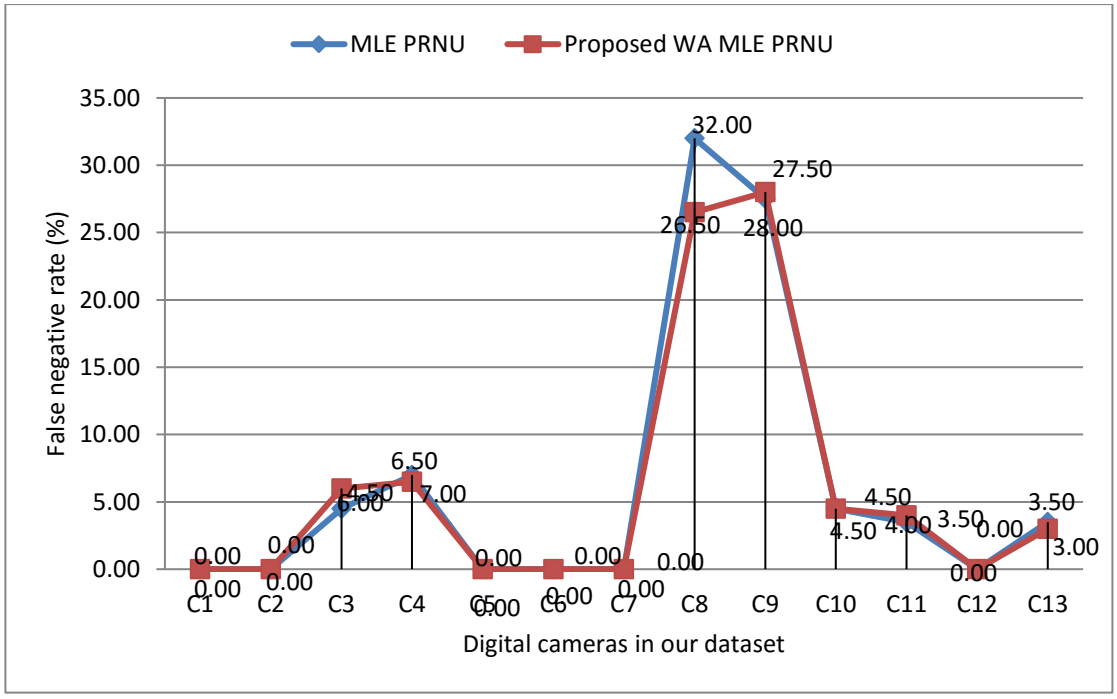

Figure 5-30 False negative rate (%) of MLE-PRNU and proposed WA MLE-PRNU for our dataset (image size 512×512).

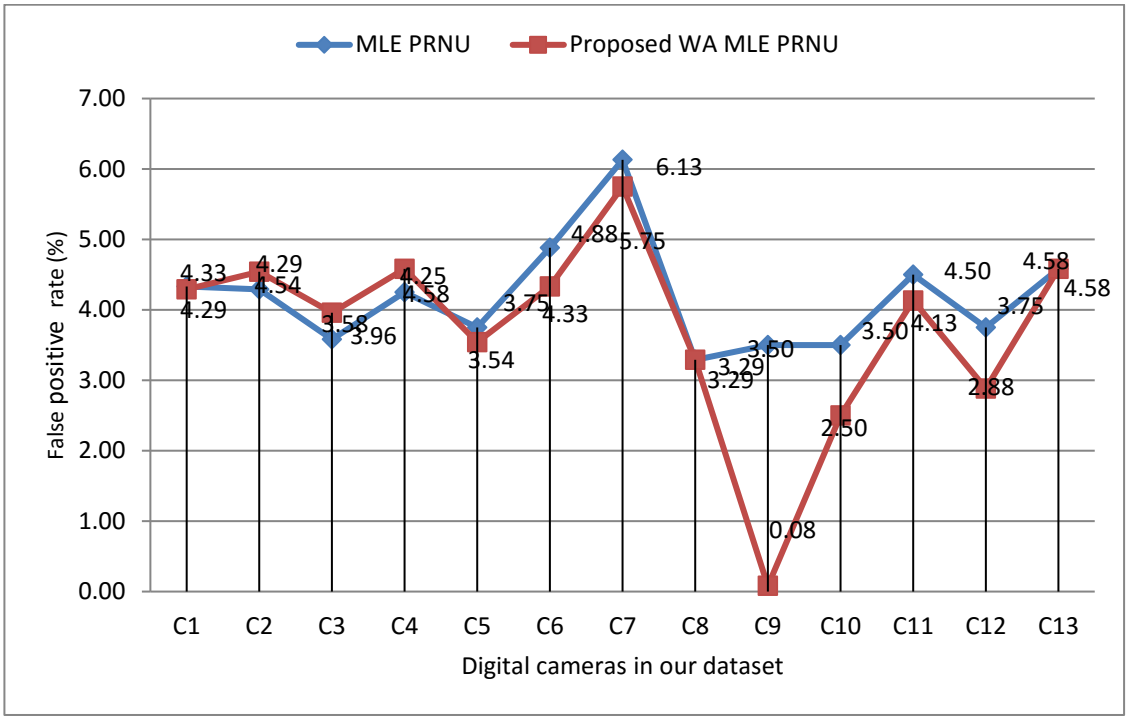

Figure 5-31 False positive rate (%) of MLE-PRNU and proposed WA MLE-PRNU for our dataset (image size 64×64).

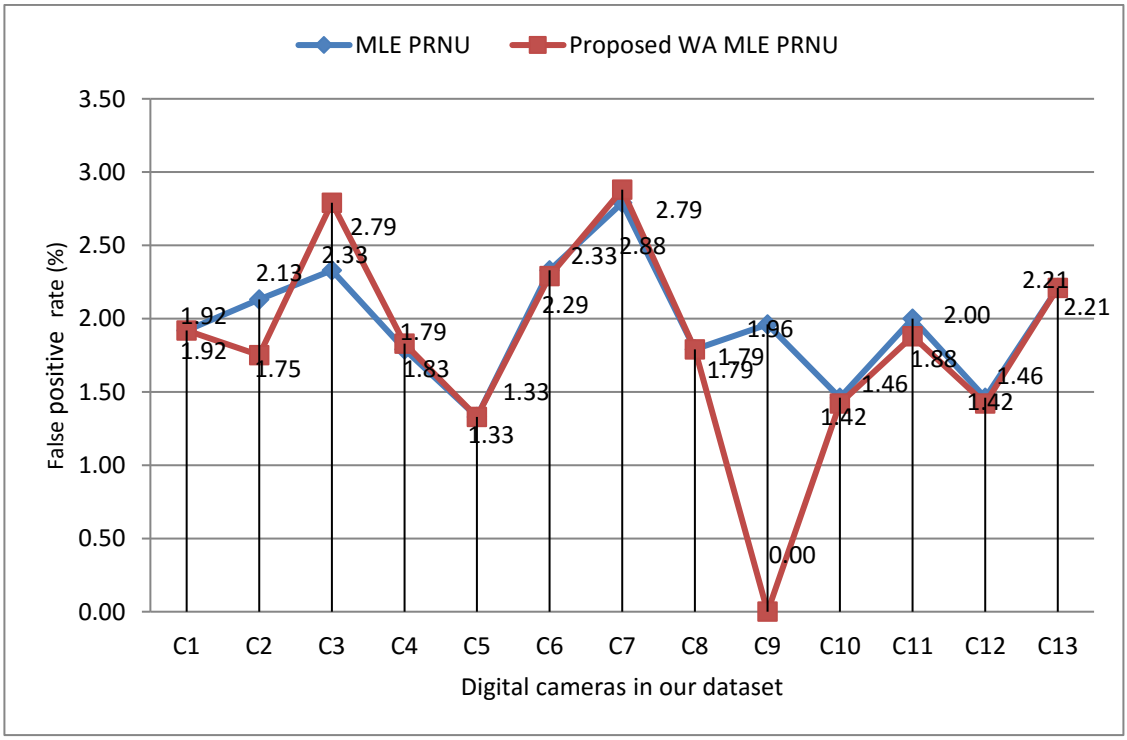

Figure 5-32 False positive rate (%) of MLE-PRNU and proposed WA MLE-PRNU for our dataset (image size 128×128).

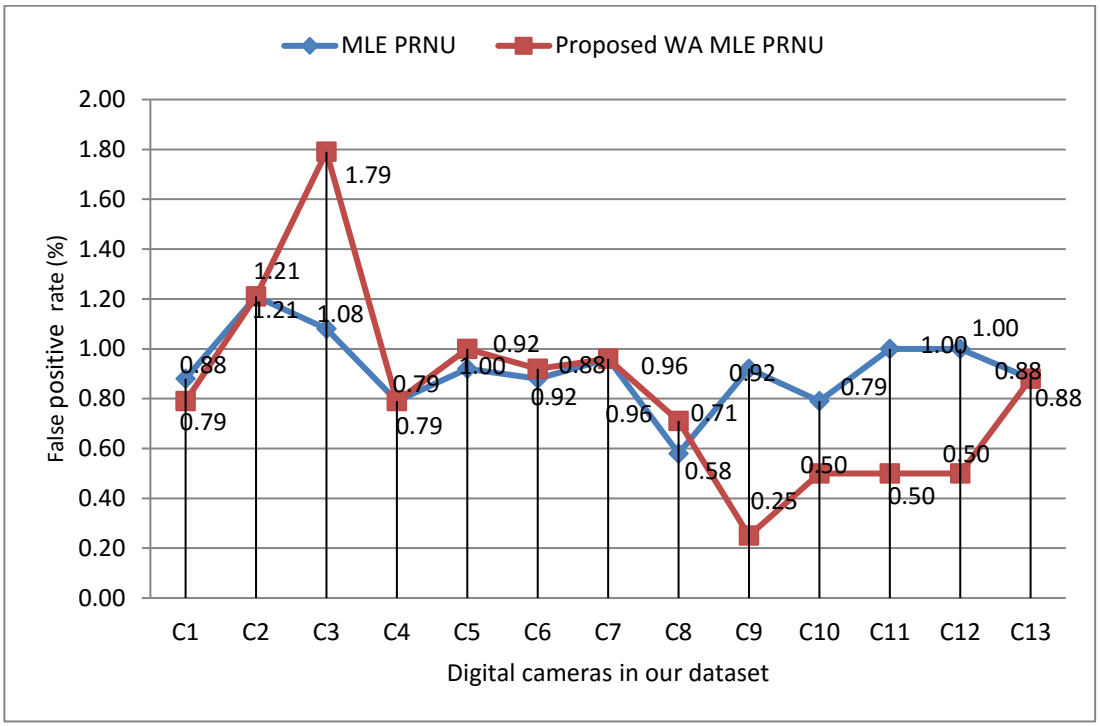

Figure 5-33 False positive rate (%) of MLE-PRNU and proposed WA MLE-PRNU for our dataset (image size 256×256).

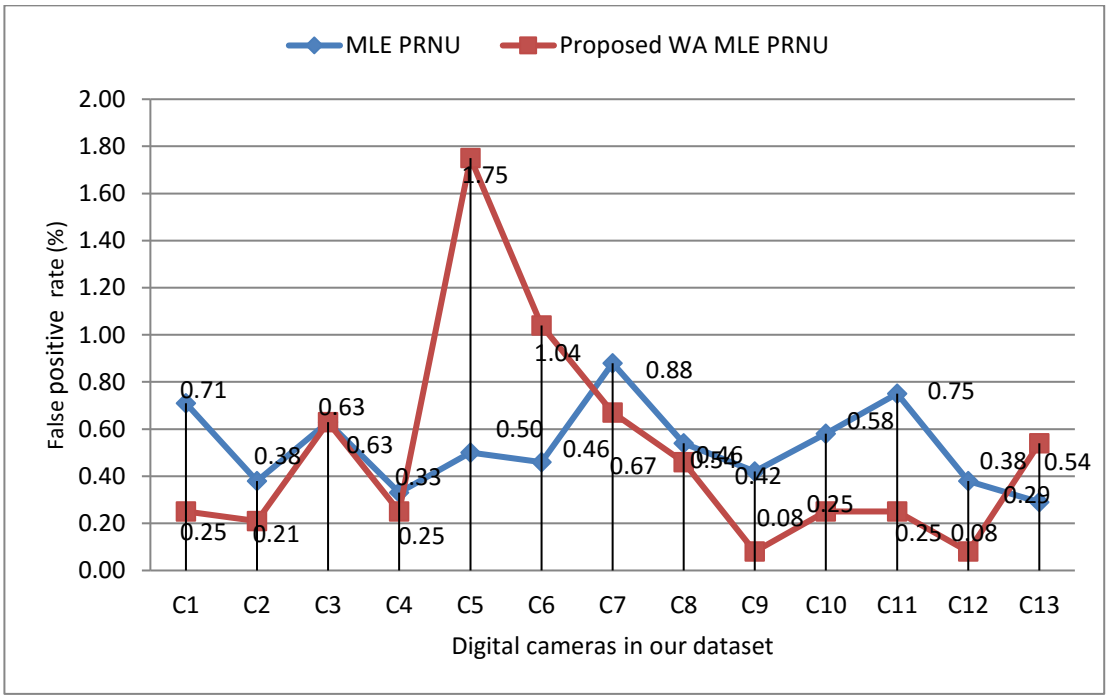

Figure 5-34 False positive rate (%) of MLE-PRNU and proposed WA MLE-PRNU for our dataset (image size 512×512).

To summarize the performance of WA MLE-PRNU and MLE-PRNU techniques, the overall false negative and false positive rates needs to be considered. The results have shown that the proposed WA MLE-PRNU can achieve better performance than MLE-PRNU in both dataset. This is true among all image sizes as shown in table 5.3 and table 5.4. As can be seen in table 5.3, significant enhancements are achieved especially on with Dresden dataset where the decrease in overall false negative rate reaches 9%, 21%, 18% and 25%, while the decreases in overall false positive rate goes down to 14%, 22%, 26% and 14% with images of sizes 64×64, 128×128, 256×256 and 512×512 respectively. Regarding our dataset, the WA MLE-PRNU technique achieves less improvement for all image sizes. The improvement in overall false negative rate moves down to more than 4%, 2%, 9% and 8%, while the overall false positive rate decreases by almost 10%, 7%, 5% and 5% with images of size 64×64, 128×128, 256×256 and 512×512 respectively (see table 5.4).

Technique	FNR (%)				FPR (%)			
	Image size 64×64	Image size 128×128	Image size 256×256	Image size 512×512	Image size 64×64	Image size 128×128	Image size 256×256	Image size 512×512
MLE-PRNU	51.64	28.45	10.34	2.46	5.74	3.16	1.12	0.28
WA MLE-PRNU	46.91	22.42	8.41	1.84	4.94	2.46	0.82	0.24

Table 5.3 Overall FNR and FPR for each technique on Dresden dataset.

Technique	FNR (%)				FPR (%)			
	Image size 64×64	Image size 128×128	Image size 256×256	Image size 512×512	Image size 64×64	Image size 128×128	Image size 256×256	Image size 512×512
MLE-PRNU	49.12	23.62	11.04	6.35	4.18	1.96	0.91	0.53
WA MLE-PRNU	47.04	23.08	10.00	6.04	3.73	1.81	0.83	0.50

Table 5.4 Overall FNR and FPR for each technique on our dataset.

5.5 Conclusion

Existing PRNU estimation techniques depend heavily on the idea of averaging residue signals estimated from a number of digital images. The residue signals can be seen as noisy observations of the PRNU. As opposed to existing studies, the proposed technique is based on weighted averaging in order to enhance PRNU estimation. This is justified by the fact that residue signals can carry noise of dissimilar variance since every instance of noise is image-dependent. The weighted averaging technique is applicable with any current PRNU estimation technique and it has been validated against two recent techniques (Basic PRNU and MLE-PRNU). Extensive experiments on two different datasets have shown that the performance of the PRNU estimation techniques for source camera identification is considerably improved with different sizes of images.

CHAPTER 6 IMPROVED LOCALLY ADAPTIVE DISCRETE COSINE TRANSFORM FILTER for SOURCE CAMERA IDENTIFICATION

6.1 Introduction

The PRNU estimation process can be faced with the presence of image-dependent information in addition to other non-unique noise components. Researchers have developed several techniques, in order to decrease such undesirable effects. For example wavelet based de-noising is one of the commonly used filtering technique for image restoration or enhancement applications and it has been recommended by researchers for better PRNU extraction. Wavelet-based denoising could perform well using criteria such as the mean squared error or peak-signal-to-noise ratio (Cooper, 2013). Nonetheless, Matsushita and Kitazawa (2009) pointed out that, using the wavelet may lead to a diffusion of the details, and edges of an image and producing a noise residue carries many disturbing signals around these areas. As a consequence, a new efficient filter is required to improve camera identification rate. Based on this observation, an improved version of the locally adaptive discrete cosine transform (LADCT) filter is proposed in this chapter, in order to improve the camera identification rate. The locally adaptive DCT filter has been originally designed by (Öktem *et al.*, 2007). This chapter is organized as follows; the advantages of the current LADCT filter are introduced in section two, and the improved version of the

LADCT fitter is presented in section three. The efficiency of the improved LADCT filter is then discussed in sections four and five. The conclusions are presented in section six.

6.2 Locally adaptive discrete cosine transform (LADCT)

The discrete cosine transform (DCT) has generally been used in image processing applications including feature extraction, quality assessment, filtering, and compression (Kurkin *et al.*, 2012). The locally adaptive DCT filter (LADCT) has a number of advantages compared to other filters that operate on full images, such as wavelets and it is claimed to perform well on images affected by image-dependent noise including the multiplicative noise (Öktem *et al.*, 2007). This provides a logical reason for adopting this filter because the PRNU is also multiplicative. The LADCT filter is also different from wavelet filters in that , it operates on sliding blocks (local action filter), which might provide more information about the spatial correlation properties of noise in an easier method (Ponomarenko *et al.*, 2008). Furthermore, Lukin *et al.* (2010) reported that the LADCT can perform well with several noise models such as film-grain and Poisson types. In addition, averaging several de-noised estimates for each pixel in the block will overcome the problem of undershoots and overshoots which occur around the neighborhood of discontinuities as a result of the Gibbs Phenomenon (Coifman and Donoho, 1995) and this is directly linked to the problem of scene details in PRNU estimation. Öktem *et al.* (2007) proposed the LADCT filter for a type of noise that may contaminate the signal through a multiplicative rule. The authors used a sliding block window in order to gain de-noised

estimates of neighbouring and overlapping blocks. The multiple estimates can then be averaged to suppress artefacts produced by undershoots and overshoots around the highly textured regions (Ponomarenko *et al.*, 2008). The threshold for every block is based on the local mean of the block and the local noise variance. In the rest of the thesis, the filter of Öktem *et al.* (2007) is referred to as LADCT_1. Due to the present concern with the estimation of PRNU, which is a multiplicative type of noise, for camera source identification, the advantages of the LADCT_1 filter are exploited in order to improve PRNU estimation. To the best of the present author's knowledge, this filter has not yet been applied in the field of image forensics. The main steps of LADCT_1 are summarized below.

- The digital image is first divided into blocks of $N \times N$. Let S be a shift in pixels ($S = 1$) row or column-wise between two neighbouring blocks. According to Öktem *et al.* (2007), the best performance of the LADCT filter could be reached when S=1 and N=8 (This is why the number 1 is included in the notation of LADCT_1).
- For every block x, with the upper left corner at (m,l), the DCT coefficients can be computed as:

$$B(p,q) = c(p)c(q) \times \sum_{\mathrm{m}=0}^{\mathrm{N}-1} \sum_{\mathrm{l}=0}^{\mathrm{N}-1} \mathrm{b}(\mathrm{m},\mathrm{l}) \cos\left(\frac{(2\mathrm{m}+1)\mathrm{p}\pi}{2\mathrm{N}}\right) \cos\left(\frac{(2\mathrm{l}+1)\mathrm{q}\pi}{2\mathrm{N}}\right) \qquad 6.1$$

where

$$c(p) = \begin{cases} \sqrt{\frac{2}{N}} & 1 \leq p \leq N-1, \\ \frac{1}{\sqrt{N}} & p = 0, \end{cases}$$

$$c(q) = \begin{cases} \sqrt{\frac{2}{N}} & 1 \leq q \leq N-1, \\ \frac{1}{\sqrt{N}} & q = 0, \end{cases}$$

- A hard threshold is applied for each DCT coefficient X(p, q) as follows:

$$B'(p,q) = \begin{cases} \mathrm{B(p,q)}, & \text{if } |\mathrm{B(p,q)}| > T_1 \\ 0, & \text{Otherwise} \end{cases} \quad 6.2$$

- The threshold for each block can be computed as:

$$T_1 = k \,.\, \sigma_c \,.\, \bar{g} \quad 6.3$$

where k is a constant value to control the threshold value and it has been found empirically to be equal to 2.6, $\bar{\mathrm{g}}$ denotes the local mean for that block, and σ_c represents the noise standard deviation.

- The inverse DCT can be applied as:

$$b'(m,l) = c(p)c(q) \times \sum_{p=0}^{N-1} \sum_{q=0}^{N-1} B'(p,q) \cos\left(\frac{(2m+1)\,p\pi}{2N}\right) \cos\left(\frac{(2l+1)q\pi}{2N}\right) \quad 6.4$$

- The final estimate for a pixel at (*m*,*l*) can be computed by averaging the multiple estimates at the same location which were gained from overlapping blocks due to the shifting process. Figure 6-1 shows the process of estimating the PRNU based on the original LADCT_1 as proposed in work of Öktem *et al.* (2007).

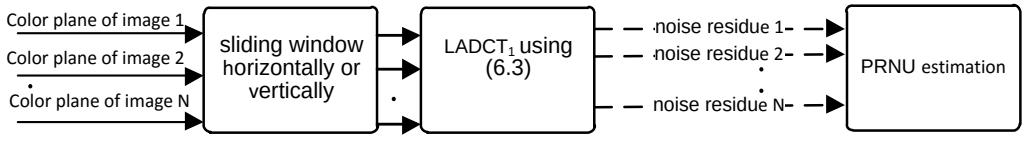

Figure 6-1: Estimating the PRNU based on original LADCT_1.

6.3 Improved LADCT for source camera identification

It is worth pointing out that the idea underlying LADCT_1 assumes that the multiplicative noise is stationary for every block with similar statistical means. That is, the standard deviation of the noise σ_c used in equation 6.3 is assumed to be constant. Nonetheless, the PRNU cannot be stationary as it depends on the homogeneity of the silicon in the imaging device sensor. It is consequently more sensible to suppose that the variance of the PRNU would differ particularly through blocks of small size (8×8). In order to adjust the LADCT_1 filter for PRNU estimation, an improved version of the filter is therefore proposed.

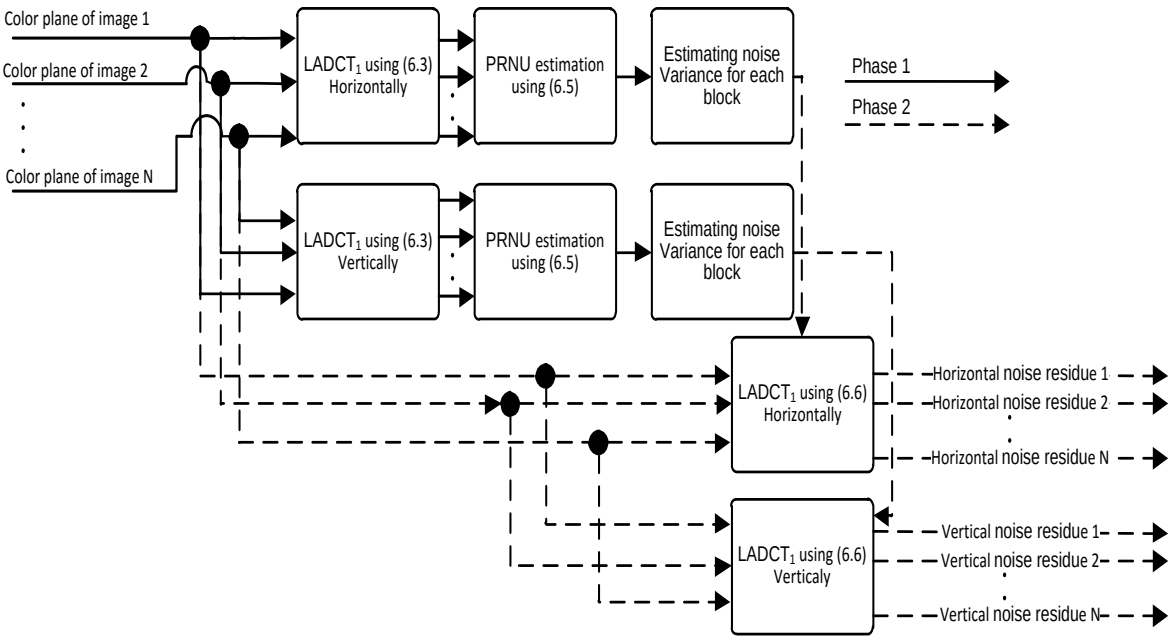

Figure 6-2 Extraction of noise residues corresponding to a single color plane for PRNU estimation based on improved LADCT1

As demonstrated in figure 6-2, two improvements of the LADCT_1 are proposed. The first improvement relies on estimating the noise variance for each block independently using the threshold as described in the previous section (steps 1-6). This is used to estimate a block-dependent threshold which will be applied in another stage of the LADCT_1 filtering. The proposed technique for estimating a threshold for each block contains two steps as follows:

Step 1:

Let us define an estimate of the sensor pattern noise K (see equation 1.3) as.

$$\widehat{K} = \frac{\sum_{i=1}^{N}\left(I_i - f(I_i)\right)}{\sum_{i=1}^{N} f(I_i)} \qquad 6.5$$

where I_i is the i^{th} observed image and $f(I_i)$ represents its filtered version with the conventional LADCT_1 where σ_c^2 = 0.002. Then,

Step 2:

The following threshold is proposed for each block *b* as

$$T_b = \propto \sqrt{\frac{\sigma_{\widehat{K}}^2}{\sigma_{\widehat{K}_b}^2} E[b^2]} \qquad 6.6$$

where α is a constant which could be determined empirically. $\sigma_{\widehat{K}}^2$ is the variance of the estimated PRNU $\widehat{K}$ as described in equation 6.5 and $\sigma_{\widehat{K}_b}^2$ is the variance of the estimated noise within the block b. $E[b^2]$ is the second moment of the block. The idea underlying such a threshold value is based on the fact that the statistical variance of the estimated noise might differ significantly across blocks. Hence, blocks in which the estimated noise has high variance should be filtered with a relatively small threshold in

the DCT domain to retain the image content because the high activity of the estimated noise in such blocks could be likely from texture and edges. On the other hand, low variance noise within a block might well represent the actual PRNU and therefore should be filtered out with a relatively large threshold in the DCT domain. $\sigma_{\hat{K}}^2$ is used in the ratio as a reference in order to measure the extent to which the estimated noise has high or low activity in a specific block. Finally, the second moment in equation 6.6 allows bright regions to be exploited more than dark ones, as the multiplicative nature of the PRNU means that its presence is stronger in bright regions. Regarding the second technique of enhancement, it is worth mentioning that the LADCT_1 filter was initially used by Öktem *et al.* (2007) in just one direction. This might be a reasonable process for image de-noising purposes because the size of the filtered image must be the same as the original. Nonetheless, in our application we can have two versions of the filtered image and hence two PRNUs, each estimated in one direction (horizontal and vertical). The logic behind this process is to increase the size of the PRNU camera reference and noise residue in order to decrease the probability of false alarms (i.e. reducing the similarity among different camera PRNUs and noise residues). Indeed, there might be some components of the PRNU that can be difficult to estimate in the horizontal direction but which are estimable in the vertical direction and vice versa. The LADCT_1H & V refers to the combination of the PRNUs in the horizontal and vertical directions.

6.4 Analysis of enhanced LADCT_1 filtering

In this section, the advantages of the proposed enhancements to the conventional LADCT_1 (Öktem *et al.*, 2007) for source camera identification are demonstrated. The evaluation has been conducted using our dataset and the Dresden database. In this experimental evaluation, each PRNU is estimated from 50 natural images (green channel) captured by the same sensor. To evaluate the performance of the filter and its improved versions, the false negative rate (FNR) and false positive rate (FPR) are calculated. Note that constant averaging is used to obtain the PRNU in this section which only and compares the results of the improved LADCT with those of the wavelet filter as described in the work of Lukas *et al.* (2006). With regards to the conventional LADCT_1, the noise variance for each image block is constant. In order to derive the optimal parameter setting for LADCT_1 for both datasets, different values of variance σ^2 are tested in the two datasets. Table 6.1 and table **6.2** respectively show that the best results for overall FNR and overall FPR correspond to a value of σ^2 equal to 0.002.

Noise variance for each block	Overall FNR (%)			Overall FPR (%)		
	Image size 128×128	Image size 256×256	Image size 512×512	Image size 128×128	Image size 256×256	Image size 512×512
0.012	42.38	19.81	9.50	3.53	1.65	0.79
0.007	35.54	16.42	8.81	2.96	1.37	0.73
0.004	32.96	14.77	7.81	2.75	1.24	0.65
0.002	**29.50**	**14.62**	**7.38**	**2.46**	**1.22**	**0.62**
0.001	30.15	14.73	7.42	2.48	1.24	**0.62**

Table 6.1 Overall FNR and FPR with constant noise variance for our dataset.

Noise variance for each block	Overall FNR (%)			Overall FPR (%)		
	Image size 128×128	Image size 256×256	Image size 512×512	Image size 128×128	Image size 256×256	Image size 512×512
0.012	55.80	31.06	12.13	6.20	3.45	1.35
0.007	48.12	24.40	8.31	5.35	2.71	0.92
0.004	41.64	18.99	5.56	4.63	2.11	0.62
0.002	**36.47**	**16.28**	**5.41**	**4.05**	**1.79**	**0.60**
0.001	37.00	16.60	**5.41**	4.14	1.85	0.61

Table 6.2 Overall FNR and FPR with constant noise variance for the Dresden dataset

The results of the false negative and false positive rate based on constant noise variance for each digital camera is shown in appendix A. Regarding the improved LDACT filter, table 6.3 and table 6.4 summarize the camera identification performance by using LADCT_1 in the horizontal and vertical directions denoted here to as LADCT_1H&V, as well as the improvement of the proposed enhancement using block-based noise variance (i.e. block-based σ^2). As can be seen, the proposed enhancements significantly reduce the overall false negative and the false overall positive rates when compared with the conventional LADCT_1 filter.

Filter	Overall FNR (%)			Overall FPR (%)		
	Image size 128×128	Image size 256×256	Image size 512×512	Image size 128×128	Image size 256×256	Image size 512×512
Conventional filter (LADCT_1H with constant $\boldsymbol{\sigma^2}$)	29.50	14.62	7.38	2.46	1.22	0.62
LADCT_1H&V with constant $\boldsymbol{\sigma^2}$	24.85	12.77	6.92	2.07	1.06	0.58
LADCT_1H with block based $\boldsymbol{\sigma^2}$	27.96	13.58	7.12	2.33	1.13	0.59
LADCT_1H&V with block based $\boldsymbol{\sigma^2}$	**23.65**	**12.04**	**6.77**	**1.97**	**1.00**	**0.56**

Table 6.3 Overall FNR and FPR for each LADCT filter technique for our dataset.

Filter	Overall FNR (%)			Overall FPR (%)		
	Image size 128×128	Image size 256×256	Image size 512×512	Image size 128×128	Image size 256×256	Image size 512×512
Conventional filter (LADCT_1H with constant $\boldsymbol{\sigma^2}$)	36.47	16.28	5.41	4.05	1.79	0.60
LADCT_1H&V with constant $\boldsymbol{\sigma^2}$	29.71	11.21	3.57	3.30	1.25	0.40
LADCT_1H with block base $\boldsymbol{\sigma^2}$	33.14	13.77	4.69	3.68	1.53	0.52
LADCT_1H&V with block based $\boldsymbol{\sigma^2}$	**25.75**	**9.23**	**2.61**	**2.86**	**1.05**	**0.32**

Table 6.4 Overall FNR and FPR for each filter technique (Dresden dataset).

In our dataset the overall false negative rate for different image sizes is reduced from 29.50%, 14.62% and 7.38% using the conventional LADCT_1H with constant σ^2 to 23.65%, 12.04% and 6.77% respectively when using the proposed LADCT_1H&V with block based σ^2. Also the decrease in overall false positive rate reaches 19%, 18%, and 9% with image sizes equal to 128×128, 256×256 and 512×512 respectively (see table 6.3). Regarding the Dresden dataset, a significant improvement is shown in table 6.4, where the enhancement of the overall false negative and false positive rates compared to conventional LADCT_1H with constant σ^2 is more than 29%, 43%, and 51% with image sizes of 128×128, 256×256 and 512×512 respectively (see table 6.4). The improvements due to the proposed filter based on each digital camera, and for and both datasets are shown in table 6.5- table 6.8.

Image size	Filter	C1	C2	C3	C4	C5	C6	C7	C8	C9	C10	C11	C12	C13
128×128	LADCT_1H with constant σ^2	33.00	24.50	22.50	40.50	48.00	10.50	6.00	71.50	63.00	28.50	20.50	1.50	13.50
	LADCT_1H&V with constant σ^2	22.50	16.00	16.00	33.00	38.00	9.00	3.00	72.00	61.50	23.00	18.00	1.00	10.00
	LADCT_1H with block base σ^2	26.50	22.50	19.50	36.00	48.00	10.50	6.50	71.00	61.50	26.50	19.50	3.00	12.50
	LADCT_1H&V with block based σ^2	20.00	15.00	12.50	33.00	40.00	9.00	4.00	71.00	56.50	20.00	18.00	1.00	7.50
256×256	LADCT_1H with constant σ^2	10.00	3.00	8.00	17.00	16.50	2.50	1.50	58.00	51.00	10.50	9.00	0.00	3.00
	LADCT_1H&V with constant σ^2	7.00	2.00	8.00	16.50	13.50	2.00	0.50	53.50	43.50	9.50	7.50	0.00	2.50
	LADCT_1H with block base σ^2	8.50	1.50	9.50	17.50	14.50	3.50	0.50	54.00	46.00	11.00	7.50	0.00	2.50
	LADCT_1H&V with block based σ^2	7.00	1.50	8.50	17.00	11.50	2.50	0.50	50.00	38.00	11.00	6.50	0.00	2.50
512×512	LADCT_1H with constant σ^2	1.00	0.00	7.00	10.50	0.50	0.00	0.00	35.50	29.00	6.00	3.50	0.00	3.00
	LADCT_1H&V with constant σ^2	1.00	0.00	6.00	9.00	0.50	0.00	0.00	33.50	27.00	5.50	3.50	0.00	4.00
	LADCT_1H with block base σ^2	1.00	0.00	7.50	11.00	0.50	0.00	0.50	32.50	28.00	6.00	3.00	0.00	2.50
	LADCT_1H&V with block based σ^2	1.00	0.00	6.00	9.00	0.00	0.00	0.00	32.00	26.50	6.50	3.50	0.00	3.50

Table 6.5 False negative rate for each digital camera using different LADCT filter methods (our dataset).

Image size	Filter	C1	C2	C3	C4	C5	C6	C7	C8	C9	C10	C11	C12	C13
128×128	(LADCT_1H with constant σ^2)	2.04	2.38	2.58	2.21	2.00	2.58	3.08	2.08	2.75	2.21	3.13	2.04	2.88
	LADCT_1H&V with constant σ^2	1.58	1.92	2.08	2.00	1.38	2.04	2.71	1.83	2.00	2.33	2.29	2.08	2.67
	LADCT_1H with block base σ^2	2.13	2.50	2.50	2.17	1.71	2.46	3.13	2.08	2.33	2.00	2.42	2.38	2.50
	LADCT_1H&V with block based σ^2	2.08	1.83	1.67	1.92	1.17	1.88	2.71	1.42	1.83	1.79	2.63	2.38	2.38
256×256	(LADCT_1H with constant σ^2)	1.25	1.21	1.54	1.42	1.13	0.92	1.33	1.04	1.04	1.33	1.21	1.33	1.08
	LADCT_1H&V with constant σ^2	1.25	0.96	1.21	1.08	1.00	0.92	0.96	0.88	0.92	1.04	1.08	1.21	1.33
	LADCT_1H with block base σ^2	1.25	1.04	1.71	1.25	0.67	1.17	1.33	1.08	0.83	0.83	1.21	1.13	1.21
	LADCT_1H&V with block based σ^2	1.21	1.00	1.21	0.83	0.58	0.96	1.25	0.83	0.58	1.25	0.96	1.13	1.25
512×512	(LADCT_1H with constant σ^2)	0.79	0.79	0.75	0.29	0.38	0.58	0.63	0.63	0.71	0.58	0.58	0.50	0.79
	LADCT_1H&V with constant σ^2	0.71	0.71	0.67	0.54	0.38	0.29	0.75	0.42	0.33	0.63	0.63	0.54	0.92
	LADCT_1H with block base σ^2	0.58	0.67	0.79	0.46	0.54	0.58	0.54	0.50	0.63	0.75	0.50	0.46	0.71
	LADCT_1H&V with block based σ^2	0.71	0.79	0.58	0.79	0.33	0.42	0.83	0.38	0.33	0.42	0.71	0.42	0.63

Table 6.6 False positive rate for each digital camera using different LADCT filter methods (our dataset).

Image size	Filter	DC1	DC2	DC3	DC4	DC5	DC6	DC7	DC8	DC9	DC10
128×128	(LADCT_1H with constant σ^2)	42.03	31.88	51.69	49.28	51.21	40.10	36.23	29.95	12.08	20.29
	LADCT_1H&V with constant σ^2	36.23	28.50	43.96	43.96	43.00	28.50	31.40	20.29	6.76	14.49
	LADCT_1H with block base σ^2	44.44	28.02	48.31	46.38	46.86	30.92	36.23	27.05	8.21	14.98
	LADCT_1H&V with block based σ^2	36.71	20.77	35.75	39.61	37.20	21.74	29.47	20.29	5.31	10.63
256×256	(LADCT_1H with constant σ^2)	20.77	9.18	31.88	28.99	28.50	15.94	10.63	11.59	0.97	4.35
	LADCT_1H&V with constant σ^2	14.49	4.35	21.74	22.22	17.87	11.59	7.73	10.14	0.00	1.93
	LADCT_1H with block base σ^2	17.87	6.28	31.40	24.64	24.15	9.18	8.70	11.59	0.48	3.38
	LADCT_1H&V with block based σ^2	13.04	2.90	17.39	17.39	15.94	6.28	7.73	9.66	0.48	1.45
512×512	(LADCT_1H with constant σ^2)	6.28	1.45	12.56	12.56	8.21	1.45	3.38	7.73	0.00	0.48
	LADCT_1H&V with constant σ^2	5.80	1.45	4.83	8.70	5.31	0.48	1.93	7.25	0.00	0.00
	LADCT_1H with block base σ^2	7.73	1.45	10.14	9.66	5.80	0.97	3.38	6.76	0.00	0.97
	LADCT_1H&V with block based σ^2	4.83	0.97	3.38	7.25	2.90	0.00	1.93	4.83	0.00	0.00

Table 6.7 False negative rate for each digital camera using different LADCT filter methods (Dresden dataset).

Image size	Filter	DC1	DC2	DC3	DC4	DC5	DC6	DC7	DC8	DC9	DC10
128×128	(LADCT_1H with constant σ^2)	3.97	3.92	3.86	3.44	3.92	4.40	3.60	4.46	4.29	4.67
	LADCT_1H&V with constant σ^2	2.95	3.49	3.06	2.79	3.11	3.22	2.79	4.67	3.65	3.27
	LADCT_1H with block base σ^2	3.11	3.11	3.60	3.81	3.54	3.11	3.44	4.72	3.65	4.72
	LADCT_1H&V with block based σ^2	1.99	3.70	2.90	2.25	2.52	2.47	2.58	3.92	3.11	3.11
256×256	(LADCT_1H with constant σ^2)	1.61	1.61	1.72	1.40	1.77	1.93	1.18	1.99	2.15	2.52
	LADCT_1H&V with constant σ^2	1.13	1.29	1.02	0.97	0.97	1.29	1.23	1.07	1.83	1.66
	LADCT_1H with block base σ^2	1.18	1.50	1.56	1.61	1.07	1.77	1.34	1.13	1.88	2.25
	LADCT_1H&V with block based σ^2	1.29	0.97	0.97	0.64	0.59	1.23	1.07	0.81	1.40	1.56
512×512	(LADCT_1H with constant σ^2)	0.59	0.54	0.64	0.38	0.70	0.59	0.43	0.59	0.86	0.70
	LADCT_1H&V with constant σ^2	0.43	0.27	0.27	0.16	0.38	0.32	0.48	0.27	0.64	0.75
	LADCT_1H with block base σ^2	0.64	0.54	0.48	0.48	0.48	0.43	0.38	0.38	0.75	0.64
	LADCT_1H&V with block based σ^2	0.21	0.27	0.21	0.32	0.38	0.11	0.21	0.16	0.64	0.59

Table 6.8 False positive rate for each digital camera using different LADCT filter methods (Dresden dataset).

6.5 Improved LADCT Filter vs Wavelet Filter

In this section, the proposed LADCT filter is assessed in comparison with the wavelet filter for source camera identification. It is worth mentioning that, for a fair comparison each PRNU is extracted from the green channel captured by the same sensor and the normalized correlation is applied to measure the similarity between the camera's reference PRNU and the image noise residue. To evaluate the performance of each filter, the overall error rates for FNR and FPR are then computed. The results show that the proposed LADCT filter offers the most significant improvements compared to the wavelet filter. With the Dresden dataset, using the improved LADCT_1 filter reduces the overall false negative rate from 30.48% to 25.75 %, 11.40 % to 9.37 %, and 3.09% to 2.80% while the decrease in overall false positive rate reaches 15%, 12%, 13% with image sizes of 128×128, 256×256, and 512×512 respectively (see table 6.9). These improvements are also illustrated in figure 6-3 in terms of the mean error rate for overall false negatives and overall false positives.

Filter technique	Overall FNR (%)			Overall FPR (%)		
	Image size 128×128	Image size 256×256	Image size 512×512	Image size 128×128	Image size 256×256	Image size 512×512
Wavelet filter	30.48	11.40	2.75	3.37	1.20	0.37
LADCT_1H&V with block based σ^2	25.75	9.23	2.61	2.86	1.05	0.32

Table 6.9 Overall FNR and FPR for the wavelet and proposed LADCT filters (Dresden dataset).

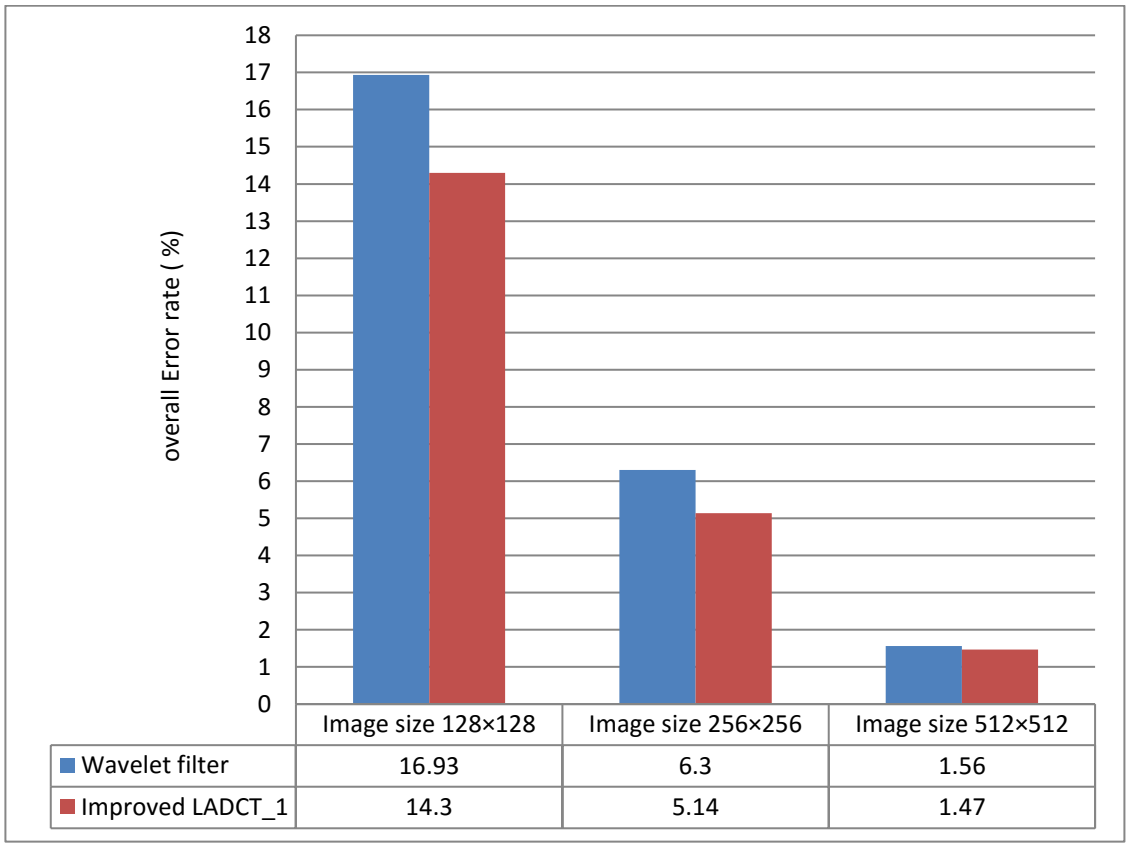

Figure 6-3 Overall error rate for the wavelet and improved LADCT filters (Dresden dataset).

However, only minor improvements have been achieved in our dataset. As shown in table 6.10, when compared to the wavelet filter the improved LADCT_1 filter reduced the overall false negative rate approximately by 5%, 1% and 4% and the overall false positive rate by 6%, 5%, and 8% with image sizes of 128×128, 256×256, and 512×512 respectively. Figure 6-4 shows these minor improvements in overall error rate for all FNR and FPR. The results for the wavelet filters and improved LADCT_1 filters based on each digital camera can be seen in table 6.11- table **6.14**.

Filter technique	Overall FNR (%)			Overall FPR (%)		
	Image size 128×128	Image size 256×256	Image size 512×512	Image size 128×128	Image size 256×256	Image size 512×512
Wavelet filter	24.96	12.15	7.08	2.10	1.06	0.61
LADCT_1H&V with block based σ^2	23.65	12.04	6.77	1.97	1.00	0.56

Table 6.10 Overall FNR and FPR for the wavelet and proposed LADCT filters (our dataset).

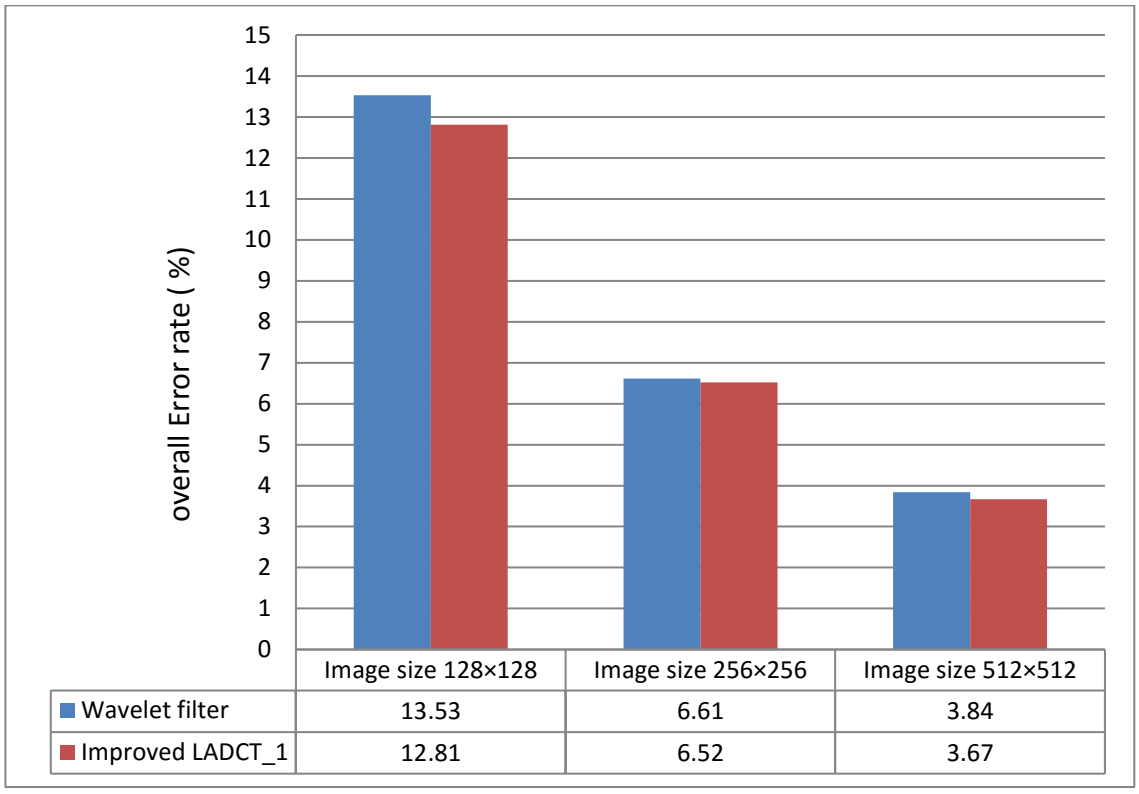

Figure 6-4 Overall error rate for wavelet and improved LADCT filter (our dataset).

Image size	Filter	DC1	DC2	DC3	DC4	DC5	DC6	DC7	DC8	DC9	DC10
128×128	Wavelet	35.27	25.60	44.44	43.00	45.89	28.50	32.85	27.05	8.70	13.53
	Improved LADCT_1	36.71	20.77	35.75	39.61	37.20	21.74	29.47	20.29	5.31	10.63
256×256	Wavelet	13.04	6.28	21.74	22.22	17.87	10.63	11.11	8.70	0.97	1.45
	Improved LADCT_1	13.04	2.90	17.39	17.39	15.94	6.28	7.73	9.66	0.48	1.45
512×512	Wavelet	4.35	1.93	4.35	4.35	4.35	0.48	2.9	4.83	0	0
	Improved LADCT_1	4.83	0.97	3.38	7.25	2.9	0	1.93	4.83	0	0

Table 6.11 False negative rate for the wavelet and improved LADCT filters (Dresden dataset).

Image size	Filter	DC1	DC2	DC3	DC4	DC5	DC6	DC7	DC8	DC9	DC10
128×128	Wavelet	2.68	3.49	2.90	3.22	3.22	3.97	3.60	3.38	3.81	3.44
	Improved LADCT_1	1.99	3.70	2.90	2.25	2.52	2.47	2.58	3.92	3.11	3.11
256×256	Wavelet	0.91	0.97	1.13	1.18	1.18	1.29	0.91	0.91	1.77	1.72
	Improved LADCT_1	0.91	0.97	0.97	0.64	0.59	1.23	1.07	0.81	1.40	1.56
512×512	Wavelet	0.21	0.32	0.32	0.38	0.16	0.54	0.21	0.16	0.75	0.64
	Improved LADCT_1	0.21	0.27	0.21	0.32	0.38	0.11	0.21	0.16	0.64	0.59

Table 6.12 False positive rate for the wavelet and improved LADCT filters (Dresden dataset).

Image size	Filter	C1	C2	C3	C4	C5	C6	C7	C8	C9	C10	C11	C12	C13
128×128	Wavelet	25.50	20.00	17.00	31.50	44.00	6.00	2.00	67.00	60.50	20.00	21.00	1.00	9.00
	Improved LADCT_1	20.00	15.00	12.50	33.00	40.00	9.00	4.00	71.00	56.50	20.00	18.00	1.00	7.50
256×256	Wavelet	4.00	2.50	7.50	17.00	10.50	1.50	0.00	50.00	47.50	8.50	7.00	0.00	2.00
	Improved LADCT_1	7.00	1.50	8.50	17.00	11.50	2.50	0.50	50.00	38.00	11.00	6.50	0.00	2.50
512×512	Wavelet	0.50	0.00	5.50	9.50	0.50	0.00	0.00	35.50	28.00	5.00	4.00	0.00	3.50
	Improved LADCT_1	1.00	0.00	6.00	9.00	0.00	0.00	0.00	32.00	26.50	6.50	3.50	0.00	3.50

Table 6.13 False negative rate for the wavelet and improved LADCT filters (our dataset).

Image size	Filter	C1	C2	C3	C4	C5	C6	C7	C8	C9	C10	C11	C12	C13
128×128	Wavelet	2.42	1.71	2.46	1.96	1.33	2.75	2.88	1.96	1.96	1.58	2.04	1.46	2.63
	Improved LADCT_1	2.08	1.71	1.67	1.92	1.17	1.88	2.71	1.42	1.83	1.79	2.63	2.38	2.38
256×256	Wavelet	1.04	1.00	1.50	0.92	1.04	1.21	1.17	0.96	1.17	0.88	1.21	0.79	0.96
	Improved LADCT_1	1.21	1.00	1.21	0.83	0.58	0.96	1.25	0.83	0.58	1.25	0.96	1.13	1.25
512×512	Wavelet	0.92	0.46	0.75	0.33	0.54	0.71	1.04	0.58	0.33	0.63	0.54	0.63	0.50
	Improved LADCT_1	0.71	0.79	0.58	0.79	0.33	0.42	0.83	0.38	0.33	0.42	0.71	0.42	0.63

Table 6.14 False negative rate for the wavelet and improved LADCT filters (our dataset).

6.6 Conclusion

The PRNU estimation process can be affected by the existence of image-dependent information, and also some non-unique noise components. With the aim to reduce such undesirable effects, a new improved version of LADCT filter was proposed in this chapter. The LADCT filter can provide a number of advantages compared to other filters such as wavelets. The LADCT filter performs well with images affected by image-dependent noise, including multiplicative noise, and it also works on sliding blocks, which can provide more information about the spatial correlation properties of noise in an easier technique. The original LADCT_1 filter relies on the fact that the multiplicative noise is fixed for every block with similar statistical means, while the PRNU may not be stationary depending on the homogeneity of the silicon in the imaging device sensor. Therefore, two improvements of LADCT_1 are proposed, the first of which relies on estimating the noise variance for each block independently. The second technique of enhancement aims to capture more information about the PRNU to decrease to probability of false alarms) by applying the LADCT_1 in the horizontal and vertical directions. The improved LADCT_1 has been compared with the wavelet filter. The results show that the improved LADCT_1 filter can reduce the overall false negative and false positive rates more than wavelet filter and this is more clearly demonstrated with the Dresden dataset. In the future, it would be sensible to use a large number of images in estimation stage to overcome the issue of inter-class similarity and the high-resolution images. In addition, to obtain the actual and predicted classification, the confusion matrix should be applied.

CHAPTER 7 PROPOSED DIGITAL CAMERA IDENTIFICATION SYSTEM USING COLOUR PRNU COMBINATION

7.1 Introduction

In this chapter, a new PRNU-based source camera identification system is presented. The system uses enhanced components in several stages of the process. Firstly, the improved version of the locally adaptive discrete cosine transform filter is applied in the filtering stage. In the estimation stage, the weighted averaging technique as seen in chapter 5 is adopted. The post-estimation stage consists of combining the PRNU estimated from each colour plane, aiming to take advantage of the presence of physical PRNU components in different channels. Although most researchers have used a gray version of the image or sometimes the green channel, exploiting RGB planes may lead to reducing the effect of colour interpolation and hence to more accurate estimation since this involves a larger number of observed signals. The experimental analysis covers three application scenarios: source camera identification, source camera verification and the purity of PRNU estimation. Experimental results with two image datasets acquired by various camera devices show a significant gain obtained with the proposed enhancements in each stage and the superiority of the overall system over state-of-the-art source camera identification systems. The rest of this chapter is structured as follows: section two describes the proposed colour planes for PRNU estimation, and the proposed digital camera identification system is introduced in

section three. Experimental results and analysis are provided in section four and the conclusions are drawn in section five.

7.2 Colour Planes for PRNU Estimation

A challenging task in estimating the PRNU is to consider the colour channel at each pixel location. Because there are three primary colours; i.e. red, green and blue, the sensor exhibits a physical noise pattern in one colour component only at each pixel location, while the other components are estimated through interpolation involving the neighboring pixels (Lukas *et al.*, 2006). Some PRNU estimation techniques, such as the techniques of Cooper (2013) and Chenyang *et al.* (2012) depend on the gray-scale version of images in order to extract the PRNU. On the other hand, others such as Goljan *et al.* (2008), Lukas *et al.* (2006), Li *et al.* (2014), and Goljan (2008) have estimated the PRNU from each channel individually and then combined them linearly to derive a colour-to-luminance PRNU. The common rule for calculating the luminance component is:

$$Y = 0.3\,R + 0.59\,G + 0.11\,B \tag{7.1}$$

where Y represents the luminance component and R, G and B stand for the red, green and blue channels respectively (Kanan and Cottrell, 2012). Other techniques use only the green channel in order to extract the PRNU as it contains more physical PRNU information when compared to the other channels (Kang *et al.*, 2012; Qu *et al.*, 2013). However, a linear combination of the colour channels with fixed weights would include some interpolation noise if a certain colour location does not correspond to the

physical light information. On the other hand, if only the green channel is used the physical PRNU information which could exist in the other two colour components; i.e. red and blue are not taken into account. In the work of Hu *et al.* (2010), a non-linear combination is applied by extracting the PRNU from each colour channel separately, and then the largest coefficient in magnitude at each location is chosen. In this thesis, the PRNU is estimated from every channel separately and then the resulting PRNUs are concatenated to form a combined PRNU. Similarly, a combined noise residue can be obtained from the test image through the concatenation of the three noise residues, each corresponding to a colour plane. This way the physical information characterizing the PRNU can be exploited efficiently.

7.3 Proposed digital camera identification system using colour PRNU combination

Figure 7-1 shows the proposed source camera identification system. Firstly, digital images can be considered in the form of individual colour channels. Next, an improved version of the LADCT de-noising filter is adopted in order to decrease the effect of scene details on noise residues. Then, for effective PRNU estimation, the obtained noise residues are averaged using the proposed WA technique. Finally, concatenating the PRNUs estimated from the primary colour planes is proposed in order to exploit the presence of physical PRNU components in different colour channels. It worth noting that the proposed system performs the circular correlation norm (CCN) as

proposed by Kang *et al.* (2012) to measure the similarity between the PRNU and a noise residue estimated from a query image.

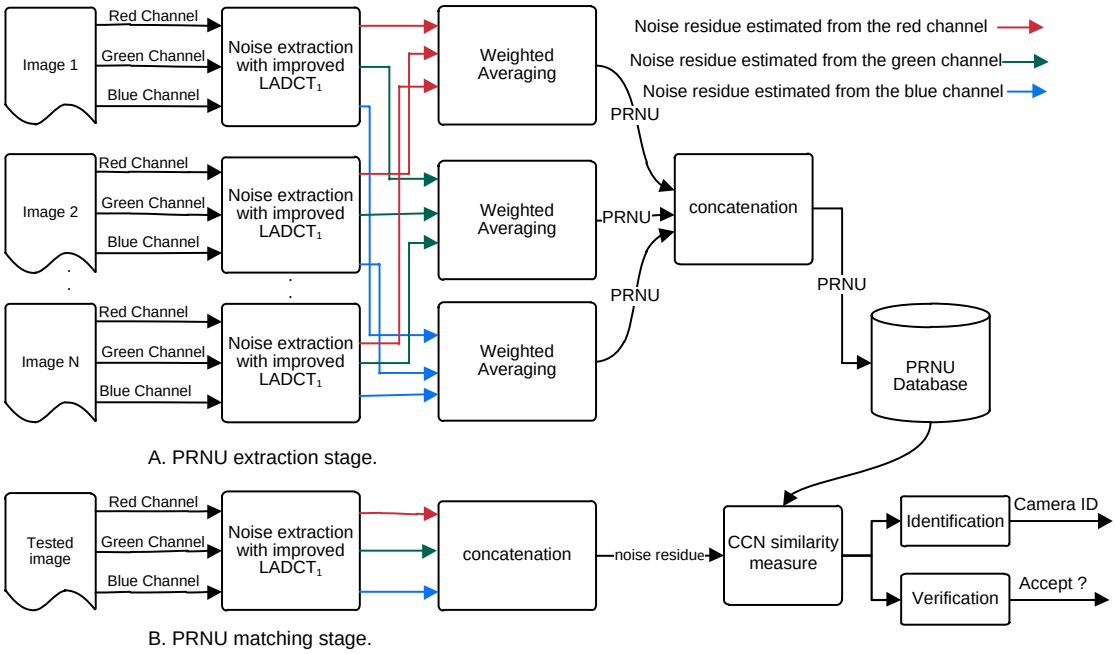

Figure 7-1 Proposed source camera identification and verification system.

7.4 Experimental Work

This section describes a number of experiments conducted to assess the performance of the proposed system. The evaluation has been conducted using two different datasets: our dataset and the Dresden database. In the rest of this chapter, the improved LADCT_1 filter, that is, the LADCT_1H&V with block-based noise variance, is used unless otherwise stated.

7.4.1 Colour PRNU Evaluation

Here the WA technique as discussed in chapter 5 is adopted. Different techniques for combining colour channels in PRNU estimation are assessed. That is, the green channel-based PRNU as suggested in the work of Kang et al. (2012),and Qu et al. (2013), the luminance image-based PRNU estimation as mentioned in Cooper (2013) and Chenyang *et al.* (2012) , and the colour -to-luminance PRNU technique as proposed in the technique of Goljan *et al.* (2008), Lukas *et al.* (2006), and Li *et al.* (2014) as well as, finally the colour combination scheme developed by Hu *et al.* (2010). Note that Hu *et al.* (2010) developed three schemes, but in this thesis their scheme 3 is used because it has been found to deliver the best performance. The results shown in table 7.1 and table **7.2** reveal an interesting finding in that the PRNU estimated from gray-level images seems to offer better source camera identification than that of the green channel for both datasets. The main reason of such results could be that, the gray-level image includes more physical PRNU components than the green images (the PRNU components could exist in the other two colour components). Moreover, it is clear that the combination of the three RGB channels as recommended by Hu et al. (2010) outperforms the techniques which use the green channel only, the Luminance image and the luminance PRNU. Finally, the proposed combination achieves the best performance among all methods tested. The results of FNR and FPR for each digital camera based on each colour component are shown in appendix B.

Methods	Overall FNR (%)			Overall FPR (%)		
	Image size 128×128	Image size 256×256	Image size 512×512	Image size 128×128	Image size 256×256	Image size 512×512
Green image (Kang *et al.*, 2012), (Qu *et al.*, 2013)	23.58	11.12	6.69	1.96	0.92	0.55
Gray image (Cooper, 2013),(Chenyang *et al.*, 2012)	23.35	10.73	6.42	1.95	0.89	0.54
Grey Colour -to-luminance PRNU Lukas *et al.* (2006), Li *et al.* (2014)	22.46	10.42	6.40	1.87	0.90	**0.52**
RGB scheme 3 (Hu *et al.*, 2010)	22.46	10.58	6.31	1.87	0.88	**0.52**
Proposed method	**21.35**	**10.20**	**6.12**	**1.78**	**0.85**	**0.52**

Table 7.1 Overall FNR and FPR based on each colour component (our dataset).

Methods	Overall FNR (%)			Overall FPR (%)		
	Image size 128×128	Image size 256×256	Image size 512×512	Image size 128×128	Image size 256×256	Image size 512×512
Green image (Kang *et al.*, 2012), (Qu *et al.*, 2013)	21.69	6.62	1.79	2.41	0.74	0.20
Gray image (Cooper, 2013),(Chenyang *et al.*, 2012)	20.10	6.09	1.64	2.23	0.68	0.18
Grey Colour-to-luminance PRNU Lukas *et al.* (2006), Li *et al.* (2014)	19.28	5.60	1.60	2.14	0.60	0.20
RGB scheme 3 (Hu *et al.*, 2010)	18.31	5.41	1.55	2.03	0.60	0.17
Proposed method	**14.40**	**4.15**	**1.45**	**1.72**	**0.51**	**0.16**

Table 7.2 Overall FNR and FPR based on each colour component (Dresden dataset).

7.4.2 Comparison with State-of the- art Systems

In this sub-section, the proposed system is assessed in comparison with existing state-of the- art systems, namely the basic-PRNU (Lukas *et al.*, 2006), the MLE-PRNU[1] (Chen *et al.*, 2008), Phase-PRNU (Kang *et al.*, 2012), CD_PRNU (Chang-Tsun and Yue, 2012), WA (Lawgaly *et al.*, 2014), and Wiener_median PRNU (Cooper, 2013). The comparative analysis covers three different aspects, i.e., source camera

[1] Note that the MLE method (Chen *et al.*, 2008) delivered adversary results for $\sigma = 5$ as opposed to the best performance shown here with $\sigma = 3$.

identification, source camera verification, and the purity of PRNU estimation. It is worth mentioning that CCN has been used in the proposed system.

7.4.2.1 Source Camera Identification

In source camera identification, the forensic analyst possesses a number of cameras and the objective is to identify the specific camera used to take a picture. Here, it is assumed that the picture has been taken by one of the cameras available. Therefore, a test image is assigned to a specific camera if the corresponding PRNU provides the highest similarity when compared with the noise residue extracted from that image. The results for overall false negative rate and overall false positive rate for our dataset and the Dresden dataset are illustrated in table 7.3 and table 7.4, respectively. As can be seen, the proposed system offers the best performance with the two datasets for all different image sizes. The difference is more significant on the Dresden dataset with clear enhancements to overall false negative and false positive rates exceeding 50% when compared with other techniques (see table 7.4).

Technique	FNR (%)			FPR (%)		
	Image size 128×128	Image size 256×256	Image size 512×512	Image size 128×128	Image size 256×256	Image size 512×512
Basic PRNU(Lukas *et al.*, 2006)	24.15	11.27	6.88	2.06	0.94	0.58
MLE PRNU(Chen *et al.*, 2008)	23.54	11.04	6.35	1.96	0.91	0.53
Phase-PRNU (Kang *et al.*, 2012)	23.27	11.00	6.31	1.94	0.92	0.53
CD_PRNU (Chang-Tsun and Yue, 2012)	23.88	10.20	5.81	1.99	0.85	0.50
WA (Lawgaly *et al.*, 2014)	22.31	10.58	6.23	1.89	0.90	0.54
Wiener & median PRNU(Cooper, 2013)	29.15	13.08	6.38	2.43	1.09	0.54
The proposed system	**21.27**	**9.85**	**5.46**	**1.77**	**0.82**	**0.48**

Table 7.3 Overall FNR and FPR for each technique on our dataset.

Technique	FNR (%)			FPR (%)		
	Image size 128×128	Image size 256×256	Image size 512×512	Image size 128×128	Image size 256×256	Image size 512×512
Basic PRNU(Lukas *et al.*, 2006)	29.90	10.53	2.51	3.26	1.13	0.28
MLE PRNU(Chen *et al.*, 2008)	28.45	10.34	2.46	3.16	1.12	0.27
Phase-PRNU (Kang *et al.*, 2012)	28.45	10.10	2.03	3.14	1.12	0.23
CD_PRNU (Chang-Tsun and Yue, 2012)	31.25	10.48	2.41	3.50	1.10	0.26
WA (Lawgaly *et al.*, 2014)	23.72	7.44	1.69	2.62	0.92	0.20
Wiener & median PRNU(Cooper, 2013)	30.00	10.92	2.37	3.33	1.21	0.26
The proposed system	**14.11**	**3.96**	**0.93**	**1.72**	**0.70**	**0.10**

Table 7.4 Overall FNR and FPR for each technique on Dresden dataset.

The results for FNR are FPR for each technique based on each digital camera are shown in appendix C. These enhancements are better illustrated in table 7.5 and table 7.6 where the basic PRNU estimation technique(Lukas et al., 2006) has been used as a reference point. Note that the Wiener & median PRNU technique (Cooper, 2013) does not bring improvements compared to the reference technique. This could be justified by the fact that the number of images used for PRNU estimation by Cooper (2013) is more than 100 images. Furthermore, the authors adopted blue sky images in their experiments though this setting might not be available in practical scenarios. It is however worth highlighting some improvements with larger size images which suggest that the technique's performance is also sensitive to the image size (see table 7.5 and table 7.6).

Technique	Gain for FNR (%)			Gain for FPR (%)		
	Image size 128×128	Image size 256×256	Image size 512×512	Image size 128×128	Image size 256×256	Image size 512×512
MLE PRNU(Chen *et al.*, 2008)	+2.53	+2.04	+7.70	+4.85	+3.19	+7.02
Phase-PRNU (Kang *et al.*, 2012)	+3.64	+2.40	+8.28	+5.83	+2.13	+7.02
CD_PRNU (Chang-Tsun and Yue, 2012)	+1.12	+9.58	+15.55	+3.40	+9.57	+12.28
WA(Lawgaly *et al.*, 2014)	+7.62	+6.12	+9.45	+8.25	+4.26	+5.26
Wiener & median PRNU(Cooper, 2013)	-20.70	-16.06	+7.27	-17.96	-15.96	+5.26
The proposed system	**+11.93**	**+12.60**	**+20.64**	**+14.08**	**+12.77**	**+15.79**

Table 7.5 Obtained source camera identification gain on our dataset.

Technique	Gain for FNR (%)			Gain for FPR (%)		
	Image size 128×128	Image size 256×256	Image size 512×512	Image size 128×128	Image size 256×256	Image size 512×512
MLE PRNU(Chen *et al.*, 2008)	+4.85	+1.80	+1.99	+3.07	+0.88	+3.57
Phase-PRNU (Kang *et al.*, 2012)	+4.85	+4.08	+19.12	+3.68	+0.88	+17.86
CD_PRNU (Chang-Tsun and Yue, 2012)	-4.52	+0.47	+7.57	-7.36	+2.65	+7.14
WA(Lawgaly *et al.*, 2014)	+20.67	+29.34	+32.67	+19.63	+18.58	+28.57
Wiener & median PRNU(Cooper, 2013)	-0.33	-3.70	+5.58	-2.15	-7.08	+7.14
The proposed system	**+52.81**	**+62.39**	**+62.95**	**+46.63**	**+38.05**	**+64.29**

Table 7.6 Obtained source camera identification gain (%) on Dresden dataset.

7.4.2.2 Source Camera Verification

The task of the investigator in source camera verification is to verify whether a specific camera has been used to acquire a given picture. Because a threshold must be set in order to reach such a decision[2], one can measure the performance of the system, i.e., FPR and FNR, for each threshold value. This leads us to what is known in the literature as the Receiver Operating Characteristics (ROC) curve. In this experiment, 23 cameras (our dataset combined with the Dresden dataset) have been used to calculate the values of similarity between each source camera PRNU and the noise

[2] This threshold represents the least possible similarity between the reference PRNU of a camera and the noise residue of an image acquired by the same device.

residues of images captured by different cameras. This will enable us to determine the false positive rate for each threshold value. On the other hand, the values of similarity between every source camera PRNU and the noise residues of images acquired by the same camera have been calculated. This is to define the false negative rate (i.e., 1-TPR) for each threshold value. It is worth mentioning here that the process of removing non-unique components is applied as proposed by Goljan (2008) in order to decrease the correlation between the PRNUs extracted from different cameras. The ROC curve performance of the proposed system along with that of existing state-of-the-art techniques are demonstrated in figure 7-2- figure 7-4 for a various image sizes respectively. In practical applications, it is extremely important to ensure a sufficiently low false positive rate, and so the ROC performance in cases of low false positive rate is more critical; consequently, the horizontal axis of all the ROC curves is adjusted, in order to illustrate the detail of the ROC with a low false positive rate accordingly. The experimental results show that the proposed system performs better than its competitors. This is true for all image sizes. In table 7.7 the true positive rate (TPR) at fixed values for FPR (10^{-2} and 10^{-3}) are depicted. As can be seen, the systems perform differently in source camera verification when compared to the results of source camera identification. Indeed, the CD PRNU technique is outperformed by the basic PRNU technique. Also, the Wiener-median PRNU technique appears significantly more powerful than CD PRNU and Basic PRNU on images with size 256×256 and 512×512 and close to the phase PRNU. These results also confirm the superiority of the proposed system. Surprisingly, CD PRNU performs worse than the Basic PRNU and MLE in camera verification. Note that CD PRNU has been shown in the work of

Chang-Tsun and Yue (2012) to outperform MLE in a number of PRNU-based image authentication experiments but these were slightly different from my approach. Indeed, in the ROC curves plotted in in the work of Chang-Tsun and Yue (2012), the estimated the values of TPR and FPR for an individual camera by varying a certain threshold. This is a single camera verification problem and such a different setting could justify the different performance here since my varying threshold is applied to multiple cameras in order to estimate the overall TPR and FPR. In this context, it is worth noting that experiments on single and multiple camera verification were conducted in work of (Swaminathan *et al.*, 2008) ,where it was shown that the performance of their system differs in each experiment. Overall, the results of source camera verification confirm the superiority of the proposed system.

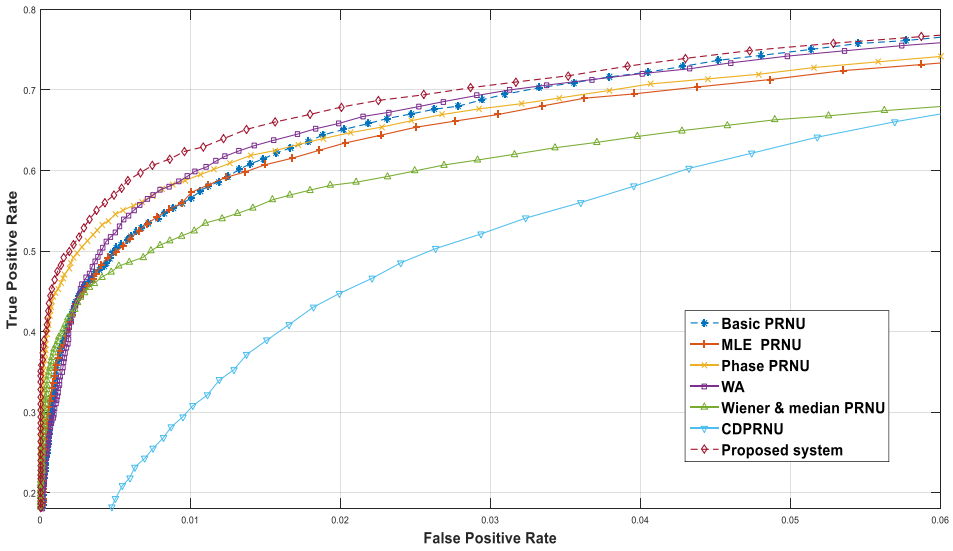

Figure 7-2 Overall ROC curve for our dataset and Dresden dataset, image size 128×128.

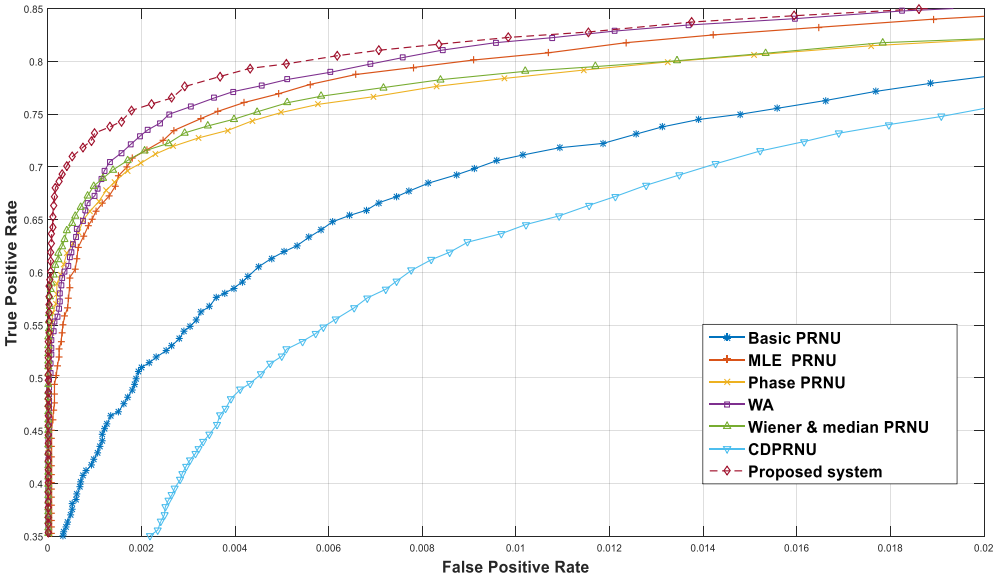

Figure 7-3 Overall ROC curve for our dataset and Dresden dataset, image size 256×256.

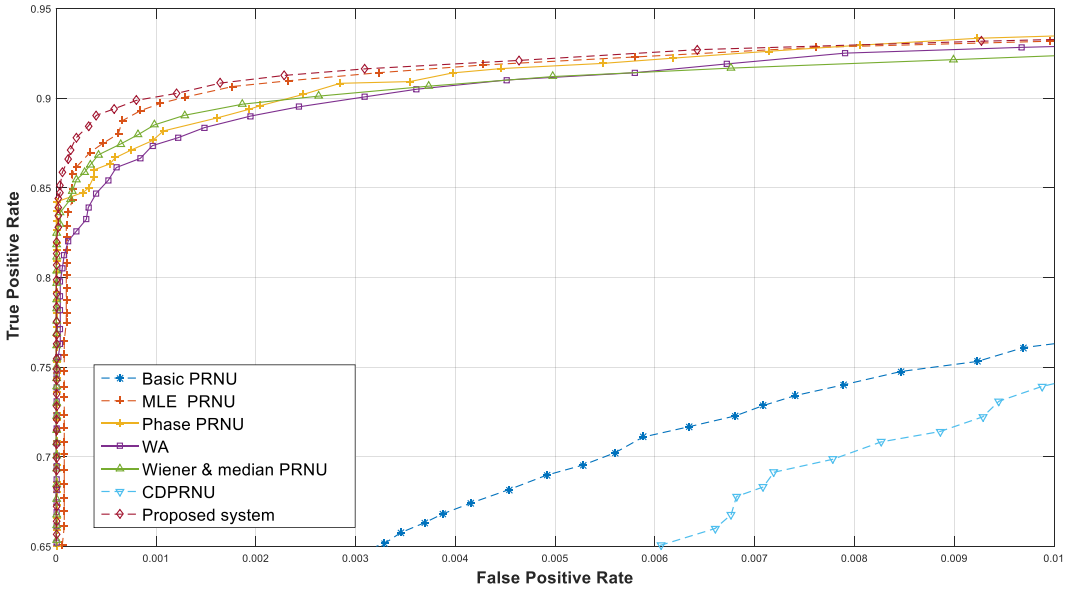

Figure 7-4 Overall ROC curve for our dataset and Dresden dataset, image size 512×512.

Technique	TPR at low FPR of 10^{-2}			TPR at low FPR of 10^{-3}		
	Image size 128×128	Image size 256×256	Image size 512×512	Image size 128×128	Image size 256×256	Image size 512×512
Basic PRNU(Lukas *et al.*, 2006)	0.5660	0.7113	0.7608	0.3358	0.4230	0.5289
MLE PRNU(Chen *et al.*, 2008)	0.5730	0.8081	0.9286	0.3527	0.6578	0.8965
Phase-PRNU (Kang *et al.*, 2012)	0.5878	0.7839	**0.9317**	0.4480	0.6772	0.8970
CD_PRNU (Chang-Tsun and Yue, 2012)	0.3079	0.6460	0.7392	0.0300	0.1480	0.3947
WA(Lawgaly *et al.*, 2014)	0.5929	0.8178	0.9283	0.3116	0.6728	0.8734
Wiener & median PRNU(Cooper, 2013)	0.5251	0.7906	0.9214	0.3827	0.6820	0.8850
The proposed system	**0.6238**	**0.8227**	**0.9317**	**0.4647**	**0.7321**	**0.9026**

Table 7.7 TPR values of the different methods at a low FPR of 10^{-2} and 10^{-3}

7.4.2.3 Purity of PRNU Estimation

In this experiment, we aim to quantify the purity of the estimated PRNU with the proposed system as well as with other competing systems. The idea underlying this experiment is that the similarity between PRNUs extracted from the same sensor must be equal to the highest possible value while the similarity between PRNU's estimated from different cameras must be minimum because the actual PRNUs are statistically independent and similar to a white Gaussian noise. Five PRNUs have been estimated for each digital camera where each uses 50 different images. Different block size values are considered of 64×64, 128×128 and 256×256. The equal error rate (EER) has also been adopted in this experiment in order to illustrate the purity of PRNU estimation for each technique. The EER defines the point where the false negative rate becomes equal to the false positive rate. As can be seen in table 7.8, the proposed system offers the smallest EER values. It is clear that all techniques provide a better PRNU estimation than the one given by the Basic PRNU technique.

Furthermore, although MLE and WA outperform the Basic PRNU, their estimated PRNUs are less accurate than those obtained with other techniques for the block size of 128 × 128. This suggests that the estimation of the noise residue from individual images plays a crucial role in source camera identification and verification.

Technique	EER (%)		
	Image size 64×64	Image size 128×128	Image size 256×256
Basic PRNU(Lukas *et al.*, 2006)	2.62	2.60	2.18
MLE PRNU(Chen *et al.*, 2008)	2.20	1.31	0.007
Phase-PRNU (Kang *et al.*, 2012)	2.54	0.87	**0**
CD_PRNU (Chang-Tsun and Yue, 2012)	3.09	0.90	**0**
WA(Lawgaly *et al.*, 2014)	2.28	1.31	**0**
Wiener & median PRNU(Cooper, 2013)	2.64	0.95	**0**
The proposed system	**2.17**	**0.51**	**0**

Table 7.8 EER for each technique based on the purity of PRNU estimation.

7.5 Conclusion

In this chapter, an efficient source camera identification system has been introduced. The idea uses an improved locally adaptive DCT Filter followed by a weighted averaging technique to exploit the content of images carrying the PRNU efficiently. Furthermore, since the physical PRNU is present in all colour planes, the estimated colour PRNUs has been combined for better matching. The system has been thoroughly assessed where the gain obtained with each of its components has been highlighted through intensive experiments on two different image datasets considering various image sizes. Finally, an experimental analysis covering three application scenarios in digital image forensics has shown the superiority of the proposed system over state of the art techniques. However, when the UM technique is combined with our source camera identification system, it does not show a significant gain. This shows that the filtering stage followed by weighted averaging contribute significantly to the final performance and seem to capture well the PRNU components that exist in high frequencies. In the future, it would be sensible to examine the performance of our source camera identification system by applying different image sharpening techniques such as Gaussian-based unsharp masking (Laplacian of Gaussian).

CHAPTER 8 **CONCLUSIONS**

8.1 Contributions of the thesis

Over the last decade, digital multimedia has acquired great relevance in many aspects of our lives and represents one of the main forms of information that could affect public opinion. In specific situations, such as in the forensics field, visual information might be exploited as promising evidence in a courtroom, therefore supporting the final outcome. In such scenarios, it is very important to know the history and the origin of multimedia documents involved in order to be able to guarantee that such information has not been altered. Multimedia forensics could deliver evidence on a digital asset by analysing the intrinsic fingerprints which characterise a piece of information throughout its life time. In other words, the evaluation of such patterns could result in identifying the origin of a video or image and establishing data integrity. Consequently, to increase the reliability of digital images, image authentication and copyright protection must be accomplished. Motivated by this, the present research has investigated the performance of existing techniques which are based on estimating photo response non-uniformity (PRNU), in order to contribute to the development of new estimation approaches to improve the performance of digital camera identification. The principles and motivations of digital image forensics are considered and new methods in digital image forensics are offered in this thesis.

In chapter 3, different techniques of image authentication have been investigated. More specifically, techniques of sensor fingerprint estimation based on photo response non-uniformity have been examined. PRNU noise is mainly caused by the sensitivity of pixels to light which is produced due to the imperfections and non-homogeneity of silicon wafers during the manufacture of camera sensor. PRNU has been generally used for source camera identification and image authentication. The abundant information that sensor pattern noise carries in terms of frequency content makes it unique and hence suitable for identifying the source camera and detecting image forgeries. Nonetheless, the PRNU estimation process is inevitably faced with the presence of image-dependent information as well as other non-unique noise components. With the aim to reduce such undesirable effects, new novel techniques are proposed in this thesis in different stages of the digital camera identification system: the pre-processing stage, the filtering stage, the estimation stage, and the post-estimation stage.

In chapter 4, an image sharpening technique has been suggested to enhance the source camera identification based on PRNU estimation. The proposed pre-processing Unsharp masking technique, aims to amplify the PRNU noise present in the digital image in order improve the accuracy of its estimation, which may rely on differences among a set of digital images and their smoothened versions in order to identify the characteristics of the sensor. Therefore, such a process can use part of the content of the sensor noise which can be concentrated in the high frequency range and present in contours, edges and textured areas of digital images. Motivated by this, the unsharp

masking technique is utilized to amplify the high frequency content of the PRNU, and consequently of strengthen its presence in sample images in order to facilitate efficient source camera identification. The results of extensive experiments have shown that the proposed sharpening technique achieves significant improvements to two recent state-of the-art source camera identification schemes with different sizes of images.

In chapter 5, a new PRNU estimation technique based on weighted averaging is proposed to enhance PRNU estimation. The traditional technique of PRNU estimation uses a set of digital images where a pattern residue signal is extracted from each image. The extracted residue signals are then averaged in order to obtain the sensor pattern noise. This constant averaging technique has been used in most PRNU estimation studies. The common assumption made in these studies is that every residue signal is a noisy observation of the sensor pattern noise and then each observation is multiplied by the same constant factor 1/N. Theoretically, the constant averaging technique is optimal only if the variance of noise is constant in all observations, and such an assumption is not justified in practice since digital images can be obtained in various conditions, creating the corresponding residue signals which are different from each other (bright digital images can provide better PRNU estimation than dark digital images). Moreover, saturated pixels can increase the estimation error in residue signals because each signal could carry undesirable image-dependent noise. Based on this observation, the weighted averaging technique is proposed for effective PRNU estimation. The technique depends on the principle of estimating an unknown signal from noisy observations. Note that the weighted averaging technique is only applied in

the estimation stage. The weighted averaging technique is applicable with any existing PRNU estimation technique and it has been validated against two recent techniques (basic PRNU and MLE-PRNU). Intensive experiments have shown that the performance of WA technique for source camera identification is considerably improved with different sizes of images.

In chapter 6, an improved version of the locally adaptive discrete cosine transform (LADCT) filter is proposed to improve camera identification performance. The LADCT filter can offer several advantages compared to other filters such as wavelets that operate on full images, and it is claimed to perform well on images affected by image-dependent noise including the multiplicative noise. Also, the LADCT performs well with several noise models. Furthermore, averaging numerous de-noised estimates for each pixel in the block can lead to resolving the problem of undershoots and overshoots which can be directly linked to the problem of scene details in PRNU estimation. Two improvements of the LADCT_1 are suggested, the first depending on estimating the noise variance for each block individually in order to estimate a threshold for each block. The principal idea of such a threshold value is based on the fact that the statistical variance of the estimated noise might differ considerably across blocks. Therefore, blocks in which the estimated noise may have high variance would be filtered with a relatively small threshold in the DCT domain as the high activity of the estimated noise in such blocks could be more likely to arise from texture and edges. In contrast, low variance noise within a specific block could well represent the actual PRNU and therefore should be retained by applying a

relatively large threshold in the DCT domain. The second technique of enhancement is based on applying the improved LADCT_1 in both the horizontal and vertical directions. This process can lead to two PRNUs, each estimated in one direction. The logic behind this process is to increase the size of the PRNU camera reference and noise residue in order to decrease the probability of false alarms. Also, it could be that some components of the PRNU that may be hard to estimate in the horizontal direction and will be easier to estimate in the vertical direction and vice versa. The improved LADCT_1 is validated against the wavelet filter, and the results show that the improved LADCT_1 filter can reduce the overall false negative and the overall false positive rates more than the wavelet filter.

In chapter 7, a novel source camera identification system based on colour PRNU combination is presented by adopting enhancements in several stages of the process. The camera sensor exhibits a physical noise pattern in one colour component only at every pixel location, while the other components can be estimated through interpolation involving the neighboring pixels. Some PRNU estimation techniques rely on the luminance rule to estimate the final PRNU; however, a linear combination of the colour channels with fixed weights may contain some interpolation noise. Furthermore if the green channel only is utilized, the physical PRNU information which could exist in other colour components is not taken into account. Motivated by this, the PRNU is estimated from each channel individually and then the resulting PRNUs are concatenated to form a combined PRNU. The use of this technique means that the physical information characterizing the PRNU would be exploited efficiently.

The improved locally adaptive DCT Filter followed by a weighted averaging techniqueis adopted in order to efficiently exploit the content of images carrying the PRNU. The results show that the PRNU estimated from gray-level images appears to give better source camera identification than the green channel. Moreover, the recommended colour combination achieves the best performance among all methods tested. The proposed system has been thoroughly validated against six recent state-of-the-art source camera identification schemes with different sizes of images. As opposed to other proposed techniques, the experimental analysis in chapter 7 covers three application scenarios in digital image forensics: source camera identification, source camera verification, and the purity of PRNU estimation. The results have shown a significant gain obtained with the proposed system over state-of- the-art source camera identification systems.

8.2 Future Work

While a number of aspects of digital image forensics mechanisms have been considered in this thesis, some particular ideas to extend the current work are as follows:

- Digital image dataset: An image dataset is essential for the assessment of a proposed algorithm. However, although some datasets are available for the research community to use, several issues that could call for the establishment of a benchmark dataset can be discussed. For example, experiments including images taken with various acquisition settings (i.e., at different resolutions) could be used

to evaluate the effect of these settings on PRNU performance. Moreover, images captured by scanners, cell phones and imaging devices operating in invisible frequencies such as ultraviolet or infrared cameras can be included for a more comprehensive work.

- Temporal digital image forensics: In several digital image forensics applications it would not be enough to identify the digital imaging device but it would be beneficial to determine a temporal localization of the digital image. For instance, in the case of an image or video with illegal content distributed over the Internet, and the digital camera involved may since have changed ownership. In this situation, estimating the date when the images with illegal content were captured may help the investigator to make a link between the camera and the owner. In order to obtain the temporal characteristics of a digital device, it is necessary to introduce a model for the identification of defective pixels over time. It would be very interesting to investigate PRNU performance in terms of temporal image forensics.
- PRNU similarity measurement: PRNU-based forensic applications normally depend on measuring the similarity among estimated PRNU signals. Although several similarity measurements have been used in the literature, such as normalized correlation, PCE and CCN, in the future it could be sensible to consider a novel similarity measure based on the statistical model of the noise residue by considering methods of signal detection in noisy environments.

- Robustness of PRNU estimation: Although several PRNU estimation techniques have been introduced, an efficient algorithm to analyse PRNU robustness against post-processing operations is still lacking. In the future it would be useful to evaluate proposed systems against some common image processing. For example how the FNR and RPR rates may changes with JPEG compression or gamma correction could be investigated. Moreover, various issues for camera identification and forgery detection could be considered in cases of application of certain types of geometrical processing, for instance cropping or resizing, which could lead to desynchronization with the PRNU.
- Application-specific PRNU Estimation: The literature review has highlighted the fact that many algorithms have been used to identify a source camera and to verify image integrity. However; each algorithm may only perform well when specific assumptions are satisfied; for instance an algorithm for PRNU estimation could work well for camera identification purposes and be less performing for forgery detection. Therefore, estimating the PRNU to target a specific application may be a better approach for optimizing the performance.

REFERENCES

Abry, P. (1997) *Ondelettes et turbulences: multirésolutions, algorithmes de décomposition, invariance d'échelle et signaux de pression*. Paris: Diderot éd.

Al-Ani, M., Khelifi, F., Lawgaly, A. and Bouridane, A. (2015), 'A novel image filtering approach for sensor fingerprint estimation in source camera identification', *Advanced Video and Signal Based Surveillance (AVSS), 12th IEEE International Conference.* Karlsruhe, 25-28 Aug. 2015. IEEE, pp. 1-5.

Amerini, I. (2010), 'Image Forensics: source identification and tampering detection', PhD thesis, Universita degli studi di Firenze, Italy.

Badamchizadeh, M. and Aghagolzadeh, A. (2004), 'Comparative study of unsharp masking methods for image enhancement', *Third International Conference on Image and Graphics (ICIG'04),* . Hong Kong, China, 18-20 Dec. 2004. IEEE, pp. 27-30.

Bataillou, E., Thierry, E., Rix, H. and Meste, O. (1995) 'Weighted averaging using adaptive estimation of the weights', *Signal Processing*, vol. 44, no. 1, pp. 51-66.

Baxes, G.A. (1994) *Digital image processing: principles and applications*. New York: Wiley.

Bayram, S., Sencar, H.T., Memon, N. and Avcibas, I. (2005), 'Source camera identification based on CFA interpolation', *Image Processing, 2005. ICIP 2005. IEEE International Conference on.* vol. 3, 11-14 Sept. 2005. IEEE, pp. III-69-72.

Bayram, S., Sencar, H.T., Memon, N. and Avcibas, I. (2006) 'Improvements on source camera-model identification based on CFA interpolation', *Proc. of WG*, vol. 11, pp. 24-27.

Bhardwaj, S. and Mittal, A. (2012) 'A survey on various edge detector techniques', *Procedia Technology*, vol. 4, pp. 220-226.

Bracewell, R.N. (1999) *The Fourier transform and its applications*. 3th edn. New York: McGraw Hill.

Burrus, C.S., Gopinath, R.A. and Guo, H. (1998) *Introduction to wavelets and wavelet transforms: a primer*. Upper Saddle River, N.J: Prentice Hall.

Celiktutan, O., Avcibas, I. and Sankur, B. 2007, 'Blind identification of cellular phone cameras', paper presented to the *Electronic Imaging 2007*.

Çeliktutan, O., Avcibaş, I. and Sankur, B. (2007), 'Blind identification of cellular phone cameras', *Electronic Imaging 2007*. vol. 6505, 15 February 2007. International Society for Optics and Photonics.

Celiktutan, O., Sankur, B. and Avcibas, I. (2008) 'Blind identification of source cell-phone model', *IEEE Transactions on Information Forensics and Security*, vol. 3, no. 3, pp. 553-566.

Chan, L.-H., Law, N.-F. and Siu, W.-C. (2013) 'A confidence map and pixel-based weighted correlation for PRNU-based camera identification', *Digital Investigation*, vol. 10, no. 3, pp. 215-225.

Chang-Tsun, L. and Yue, L. (2012) 'Color-decoupled photo response non-uniformity for digital image forensics', *IEEE Transactions on Circuits and Systems for Video Technology*, vol. 22, no. 2, pp. 260-271.

Chen, J.-S., Huertas, A. and Medioni, G. (1987) 'Fast convolution with Laplacian-of-Gaussian masks', *IEEE Transactions on Pattern Analysis and Machine Intelligence*, no. 4, pp. 584-590.

Chen, M., Fridrich, J. and Goljan, M. (2007), 'Digital imaging sensor identification (further study)', *Electronic Imaging 2007*. vol. 6505, CA, USA, Jan. 2007. International Society for Optics and Photonics, pp. 0P-0Q.

Chen, M., Fridrich, J., Goljan, M. and Lukáš, J. (2008) 'Determining image origin and integrity using sensor noise', *IEEE Transactions on Information Forensics and Security*, vol. 3, no. 1, pp. 74-90.

Chenyang, S., Yuting, S., Jing, Z. and Junyu, X. (2012), 'Sensor pattern noise in JPEG compressed images', *IEEE International Conference on Audio, Language and Image Processing (ICALIP)*. Shanghai, 16-18 July 2012. IEEE, pp. 155-159.

Chierchia, G., Parrilli, S., Poggi, G., Sansone, C. and Verdoliva, L. (2010), 'On the influence of denoising in PRNU based forgery detection', *Proceedings of the 2nd ACM Workshop on Multimedia in Forensics, Security and Intelligence*. ACM, pp. 117-122.

Chierchia, G., Poggi, G., Sansone, C. and Verdoliva, L. (2013), 'PRNU-based forgery detection with regularity constraints and global optimization', *IEEE 15th International Workshop on Multimedia Signal Processing (MMSP)*. Pula (Sardinia), Italy, 30 Sept -2 Oct. 2013. IEEE pp. 236-241.

Chierchia, G., Poggi, G., Sansone, C. and Verdoliva, L. (2014) 'A Bayesian-MRF approach for PRNU-based image forgery detection', *IEEE Transactions on Information Forensics and Security*, vol. 9, no. 4, pp. 554-567.

Cohen, K. (2007) 'Digital still camera forensics', *Small Scale Dgital Device Forensics Journal*, vol. 1, no. 1, pp. 2-8.

Coifman, R.R. and Donoho, D.L. (1995) *Translation-invariant de-noising*. New York: Springer.

Cooper, A.J. (2013) 'Improved photo response non-uniformity (PRNU) based source camera identification', *Forensic Science International*, vol. 226, no. 1, pp. 132-141.

Cortiana, A., Conotter, V., Boato, G. and De Natale, F.G. (2011), 'Performance comparison of denoising filters for source camera identification', *IS&T/SPIE Electronic Imaging*. 10 Feb.2011. International Society for Optics and Photonics.

Costa, F.D., Silva, E., Eckmann, M., Scheirer, W.J. and Rocha, A. (2014) 'Open set source camera attribution and device linking', *Pattern Recognition Letters*, vol. 39, no. 1, pp. 92-101.

Dabov, K., Foi, A., Katkovnik, V. and Egiazarian, K. (2007) 'Image Denoising by Sparse 3-D Transform-Domain Collaborative Filtering', *IEEE Transactions on Image Processing*, vol. 16, no. 8, pp. 2080-2095.

Dempster, A.P., Laird, N.M. and Rubin, D.B. (1977) 'Maximum likelihood from incomplete data via the EM algorithm', *Journal of the Royal Statistical Society. Series B (Methodological)*, pp. 1-38.

Dirik, A.E. (2010), 'New techniques in multimedia forensics', PhD thesis, New York University, New York.

Dirik, A.E., Bayram, S., Sencar, H.T. and Memon, N. (2007), 'New features to identify computer generated images', *IEEE International Conference on Image Processing, 2007. ICIP 2007.* vol. 4, San Antonio, TX, Sept. 16 2007-Oct. 19 2007. IEEE, pp. IV-433-IV-436.

Dirik, A.E., Sencar, H.T. and Memon, N. (2008) 'Digital single lens reflex camera identification from traces of sensor dust', *IEEE Transactions on Information Forensics and Security*, vol. 3, no. 3, pp. 539-552.

Donoho, D.L. (2006) 'Compressed sensing', *IEEE Transactions on Information Theory*, vol. 52, no. 4, pp. 1289-1306.

Farid, H. (2008) 'Digital image ballistics from JPEG quantization: A followup study', *Department of Computer Science, Dartmouth College, Tech. Rep. TR2008-638*.

Farid, H. (2009) 'Image forgery detection', *IEEE Signal Processing Magazine*, vol. 26, no. 2, pp. 16-25.

Fridrich, A.J., Soukal, B.D. and Lukáš, A.J. (2003), 'Detection of copy-move forgery in digital images', *in Proceedings of Digital Forensic Research Workshop*. Citeseer.

Fridrich, J. (2009a) 'Digital image forensics', *Signal Processing Magazine, IEEE*, vol. 26, no. 2, pp. 26-37.

Fridrich, J. (2009b) 'Digital image forensics introducing methods that estimate and detect sensor fingerprint', *IEEE Signal Processing Magazine*, vol. 26, no. 2, pp. 26-37.

Geradts, Z.J., Bijhold, J., Kieft, M., Kurosawa, K., Kuroki, K. and Saitoh, N. (2001), 'Methods for identification of images acquired with digital cameras', *Enabling Technologies for Law Enforcement*. International Society for Optics and Photonics, pp. 505-512.

Gisolf, F., Malgoezar, A., Baar, T. and Geradts, Z. (2013) 'Improving source camera identification using a simplified total variation based noise removal algorithm', *Digital Investigation*, vol. 10, no. 3, pp. 207-214.

Gloe, T. and Böhme, R. (2010) 'The Dresden image database for benchmarking digital image forensics', *Journal of Digital Forensic Practice*, vol. 3, no. 2-4, pp. 150-159.

Gloe, T., Franz, E. and Winkler, A. (2007), 'Forensics for flatbed scanners', *Security, Steganography, and Watermarking of Multimedia Contents IX*. vol. 6505, San Jose, CA, USA, 28 January 2007. SPIE pp. 65051I-65051I-65012.

Goljan, M. (2008), 'Digital camera identification from images estimating false acceptance probability', *Digital watermarking*. Heidelberg: Springer, pp. 454-468.

Goljan, M., Fridrich, J. and Filler, T. (2009), 'Large scale test of sensor fingerprint camera identification', *IS&T/SPIE Electronic Imaging*. 5 Feb 2009. International Society for Optics and Photonics.

Goljan, M., Fridrich, J. and Lukáš, J. (2008), 'Camera identification from printed images', *Electronic Imaging 2008.* International Society for Optics and Photonics, pp. 68190I-68112.

Gonzalez, R.C. and Woods, R.E. (2008) *Digital image processing*. Upper Saddle River, N.J: Pearson Education.

Graham, R. (1998) *Digital imaging*. Latheronwheel: Whittles.

Guangdong, W., Xiangui, K. and Liu, K.J.R. (2012), 'A context adaptive predictor of sensor pattern noise for camera source identification', *19th IEEE International Conference on Image Processing (ICIP), 2012.* Orlando, FL, Sept. 30 2012-Oct. 3 2012. pp. 237-240.

Guillon, S., Baylou, P., Najim, M. and Keskes, N. (1998) 'Adaptive nonlinear filters for 2D and 3D image enhancement', *Signal Processing*, vol. 67, no. 3, pp. 237-254.

Hany, F. (2006), *Digital image ballistics from JPEG quantization*, Technical Report TR2006-583, Department of Computer Science, Dartmouth College.

Hou, J.U. and Lee, H.K. (2016) 'Detection of Hue Modification Using Photo Response Non-Uniformity', *IEEE Transactions on Circuits and Systems for Video Technology*, vol. PP, no. 99, pp. 1-1.

Hsu, Y.-F. and Chang, S.-F. (2006), 'Detecting image splicing using geometry invariants and camera characteristics consistency', *IEEE International Conference on Multimedia and Expo.* . Toronto, Ont., 9-12 July 2006. IEEE, pp. 549-552.

Hu, Y., Li, C.-T. and Jian, C. (2010), 'Building fingerprints with information from three color bands for source camera identification', *Proceedings of the 2nd ACM Workshop on Multimedia in Forensics, Security and Intelligence.* ACM, pp. 111-116.

Hu, Y., Li, C.-T. and Lai, Z. (2015) 'Fast source camera identification using matching signs between query and reference fingerprints', *Multimedia tools and applications*, vol. 74, no. 18, pp. 7405-7428.

Hu, Y., Yu, B. and Jian, C. (2009), 'Source camera identification using large components of sensor pattern noise', *2nd International Conference on Computer Science and its Applications (CSA'09).* Jeju, Korea (South), 10-12 Dec. 2009. pp. 1-5.

Ibrahim, H. and Kong, N.S.P. (2009) 'Image sharpening using sub-regions histogram equalization', *IEEE Transactions on Consumer Electronics.*, vol. 55, no. 2, pp. 891-895.

Jain, A.K. (1989) *Fundamentals of digital image processing*. Englewood Cliffs, N.J: Prentice Hall.

Janesick, J.R. (2001) *Scientific charge-coupled devices*. vol. 117. Bellingham: SPIE press

John, M.S., Dimitrijevic, A. and Picton, T.W. (2001) 'Weighted averaging of steady-state responses', *Clinical Neurophysiology*, vol. 112, no. 3, pp. 555-562.

Johnson, M.K. and Farid, H. (2005), 'Exposing digital forgeries by detecting inconsistencies in lighting', *Proceedings of the 7th Workshop on Multimedia and Security.* 1 Aug 2005. ACM, pp. 1-10.

Johnson, M.K. and Farid, H. (2006), 'Exposing digital forgeries through chromatic aberration', *Proceedings of the 8th Workshop on Multimedia and Security*. 26 Sep 2006. ACM, pp. 48-55.

Jong-Sen, L. (1980) 'Digital image enhancement and noise filtering by use of local statistics', *IEEE Transactions on Pattern Analysis and Machine Intelligence*, vol. PAMI-2, no. 2, pp. 165-168.

Kanan, C. and Cottrell, G.W. (2012) 'Color-to-grayscale: does the method matter in image recognition?', *PloS one*, vol. 7, no. 1, p. e29740.

Kang, X., Chen, J., Lin, K. and Anjie, P. (2014) 'A context-adaptive SPN predictor for trustworthy source camera identification', *EURASIP Journal on Image and Video Processing*, vol. 2014, no. 1, pp. 1-11.

Kang, X., Li, Y., Qu, Z. and Huang, J. (2011), 'Enhancing ROC performance of trustworthy camera source identification', *IS&T/SPIE Electronic Imaging*. International Society for Optics and Photonics, pp. 788009-788011.

Kang, X., Li, Y., Qu, Z. and Huang, J. (2012) 'Enhancing source camera identification performance with a camera reference phase sensor pattern noise', *IEEE Transactions on Information Forensics and Security*, vol. 7, no. 2, pp. 393-402.

Khanna, N. (2009), 'Forensic characterization of image capture devices', PhD thesis, Purdue University, West Lafayette, Indiana.

Khanna, N., Mikkilineni, A.K., Chiu, G.T.C., Allebach, J.P. and Delp, E.J. (2007a), 'Forensic classification of imaging sensor types', *In Electronic Imaging*. vol. 6505, 15 Feb 2007. International Society for Optics and Photonics.

Khanna, N., Mikkilineni, A.K., Chiu, G.T.C., Allebach, J.P. and Delp, E.J. (2007b), 'Scanner identification using sensor pattern noise', *Security, Steganography, and Watermarking of Multimedia Contents IX*. vol. 6505, San Jose, CA, USA 28 January 2007. SPIE pp. 65051K-65051K-65011.

Khanna, N., Mikkilineni, A.K., Martone, A.F., Ali, G.N., Chiu, G.T.C., Allebach, J.P. and Delp, E.J. (2006) 'A survey of forensic characterization methods for physical devices', *Digital Investigation*, vol. 3, pp. 17-28.

Kharrazi, M., Sencar, H.T. and Memon, N. (2004), 'Blind source camera identification', *International Conference on Image Processing, 2004. ICIP'04.* . vol. 1, Singapore, 24-27 Oct. 2004. IEEE, pp. 709-712.

Kumar, M. and Saxena, R. (2013) 'Algorithm and technique on various edge detection: a survey', *Signal & Image Processing*, vol. 4, no. 3, p. 65.

Kurkin, D., Lukin, V., Abramova, V., Abramov, S., Vozel, B. and Chehdi, K. (2012), 'Image DCT coefficient statistics and their use in blind noise variance estimation', *Mathematical Methods in Electromagnetic Theory (MMET), 2012 International Conference on.* IEEE, pp. 316-319.

Laciar, E. and Jane, R. (2001), 'An improved weighted signal averaging method for high-resolution ECG signals', *Computers in Cardiology 2001*. Rotterdam, 23-26 Sep 2001. IEEE, pp. 69-72.

Langelaar, G.C., Setyawan, I. and Lagendijk, R.L. (2000) 'Watermarking digital image and video data: a state-of-the-art overview', *IEEE, Signal Processing Magazine*, vol. 17, no. 5, pp. 20-46.

Lawgaly, A., Khelifi, F. and Bouridane, A. (2013), 'Image sharpening for efficient source camera identification based on sensor pattern noise estimation', *Fourth International Conference on Emerging Security Technologies (EST).* Cambridge, 9-11 Sept. 2013. IEEE, pp. 113-116.

Lawgaly, A., Khelifi, F. and Bouridane, A. (2014), 'Weighted averaging-based sensor pattern noise estimation for source camera identification', *IEEE International Conference on Image Processing (ICIP), 2014.* Paris, 27-30 Oct. 2014. IEEE, pp. 5357-5361.

Li, C.-T. (2009), 'Source camera linking using enhanced sensor pattern noise extracted from images', *3rd International Conference on Crime Detection and Prevention (ICDP 2009).* 3 Dec 2009. IET, pp. 1-6.

Li, C.-T. (2010) 'Source camera identification using enhanced sensor pattern noise', *IEEE Transactions on Information Forensics and Security*, vol. 5, no. 2, pp. 280-287.

Li, F.M. and Nathan, A. (2005) *CCD image sensors in deep-ultraviolet: degradation behavior and damage mechanisms*. New York: Springer.

Li, R., Guan, Y. and Li, C.-T. (2014), 'PCA-based denoising of sensor pattern noise for source camera identification', *IEEE China Summit & International Conference on Signal and Information Processing (ChinaSIP), 2014* Xi'an,China, 9-13 July 2014. IEEE, pp. 436-440.

Lin, X. and Li, C.-T. (2016) 'Preprocessing reference sensor pattern noise via spectrum equalization', *IEEE Transactions on Information Forensics and Security*, vol. 11, no. 1, pp. 126-140.

Liu, B.-B., Hu, Y. and Lee, H.-K. (2010), 'Source camera identification from significant noise residual regions', *17th IEEE International Conference on Image Processing (ICIP), 2010.* Hong Kong, 26-29 Sept. 2010. IEEE, pp. 1749-1752.

Liu, B.-b., Wei, X. and Yan, J. (2015), 'Enhancing sensor pattern noise for source camera identification: an empirical evaluation', *Proceedings of the 3rd ACM Workshop on Information Hiding and Multimedia Security.* 17 Jun 2015. ACM, pp. 85-90.

Lukas, J., Fridrich, J. and Goljan, M. (2006) 'Digital camera identification from sensor pattern noise', *IEEE Transactions on Information Forensics and Security.*, vol. 1, no. 2, pp. 205-214.

Lukáš, J., Fridrich, J. and Goljan, M. (2005), 'Digital" bullet scratches" for images', *IEEE International Conference on Image Processing, ICIP 2005.* . vol. 3, 11-14 Sept. 2005. IEEE, pp. III-65-68.

Lukáš, J., Fridrich, J. and Goljan, M. (2006), 'Detecting digital image forgeries using sensor pattern noise', *Electronic Imaging 2006.* 2 Feb 2006. In Proceedings of SPIE,International Society for Optics and Photonics, pp. 60720Y-60711.

Lukin, V.V., Fevralev, D.V., Ponomarenko, N.N., Abramov, S.K., Pogrebnyak, O., Egiazarian, K.O. and Astola, J.T. (2010) 'Discrete cosine transform–based local adaptive filtering of images corrupted by nonstationary noise', *Journal of Electronic Imaging*, vol. 19, no. 2, pp. 023007-023015.

Luo, W., Qu, Z., Pan, F. and Huang, J. (2007) 'A survey of passive technology for digital image forensics', *Frontiers of Computer Science in China*, vol. 1, no. 2, pp. 166-179.

Mallat, S.p. (1999) *A wavelet tour of signal processing*. London: Academic Press.

Matsushita, K. and Kitazawa, H. (2009), 'An improved camera identification method based on the texture complexity and the image restoration', *Proceedings of the 2009 International Conference on Hybrid Information Technology*. 27 Aug. 2009. ACM, pp. 171-175.

Mihcak, M.K., Kozintsev, I. and Ramchandran, K. (1999), 'Spatially adaptive statistical modeling of wavelet image coefficients and its application to denoising', *IEEE International Conference on Acoustics, Speech, and Signal Processing* vol. 6, Phoenix, AZ, 15-19 Mar 1999. IEEE, pp. 3253-3256.

Momot, A. (2009) 'Methods of weighted averaging of ECG signals using Bayesian inference and criterion function minimization', *Biomedical Signal Processing and Control*, vol. 4, no. 2, pp. 162-169.

Momot, A. (2011), 'Methods of weighted averaging with application to biomedical signals', in G.D. Gargiulo. & A. EcEwan (eds), *Applied Biomedical Engineering.* INTECH Open Access Publisher.

Monga, V. and Evans, B.L. (2006) 'Perceptual image hashing via feature points: performance evaluation and tradeoffs', *IEEE Transactions on Image Processing*, vol. 15, no. 11, pp. 3452-3465.

Monga, V. and Mihçak, M.K. (2007) 'Robust and secure image hashing via non-negative matrix factorizations', *IEEE Transactions on Information Forensics and Security*, vol. 2, no. 3-1, pp. 376-390.

Motwani, M.C., Gadiya, M.C., Motwani, R.C. and Harris, F.C. (2004), 'Survey of image denoising techniques', *Proceedings of GSPX*. pp. 27-30.

Öktem, R., Egiazarian, K., Lukin, V.V., Ponomarenko, N.N. and Tsymbal, O.V. (2007) 'Locally adaptive DCT filtering for signal-dependent noise removal', *EURASIP Journal on Advances in Signal Processing*, vol. 2007, no. 1, pp. 1-10.

Pander, T., Przybyła, T. and Czabański, R. (2013) 'An application of the Lp-norm in robust weighted averaging of biomedical signals', *JMIT*, vol. 22, pp. 71-78.

Parker, J.R. (1997) *Algorithms for image processing and computer vision*. Chichester: Wiley.

Perona, P. and Malik, J. (1990) 'Scale-space and edge detection using anisotropic diffusion', *IEEE Transactions on Pattern Analysis and Machine Intelligence*, vol. 12, no. 7, pp. 629-639.

Petrou, M. and Petrou, C. (2010) *Image processing: the fundamentals*. Hoboken, NJ: Wiley.

Ponomarenko, N.N., Lukin, V.V., Zelensky, A.A., Astola, J.T. and Egiazarian, K.O. (2008), 'Adaptive DCT-based filtering of images corrupted by spatially correlated noise', *Electronic Imaging 2008.* 14 Feb 2008. International Society for Optics and Photonics, pp. 68120W-68111.

Popescu, A.C. and Farid, H. (2005) 'Exposing digital forgeries in color filter array interpolated images', *IEEE Transactions on Signal Processing*, vol. 53, no. 10, pp. 3948-3959.

Qu, Z., Kang, X., Huang, J. and Li, Y. (2013), 'Forensic sensor pattern noise extraction from large image data set', *IEEE International Conference on Acoustics, Speech and Signal Processing (ICASSP).* Vancouver, BC, 26-31 May 2013. IEEE, pp. 3023-3027.

Redi, J.A., Taktak, W. and Dugelay, J.-L. (2011) 'Digital image forensics: a booklet for beginners', *Multimedia Tools and Applications*, vol. 51, no. 1, pp. 133-162.

Rey, C. and Dugelay, J.-L. (2002) 'A Survey of Watermarking Algorithms for Image Authentication', *EURASIP Journal on Applied Signal Processing*, vol. 2002, no. 6, pp. 613-621.

Rudin, L.I. and Osher, S. (1994), 'Total variation based image restoration with free local constraints', *IEEE International Conference on Image Processing, ICIP-94.* vol. 1, Austin, TX, 13-16 Nov 1994. IEEE, pp. 31-35.

Rudin, L.I., Osher, S. and Fatemi, E. (1992) 'Nonlinear total variation based noise removal algorithms', *Physica D: Nonlinear Phenomena*, vol. 60, no. 1, pp. 259-268.

San Choi, K., Lam, E.Y. and Wong, K.K. (2006), 'Source camera identification using footprints from lens aberration', *Electronic Imaging 2006.* 2 Feb 2006. International Society for Optics and Photonics, pp. 60690J-60698.

Schalkoff, R.J. (1989) *Digital image processing and computer vision*. Chichester: Wiley.

Sonka, M., Hlavac, V. and Boyle, R. (1999) *Image processing, analysis, and machine vision*. Pacific Grove, Calif: PWS Publishing.

Starck, J.-L., Candès, E.J. and Donoho, D.L. (2002) 'The curvelet transform for image denoising', *IEEE Transactions on image processing*, vol. 11, no. 6, pp. 670-684.

Sutcu, Y., Bayram, S., Sencar, H.T. and Memon, N. (2007), 'Improvements on Sensor Noise Based Source Camera Identification', *IEEE International Conference on Multimedia and Expo.* Beijing, 2-5 July 2007. IEEE pp. 24-27.

Swaminathan, A., Mao, Y. and Wu, M. (2006) 'Robust and secure image hashing', *IEEE Transactions on Information Forensics and Security*, vol. 1, no. 2, pp. 215-230.

Swaminathan, A., Wu, M. and Liu, K. (2007) 'Nonintrusive component forensics of visual sensors using output images', *IEEE Transactions on Information Forensics and Security.*, vol. 2, no. 1, pp. 91-106.

Swaminathan, A., Wu, M. and Liu, K. (2008) 'Digital image forensics via intrinsic fingerprints', *IEEE Transactions on Information Forensics and Security*, vol. 3, no. 1, pp. 101-117.

Swaminathan, A., Wu, M. and Liu, K. (2009) 'Component forensics', *Signal Processing Magazine, IEEE*, vol. 26, no. 2, pp. 38-48.

Tomioka, Y., Ito, Y. and Kitazawa, H. (2013) 'Robust digital camera identification based on pairwise magnitude relations of clustered sensor pattern noise', *IEEE Transactions on Information Forensics and Security, ,* vol. 8, no. 12, pp. 1986-1995.

Tomioka, Y. and Kitazawa, H. (2011), 'Digital camera identification based on the clustered pattern noise of image sensors', *IEEE International Conference on Multimedia and Expo (ICME)* Barcelona, 11-15 July 2011. pp. 1-4.

Tran Van, L., Kai-Sen, C., Emmanuel, S. and Kankanhalli, M.S. (2007), 'A survey on digital camera image forensic methods', *IEEE International Conference on Multimedia and Expo.* Beijing, 2-5 July 2007. IEEE, pp. 16-19.

Trichili, H., Bouhlel, M.-S., Derbel, N. and Kamoun, L. (2002), 'A survey and evaluation of edge detection operators application to medical images', *IEEE International Conference on Systems, Man and Cybernetics.* vol. 4, 6-9 Oct. 2002. IEEE, p. 4 pp. vol. 4.

Valsesia, D., Coluccia, G., Bianchi, T. and Magli, E. (2015) 'Compressed fingerprint matching and camera identification via random projections', *IEEE Transactions on Information Forensics and Security*, vol. 10, no. 7, pp. 1472-1485.

Van Drongelen, W. (2006) *Signal processing for neuroscientists: an introduction to the analysis of physiological signals*. Boston: Academic Press.

van Houten, W. and Geradts, Z. (2012) 'Using anisotropic diffusion for efficient extraction of sensor noise in camera identification', *Journal of Forensic Sciences*, vol. 57, no. 2, pp. 521-527.

Van Lanh, T., Chong, K.-S., Emmanuel, S. and Kankanhalli, M.S. (2007), 'A survey on digital camera image forensic methods', *IEEE International Conference on Multimedia and Expo.* Beijing, 2-5 July 2007. IEEE, pp. 16-19.

Van, L.T., Emmanuel, S. and Kankanhalli, M.S. (2007), 'Identifying source cell phone using chromatic aberration', *IEEE International Conference on Multimedia and Expo.* Beijing, 2-5 July 2007. IEEE, pp. 883-886.

Yang, O. and Rhee, K.H. (2010) 'A Survey on Image Hashing for Image Authentication', *IEICE TRANSACTIONS on Information and Systems*, vol. 93, no. 5, pp. 1020-1030.

Zimba, M. and Xingming, S. (2011) 'DWT-PCA(EVD) Based Copy-move Image Forgery Detection', *International Journal of Digital Content Technology and its Applications*, vol. 5, no. 1.

Appendices

Appendix A: LADCT filter results based on constant noise variance.

Image size	Noise variance for each block	C1	C2	C3	C4	C5	C6	C7	C8	C9	C10	C11	C12	C13
128×128	0.012	58.00	48.50	47.00	52.00	75.00	21.50	10.00	77.00	66.50	38.50	32.50	7.50	17.00
	0.007	42.00	36.50	31.00	40.00	60.50	16.50	7.00	78.50	69.00	33.00	31.00	4.00	13.00
	0.004	38.50	27.50	27.50	38.50	56.50	15.50	7.00	76.00	69.50	31.50	26.00	3.50	11.00
	0.002	33.00	24.50	22.50	40.50	48.00	10.50	6.00	71.50	63.00	28.50	20.50	1.50	13.50
256×256	0.012	25.50	15.50	14.50	23.50	39.00	3.50	0.50	63.50	49.00	11.00	7.00	1.00	4.00
	0.007	16.00	9.00	10.50	22.00	21.00	1.50	0.50	57.00	52.50	13.00	7.50	0.00	3.00
	0.004	12.00	5.00	8.50	17.00	17.50	2.00	0.50	56.00	51.50	10.00	8.00	0.00	4.00
	0.002	10.00	3.00	8.00	17.00	16.50	2.50	1.50	58.00	51.00	10.50	9.00	0.00	3.00
512×512	0.012	3.00	1.50	7.50	14.50	2.50	0.00	0.00	46.00	35.50	5.50	4.50	0.00	3.00
	0.007	2.50	0.50	8.00	11.00	3.00	0.00	0.00	41.50	33.50	6.50	4.00	0.00	4.00
	0.004	2.00	0.00	6.50	10.50	0.50	0.00	0.00	38.00	31.00	6.50	3.00	0.00	3.50
	0.002	1.00	0.00	7.00	10.50	0.50	0.00	0.00	35.50	29.00	6.00	3.50	0.00	3.00

Table A1: False negative rate (%) based on constant noise variance with our dataset.

Image size	Noise variance for each block	C1	C2	C3	C4	C5	C6	C7	C8	C9	C10	C11	C12	C13
128×128	0.012	3.38	2.71	3.71	4.42	3.04	2.58	4.21	3.00	4.29	3.58	4.50	2.96	3.54
	0.007	3.46	2.21	3.38	2.96	2.63	2.58	2.92	2.67	3.54	2.88	3.38	2.38	3.54
	0.004	2.63	2.50	3.13	2.79	2.29	2.75	3.08	2.54	2.71	2.92	3.13	1.88	3.38
	0.002	2.04	2.38	2.58	2.21	2.00	2.58	3.08	2.08	2.75	2.21	3.13	2.04	2.88
256×256	0.012	2.17	1.38	2.04	1.83	1.29	1.25	1.71	1.13	1.67	1.83	1.79	1.42	1.96
	0.007	1.71	1.58	1.54	1.50	1.50	1.17	1.08	1.17	1.25	1.13	1.38	1.21	1.58
	0.004	1.46	1.08	1.63	1.38	1.42	1.08	1.00	1.17	1.00	1.08	1.17	0.96	1.58
	0.002	1.25	1.21	1.54	1.42	1.13	0.92	1.33	1.04	1.04	1.33	1.21	1.33	1.08
512×512	0.012	1.00	1.38	1.21	0.67	0.63	0.50	0.67	0.71	0.58	0.71	0.75	0.63	0.88
	0.007	1.08	1.13	1.25	0.58	0.75	0.50	0.92	0.58	0.67	0.50	0.46	0.38	0.75
	0.004	0.79	1.00	0.79	0.54	0.79	0.58	0.92	0.50	0.33	0.46	0.79	0.42	0.54
	0.002	0.79	0.79	0.75	0.29	0.38	0.58	0.63	0.63	0.71	0.58	0.58	0.50	0.79

Table A2: False positive rate (%) based on constant noise variance with our dataset.

Image size	Noise Variance for each block	DC1	DC2	DC3	DC4	DC5	DC6	DC7	DC8	DC9	DC10
128×128	0.012	58.94	54.11	58.45	59.42	78.26	71.50	60.87	51.69	22.22	42.51
	0.007	55.07	49.76	52.17	52.17	71.01	57.49	50.72	46.38	16.91	29.47
	0.004	44.93	36.23	49.28	46.38	67.63	54.59	43.48	36.71	13.53	23.67
	0.002	42.03	31.88	51.69	49.28	51.21	40.10	36.23	29.95	12.08	20.29
256×256	0.012	26.57	22.71	41.55	41.55	64.73	52.66	31.88	19.32	3.38	6.28
	0.007	22.71	13.04	35.27	33.33	57.49	36.71	23.19	16.91	1.45	3.86
	0.004	16.43	9.18	29.95	26.57	44.93	30.92	15.94	12.08	0.97	2.90
	0.002	20.77	9.18	31.88	28.99	28.50	15.94	10.63	11.59	0.97	4.35
512×512	0.012	9.18	6.76	19.32	16.91	37.20	18.84	6.76	5.80	0.00	0.48
	0.007	8.70	3.86	14.49	10.63	26.09	10.63	3.86	4.83	0.00	0.00
	0.004	8.21	2.90	9.18	8.70	13.53	4.35	2.42	6.28	0.00	0.00
	0.002	6.28	1.45	12.56	12.56	8.21	1.45	3.38	7.73	0.00	0.48

Table A3: False negative rate (%) based on constant noise variance with the Dresden dataset.

Image size	Noise Variance for each block	DC1	DC2	DC3	DC4	DC5	DC6	DC7	DC8	DC9	DC10
128×128	0.012	5.21	6.33	5.74	5.37	6.28	6.44	5.58	7.41	6.39	7.25
	0.007	4.78	5.42	5.05	5.58	4.56	4.78	5.26	5.58	6.12	6.33
	0.004	4.46	4.88	4.24	4.29	4.51	4.03	4.51	4.83	4.99	5.53
	0.002	3.97	3.92	3.86	3.44	3.92	4.40	3.60	4.46	4.29	4.67
256×256	0.012	3.33	3.92	2.09	3.11	3.33	3.54	3.44	3.65	3.86	4.24
	0.007	3.17	2.52	2.04	2.31	2.31	2.79	2.58	2.90	3.70	2.79
	0.004	1.99	2.25	1.93	1.93	1.93	2.25	1.88	2.15	2.84	1.93
	0.002	1.61	1.61	1.72	1.40	1.77	1.93	1.18	1.99	2.15	2.52
512×512	0.012	1.40	1.72	1.07	1.13	1.02	1.93	1.40	1.13	1.13	1.56
	0.007	1.07	0.91	0.81	1.02	1.13	1.18	0.70	0.64	0.97	0.81
	0.004	0.75	0.59	0.43	0.48	0.81	0.64	0.54	0.43	0.70	0.81
	0.002	0.59	0.54	0.64	0.38	0.70	0.59	0.43	0.59	0.86	0.70

Table A4: False positive rate (%) based on constant noise variance with the Dresden dataset.

Appendix B: Results for Colour PRNU

Image size	Methods	DC1	DC2	DC3	DC4	DC5	DC6	DC7	DC8	DC9	DC10
128× 128	Green image	43.96	14.49	34.30	32.85	14.49	20.77	25.12	10.14	7.25	13.53
	Gray image	33.82	13.53	35.27	34.78	11.59	14.01	27.54	14.01	6.28	10.14
	Grey Colour -to-luminance PRNU	33.82	13.04	37.20	29.95	13.04	10.63	25.60	13.53	4.35	11.59
	RGB scheme 3	32.37	13.53	30.43	26.09	13.53	6.28	26.09	15.94	7.25	11.59
	Proposed	31.88	12.08	19.32	20.77	10.14	8.70	17.87	6.28	3.86	13.04
256× 256	Green image	14.98	4.83	9.66	10.63	2.42	4.35	10.14	1.93	3.86	3.38
	Gray image	10.63	2.90	14.01	10.63	2.90	2.42	11.11	4.35	0.97	0.97
	Grey Colour -to-luminance PRNU	11.11	1.93	12.08	10.63	2.90	1.45	9.66	4.83	0.97	0.48
	RGB scheme 3	11.59	2.42	9.18	8.70	3.86	0.48	10.63	5.80	0.00	1.45
	Proposed	12.08	1.93	4.83	6.28	2.42	0.97	8.21	2.42	1.45	0.97
512× 512	Green image	5.31	2.42	1.45	1.45	0.97	0.48	4.83	0.00	0.97	0.00
	Gray image	4.35	0.48	3.86	1.45	0.97	0.48	4.83	0.00	0.00	0.00
	Grey Colour -to-luminance PRNU	4.35	0.48	2.90	1.45	0.48	0.48	5.31	0.48	0.00	0.00
	RGB scheme 3	2.90	0.48	2.42	0.97	0.48	0.00	4.83	3.38	0.00	0.00
	Proposed	3.38	2.42	1.93	0.97	0.48	0.48	4.83	0.00	0.00	0.00

Table B1: False negative rate (%) based on each color component with the Dresden dataset.

Image size	Methods	DC1	DC2	DC3	DC4	DC5	DC6	DC7	DC8	DC9	DC10
128×128	Green image	1.34	1.99	1.56	1.45	3.01	1.45	3.60	5.74	1.72	2.25
	Gray image	1.56	1.93	2.15	1.40	2.42	1.66	2.74	3.97	2.52	1.99
	Grey Colour -to-luminance PRNU	1.23	2.36	1.66	1.40	2.42	1.40	2.47	3.81	2.58	2.09
	RGB scheme 3	1.45	2.09	1.45	1.29	1.93	1.66	2.04	3.70	2.63	2.09
	Proposed	0.75	1.29	1.29	0.97	1.72	2.74	1.66	3.70	1.93	1.18
256×256	Green image	0.32	0.59	0.38	0.32	0.81	0.38	1.45	2.36	0.54	0.21
	Gray image	0.16	0.75	0.54	0.38	0.70	0.48	0.70	1.56	0.91	0.59
	Grey Colour -to-luminance PRNU	0.21	0.64	0.54	0.43	0.43	0.38	0.59	1.29	1.13	0.38
	RGB scheme 3	0.21	0.64	0.54	0.48	0.27	0.48	0.21	1.18	1.34	0.64
	Proposed	0.16	0.48	0.54	0.27	0.32	0.38	0.38	1.40	0.48	0.59
512×512	Green image	0.11	0.16	0.11	0.05	0.05	0.00	0.43	0.75	0.11	0.21
	Gray image	0.16	0.27	0.11	0.21	0.05	0.05	0.21	0.59	0.00	0.16
	Grey Colour -to-luminance PRNU	0.11	0.16	0.16	0.27	0.05	0.00	0.05	0.64	0.38	0.11
	RGB scheme 3	0.11	0.05	0.11	0.16	0.00	0.16	0.05	0.64	0.38	0.05
	Proposed	0.00	0.00	0.11	0.21	0.05	0.11	0.11	0.91	0.05	0.05

Table B2: False positive rate (%) based on each color component with the Dresden dataset.

Image size	Methods	C1	C2	C3	C4	C5	C6	C7	C8	C9	C10	C11	C12	C13
128× 128	Green image	20.00	12.00	15.50	33.50	42.00	16.50	1.50	69.50	51.50	19.00	17.50	1.50	6.50
	Gray image	20.00	13.00	15.50	29.50	47.00	17.00	1.50	66.50	52.00	18.50	15.50	2.00	5.50
	Grey Colour -to-luminance PRNU	15.50	10.00	15.50	30.00	43.00	16.50	1.00	65.00	53.00	18.50	17.00	1.00	6.00
	RGB scheme 3	18.50	10.50	14.00	29.50	47.00	13.50	1.50	67.00	51.50	18.00	13.50	1.50	6.00
	Proposed	15.00	9.50	14.00	26.50	42.00	14.00	1.00	64.50	50.00	18.00	17.00	1.00	4.50
256× 256	Green image	4.00	0.50	8.50	17.50	9.50	8.50	0.00	45.50	36.50	6.50	6.50	0.00	1.00
	Gray image	6.50	0.50	8.00	13.50	11.50	8.00	0.00	42.50	34.00	8.00	6.00	0.00	1.00
	Grey Colour -to-luminance PRNU	3.50	0.50	8.50	14.50	9.50	8.00	0.00	43.00	34.50	6.50	6.00	0.00	1.00
	RGB scheme 3	4.50	0.00	8.00	15.00	11.50	5.50	0.00	45.00	33.50	8.00	5.50	0.00	1.00
	Proposed	3.50	0.50	8.50	13.50	9.00	8.00	0.00	43.00	34.00	6.00	5.50	0.00	1.00
512× 512	Green image	0.50	0.00	8.00	7.00	1.00	3.50	0.00	31.50	27.50	5.00	2.50	0.00	0.50
	Gray image	0.50	0.00	8.00	6.50	0.50	3.00	0.00	30.50	27.50	4.00	2.50	0.00	0.50
	Grey Colour -to-luminance PRNU	0.50	0.00	8.00	7.50	1.00	3.00	0.00	29.50	25.50	5.50	2.50	0.00	0.50
	RGB scheme 3	1.00	0.00	8.00	5.50	1.50	3.00	0.00	29.50	26.50	4.00	2.50	0.00	0.50
	Proposed	0.50	0.00	7.50	5.50	1.00	3.00	0.00	28.50	26.00	5.00	2.00	0.00	0.50

Table B3: False negative rate (%) based on each color component with our dataset.

Image size	Methods	C1	C2	C3	C4	C5	C6	C7	C8	C9	C10	C11	C12	C13
128× 128	Green image	2.29	1.92	1.54	1.54	1.29	2.58	3.67	1.00	1.79	1.21	2.58	2.54	1.58
	Gray image	2.00	2.04	1.79	1.92	0.92	2.46	3.00	1.25	2.42	1.17	2.58	1.88	1.88
	Grey Colour -to-luminance PRNU	1.79	1.96	2.00	1.63	0.96	2.04	3.17	1.08	1.96	1.38	2.92	1.88	1.50
	RGB scheme 3	2.04	2.04	1.67	1.54	0.92	1.92	2.75	1.21	1.92	1.75	3.17	2.00	1.42
	Proposed	1.75	1.75	1.63	1.42	0.92	1.92	2.75	1.13	2.17	1.54	2.88	1.79	1.50
256× 256	Green image	1.08	0.96	0.67	0.83	0.75	1.00	2.21	0.21	0.71	1.04	0.79	1.17	0.63
	Gray image	0.88	0.63	0.79	1.00	0.67	1.04	1.63	0.54	0.75	0.92	1.08	0.83	0.88
	Grey Colour -to-luminance PRNU	1.17	0.67	0.79	0.79	0.67	0.92	1.92	0.29	0.88	0.88	0.96	0.88	0.96
	RGB scheme 3	0.88	0.54	1.04	0.83	0.63	0.88	1.33	0.38	0.88	1.13	1.17	1.04	0.75
	Proposed	1.17	0.79	0.79	0.88	0.29	1.00	1.58	0.38	0.71	0.92	1.17	0.75	0.67
512× 512	Green image	0.58	0.71	0.29	0.71	0.58	0.71	0.67	0.29	0.38	0.33	0.71	0.58	0.63
	Gray image	0.75	0.58	0.38	0.67	0.42	0.75	0.58	0.21	0.29	0.67	0.58	0.42	0.67
	Grey Colour -to-luminance PRNU	0.71	0.54	0.33	0.83	0.38	0.58	0.67	0.21	0.33	0.50	0.71	0.46	0.67
	RGB scheme 3	0.50	0.54	0.50	0.83	0.25	0.54	0.50	0.21	0.42	0.42	0.83	0.58	0.75
	Proposed	0.67	0.67	0.25	0.79	0.29	0.63	0.54	0.25	0.42	0.42	0.83	0.33	0.67

Table B4: False positive rate (%) based on each color component with our dataset.

Appendix C : Overall FNR and FPR for each technique

Image size	Technique	DC1	DC2	DC3	DC4	DC5	DC6	DC7	DC8	DC9	DC10
128× 128	Basic PRNU	34.30	24.15	40.58	39.13	45.89	32.85	32.37	26.57	6.28	16.91
	MLE PRNU	33.33	29.95	41.06	40.10	35.27	27.05	31.40	23.67	8.21	14.49
	Phase-PRNU	34.30	21.26	38.65	38.65	37.68	28.99	34.78	29.95	5.80	14.49
	CD_PRNU	32.37	28.02	39.27	49.28	31.40	32.85	29.47	32.37	14.49	23.19
	WA	32.85	19.32	40.58	36.23	25.60	16.43	29.47	21.74	6.28	8.70
	Wiener & median PRNU	36.71	21.74	38.16	33.82	38.65	28.50	37.20	29.47	14.01	21.74
	proposed system	26.57	12.08	18.84	23.19	10.14	6.76	15.94	10.14	5.80	11.59
256× 256	Basic PRNU	13.04	6.28	18.36	18.84	17.87	10.63	11.11	7.25	0.48	1.45
	MLE PRNU	12.56	8.21	18.84	22.71	13.53	8.21	11.59	7.73	0.00	0.00
	Phase-PRNU	11.59	4.83	18.36	20.29	14.98	7.73	11.59	10.63	0.48	0.48
	CD_PRNU	4.83	6.28	19.81	17.87	9.66	12.56	10.63	14.01	5.80	3.38
	WA	11.11	6.28	11.11	18.36	7.25	2.42	10.14	7.73	0	0
	Wiener & median PRNU	14.98	5.80	15.94	17.87	13.04	7.25	16.91	11.59	2.90	2.90
	proposed system	8.21	1.93	5.31	7.25	3.86	0.97	4.83	5.31	1.45	0.48
512× 512	Basic PRNU	4.35	1.93	4.35	2.42	4.35	0.00	2.90	4.83	0.00	0.00
	MLE PRNU	4.83	1.93	3.38	1.93	2.42	0.00	2.90	7.25	0.00	0.00
	Phase-PRNU	3.38	1.45	3.86	1.45	4.35	0.00	1.45	4.35	0.00	0.00
	CD_PRNU	0.97	2.90	4.83	7.73	0.48	0.48	1.93	4.35	0.48	0.00
	WA	5.80	1.45	4.35	0.97	0.48	0.48	2.90	0.48	0.00	0.00
	Wiener & median PRNU	4.35	1.93	4.35	2.90	1.93	0.97	3.86	3.38	0.00	0.00
	proposed system	2.42	0.48	1.93	1.45	0.48	0.48	0.97	0.97	0.00	0.00

Table C1: False negative rate (%) for each technique with the Dresden dataset.

Image size	Technique	DC1	DC2	DC3	DC4	DC5	DC6	DC7	DC8	DC9	DC10
128×128	Basic PRNU	3.54	3.17	3.01	3.01	3.06	3.97	2.84	3.38	3.70	2.95
	MLE PRNU	2.52	3.22	3.06	2.84	2.79	3.70	3.60	3.17	3.33	3.38
	Phase-PRNU	2.90	2.74	2.90	3.06	2.84	2.84	2.95	3.65	4.19	3.38
	CD_PRNU	3.11	3.17	3.44	2.74	4.62	4.13	3.44	3.17	4.03	3.11
	WA	1.88	2.52	2.63	1.83	2.63	2.84	2.79	2.74	3.38	2.95
	Wiener & median PRNU	2.84	2.95	3.92	3.92	3.06	3.06	3.65	3.49	3.01	3.44
	proposed system	0.97	1.29	1.56	0.81	1.45	2.74	2.58	3.17	1.72	1.02
256×256	Basic PRNU	0.91	1.02	1.07	0.91	1.18	1.45	0.59	1.13	1.45	1.56
	MLE PRNU	0.86	0.91	1.23	1.72	0.86	1.29	0.70	0.81	1.72	1.13
	Phase-PRNU	0.86	0.91	1.34	1.13	1.13	1.13	1.23	0.75	1.23	1.50
	CD_PRNU	3.33	0.32	0.48	0.11	2.42	2.68	0.59	0.27	0.43	0.32
	WA	0.64	0.86	0.81	0.75	0.59	1.13	0.64	0.75	1.77	1.23
	Wiener & median PRNU	0.81	1.07	1.50	1.23	1.07	1.72	0.86	1.29	1.34	1.23
	proposed system	0.16	0.54	0.59	0.27	0.32	3.11	0.48	0.75	0.48	0.32
512×512	Basic PRNU	0.11	0.32	0.32	0.38	0.16	0.54	0.21	0.21	0.27	0.27
	MLE PRNU	0.27	0.11	0.32	0.27	0.11	0.32	0.16	0.21	0.38	0.64
	Phase-PRNU	0.05	0.11	0.16	0.27	0.11	0.48	0.16	0.16	0.48	0.27
	CD_PRNU	0.27	0.00	0.11	0.00	0.75	0.86	0.27	0.16	0.00	0.16
	WA	0	0.05	0	0.21	0.16	0.11	0.21	0.64	0.21	0.27
	Wiener & median PRNU	0.27	0.21	0.32	0.21	0.11	0.38	0.38	0.27	0.21	0.27
	proposed system	0.05	0.00	0.16	0.21	0.05	0.11	0.11	0.11	0.21	0.05

Table C2: False positive rate (%) for each technique with the Dresden dataset.

Image size	Technique	C1	C2	C3	C4	C5	C6	C7	C8	C9	C10	C11	C12	C13
128× 128	Basic PRNU	25.50	20.50	16.00	31.50	44.00	4.50	1.00	66.00	59.00	15.00	21.00	1.00	9.00
	MLE PRNU	23.50	22.50	19.00	32.00	39.50	11.00	2.00	59.00	54.00	23.50	12.50	1.00	6.50
	Phase-PRNU	24.00	15.00	13.50	32.00	43.00	6.50	4.00	64.00	57.00	17.50	15.50	1.00	9.50
	CD_PRNU	16.50	18.50	18.50	30.00	36.50	8.00	7.50	55.50	73.00	19.50	17.00	4.50	5.50
	WA	23.00	15.50	15.00	27.50	41.00	6.00	1.00	61.50	55.00	18.50	17.00	0.50	8.50
	Wiener & median PRNU	29.00	22.50	23.50	33.50	59.50	22.50	9.00	65.50	54.00	26.00	16.00	6.00	12.00
	proposed system	14.50	8.50	14.50	27.00	40.00	9.00	2.00	65.00	53.50	18.50	18.00	1.00	5.00
256× 256	Basic PRNU	3.00	1.00	7.50	17.00	8.00	0.00	0.00	48.00	44.50	8.50	7.00	0.00	2.00
	MLE PRNU	4.00	1.50	8.00	16.50	7.00	1.00	0.00	49.50	37.50	8.50	7.50	0.00	2.50
	Phase-PRNU	3.50	1.50	8.00	14.50	10.50	0.50	0.00	46.50	40.50	9.00	6.50	0.00	2.00
	CD_PRNU	5.50	1.50	6.50	13.50	7.50	0.00	0.50	41.00	38.00	10.00	7.00	0.50	1.00
	WA	2.50	1.00	6.50	17.00	9.50	0.50	0.00	47.00	38.50	6.50	7.00	0.00	1.50
	Wiener & median PRNU	4.00	3.00	9.00	17.00	27.50	4.00	1.50	46.00	35.00	10.50	8.00	0.50	4.00
	proposed system	3.00	0.50	8.50	12.00	10.00	0.50	0.00	42.50	36.50	6.50	6.00	0.00	1.00
512× 512	Basic PRNU	0.50	0.00	5.50	9.50	0.50	0.00	0.00	35.00	26.50	5.00	3.50	0.00	3.50
	MLE PRNU	0.00	0.00	4.50	7.00	0.00	0.00	0.00	32.00	27.50	4.50	3.50	0.00	3.50
	Phase-PRNU	0.00	0.00	4.50	5.50	0.00	0.00	0.00	34.00	27.50	3.50	3.50	0.00	3.50
	CD_PRNU	1.00	0.00	4.00	5.00	0.00	0.00	0.00	25.50	30.50	4.50	4.00	0.00	1.00
	WA	0.00	0.00	5.50	6.00	0.00	0.00	0.00	30.00	28.00	4.50	4.00	0.00	3.00
	Wiener & median PRNU	1.00	0.50	6.00	8.00	1.00	0.50	0.00	29.50	24.50	5.00	4.50	0.00	2.50
	proposed system	0.50	0.00	6.00	5.50	0.00	0.00	0.00	28.00	25.00	4.00	2.00	0.00	0.00

Table C3: False negative rate (%) for each technique with our dataset.

Image size	Technique	C1	C2	C3	C4	C5	C6	C7	C8	C9	C10	C11	C12	C13
128× 128	Basic PRNU	2.33	1.75	2.54	1.88	1.63	2.75	2.46	1.92	2.00	1.75	1.92	1.46	2.42
	MLE PRNU	1.92	2.13	2.33	1.79	1.33	2.33	2.79	1.79	1.96	1.46	2.00	1.46	2.21
	Phase-PRNU	2.33	1.58	2.38	1.38	1.54	2.25	2.58	1.92	1.79	1.79	1.92	1.58	2.17
	CD_PRNU	2.38	1.46	3.46	1.79	2.83	3.58	1.75	2.67	0.08	1.17	1.17	1.38	2.17
	WA	2.25	1.67	2.46	1.88	1.33	1.71	2.42	1.63	2.00	1.67	2.29	1.33	1.96
	Wiener & median PRNU	2.63	2.33	3.08	2.50	2.13	2.46	2.29	2.04	3.04	2.00	2.58	2.25	2.25
	proposed system	1.92	1.96	1.63	1.54	1.13	2.04	2.58	1.17	1.50	1.63	2.33	1.88	1.75
256× 256	Basic PRNU	0.92	0.88	1.50	0.92	0.75	1.08	1.00	0.88	1.04	0.88	0.92	0.67	0.79
	MLE PRNU	0.88	1.21	1.08	0.79	0.92	0.88	0.96	0.58	0.92	0.79	1.00	1.00	0.88
	Phase-PRNU	1.25	1.00	1.29	0.92	0.71	1.04	0.83	0.71	1.04	0.88	0.71	0.79	0.92
	CD_PRNU	0.92	0.33	1.21	1.04	2.08	1.54	0.92	0.75	0.58	0.54	0.08	0.42	0.63
	WA	0.92	0.75	1.42	0.75	0.92	0.92	0.92	0.71	0.63	0.71	1.21	0.79	0.96
	Wiener & median PRNU	1.38	0.75	1.25	1.38	0.88	1.17	0.96	0.42	1.13	1.13	1.33	1.29	1.13
	proposed system	1.13	0.83	1.13	0.92	0.46	1.04	1.00	0.38	0.54	0.88	0.92	0.79	0.67
512× 512	Basic PRNU	0.92	0.46	0.46	0.42	0.54	0.54	0.88	0.46	0.46	0.63	0.67	0.63	0.42
	MLE PRNU	0.83	0.38	0.71	0.46	0.46	0.54	0.79	0.46	0.42	0.54	0.71	0.38	0.25
	Phase-PRNU	0.63	0.46	0.79	0.17	0.50	0.67	1.08	0.58	0.38	0.46	0.46	0.38	0.29
	CD_PRNU	0.71	0.46	0.54	0.46	0.50	0.33	0.67	0.46	0.46	0.46	0.83	0.33	0.25
	WA	0.50	0.46	0.75	0.38	0.33	0.67	0.79	0.54	0.33	0.42	0.75	0.63	0.42
	Wiener & median PRNU	0.71	0.67	0.83	0.42	0.38	0.92	0.54	0.42	0.50	0.42	0.54	0.25	0.42
	proposed system	0.67	0.71	0.29	0.92	0.33	0.33	0.25	0.25	0.29	0.42	0.63	0.54	0.58

Table C4: False positive rate (%) for each technique with our dataset.